# FINAL REPORT

## Live Site Demonstration of Advanced Geolocation Technology to Support Dynamic Classification of EMI Data Collect in GPS-challenged Areas

## ESTCP Project MR-201418

MARCH 2019

Dorota Grejner-Brzezinska
C. Toth
**Ohio State University**

***Distribution Statement A***
*This document has been cleared for public release*

ESTCP

*Page Intentionally Left Blank*

*Page Intentionally Left Blank*

# REPORT DOCUMENTATION PAGE

*Form Approved*
*OMB No. 0704-0188*



**1. REPORT DATE** *(DD-MM-YYYY)*
03-04-2018

**2. REPORT TYPE**
ESTCP FINAL REPORT

**3. DATES COVERED** *(From - To)*
Jun 2018 – Dec 2018

**4. TITLE AND SUBTITLE**
Demonstration of Advanced Geolocation Technology to Support Dynamic Classification of EMI Data Collect in GPS-challenged Areas

**5a. CONTRACT NUMBER**
W912HQ-14-C-0014

**5b. GRANT NUMBER**

**5c. PROGRAM ELEMENT NUMBER**

**6. AUTHOR(S)**
D.A. Grejner-Brzezinska and C. Toth

**5d. PROJECT NUMBER**
W74RDV33512270

**5e. TASK NUMBER**

**5f. WORK UNIT NUMBER**

**7. PERFORMING ORGANIZATION NAME(S) AND ADDRESS(ES)**

The Ohio State University
1960 Kenny Road
Columbus, OH 43210-1016

**8. PERFORMING ORGANIZATION REPORT NUMBER**
MR-201418

**9. SPONSORING / MONITORING AGENCY NAME(S) AND ADDRESS(ES)**

Environmental Security Technology Certification Program
4800 Mark Center Drive, Suite 16F16, Alexandria, VA 22350-3605

**10. SPONSOR/MONITOR'S ACRONYM(S)**
ESTCP

**11. SPONSOR/MONITOR'S REPORT NUMBER(S)** MR-201418

**12. DISTRIBUTION / AVAILABILITY STATEMENT**
Distribution A: Approved for public release; distribution unlimited.

**13. SUPPLEMENTARY NOTES**

**14. ABSTRACT**
The demonstrations performed at ARL - Blossom Point have delivered consistent performance. The AGT system was able to accurately geolocate the EMI platform in forested areas, where GNSS reception was not available or of poor quality, achieving about 30 cm at 95% CEP. A reacquisition test also showed excellent results, producing 20 cm at 95% CEP. Two prototypes were tested. Each worked well under typical field conditions and imposed very little extra effort and attention on the field crew, besides an increase in survey and data processing time. With a moderate effort engineering, the AGT system can be almost entirely integrated into the existing TEMTADS 2x2 system.

**15. SUBJECT TERMS**
UXO detection, EMI sensor, navigation, geolocation in GNSS denied areas, sensor integration, UWB positioning network

| 16. SECURITY CLASSIFICATION OF: a. REPORT | b. ABSTRACT | c. THIS PAGE | 17. LIMITATION OF ABSTRACT | 18. NUMBER OF PAGES | 19a. NAME OF RESPONSIBLE PERSON |
|---|---|---|---|---|---|
| Unclassified | Unclassified | Unclassified | Unlimited | 119 | D.A. Grejner-Brzezinska |
| | | | | | **19b. TELEPHONE NUMBER** *(include area code)* (614) 688-8136 |

*Page Intentionally Left Blank*

# FINAL REPORT
Project: MR-201418

## TABLE OF CONTENTS

**Page**

## TABLE OF CONTENTS (Continued)

**Page**

## TABLE OF CONTENTS (Continued)

**Page**

# LIST OF FIGURES

**Page**

# LIST OF FIGURES

**Page**

# LIST OF TABLES

# ACRONYMS AND ABBREVIATIONS

| | |
|---|---|
| AGC | Advanced Geophysical Classification |
| AGT | Advanced Geolocation Technology |
| ARL | US Army Research Laboratory |
| BP | US Army Research Laboratory – Blossom Point Facility |
| C/No | Carrier-to-Noise |
| CEP | Circular Error Probability |
| CORS | Continuously Operating Reference Station |
| CPU | Central Processing Unit |
| DGNSS | Differential GNSS |
| DIGINAV | Deeply Integrated GPS/INS Navigation |
| DoD | Department of Defense |
| DOF | Degree of Freedom |
| EKF | Extended Kalman Filter |
| EMI | Electromagnetic Induction |
| ESTCP | Environmental Security Technology Certification Program |
| FCC | Federal Communications Commission |
| GLONASS | Russia's Global Navigation Satellite System |
| GNSS | Global Navigation Satellite System |
| GPS | Navstar Global Positioning System |
| IDL | Interactive Data Language, a product of Harris Geospatial |
| IMU | Inertial Measurement Unit |
| INS | Inertial Navigation System |
| IR-UWB | Impulse Radio Ultra-wideband |
| IVS | Instrument Verification Strip |
| LN-CSAC | Low-Noise Chip Scale Atomic Clock |
| LOS | Line-of-sight |
| MEMS | Microelectromechanical IMU System |
| NCO | Numerically Controlled Oscillators |
| NMEA | National Marine Electronics Association |
| NRL | US Naval Research Laboratory |
| OPUS | Online Positioning User Service |
| OSU | The Ohio State University |

| | |
|---|---|
| PDOP | Position (3D) Dilution of Precision |
| POC | Point of Contact |
| PPK | Post-processed Kinematic |
| PPS | Pulse Per Signal |
| PVA | Position, Velocity, Attitude |
| QC | Quality Control |
| RAIM | Receiver Autonomous Integrity Monitoring |
| RF | Radio Frequency |
| RINEX | Receiver Independent Exchange Format |
| RMSE | Root-Mean-Square Error |
| RTK | Real Time Kinematic |
| SDR | Software Defined Radio |
| SERDP | Strategic Environmental Research and Development Program |
| SNR | Signal-to-Noise Ratio |
| SWaP | Size, Weight, and Power |
| TEM | Time-domain EMI |
| TEMTADS | Compound acronym of TEM and MTADS |
| TOF | Time of Flight |
| TW-ToA | Two-way Time of Arrival |
| USACoE | US Army Corps of Engineers |
| USB | Universal Serial Bus |
| UTC | Coordinated Universal Time |
| UTM | Universal Transverse Mercator |
| UWB | Ultra-Wideband |
| UXO | Unexploded Ordnance |
| WGS84 | World Geodetic System 84 |

# ACKNOWLEDGMENTS

We would like to thank the ARL – Blossom Point staff for their hospitality and assistance with the field tests.

*Page Intentionally Left Blank*

**ABSTRACT**

Detection and removal of buried, unexploded ordnance (UXO) from past military activities are necessary to protect human lives and the environment. A key objective of the munition response program within the ESTCP portfolio is to demonstrate the capabilities of various technologies related to UXO detection and classification. EMI-based detection of UXO has been successfully demonstrated in the recent past; for example, the US Naval Research Laboratory's (NRL) TEMTADS 2x2. The quality of the modeling results from the post-processing of EMI observations is directly related to the quality of the position and attitude information used to merge these observations into one anomaly map.

The ESTCP project, titled *Demonstration of Advanced Geolocation Technology to Support Dynamic Classification of EMI Data Collect in GPS-challenged Areas* has delivered consistent performance during the demonstration session at ARL - Blossom Point. The quadruple sensor integration based system was able to accurately geolocate the EMI platform in forested areas, where GNSS reception was not available or of poor quality. In general, all relevant project objectives, such as detection and acquisition accuracies are achieved or are within a small margin. Furthermore, the reacquisition test, which aimed to assess the performance of the AGT system for finding and flagging detected anomalies in the field, has also shown excellent results.

The technology development achieved in SERDP MM-1564 project, titled *Novel Geolocation Technology for Geophysical Sensors for Detection and Discrimination of Unexploded Ordnance*, formed the basis for the prototype systems developed for the demonstrations. As technology has advanced, the original sensor integration concept was updated to reflect the state-of-the-art in sensing, and consequently, in the data processing workflow. In short, the pseudolight and laser sensor sensors originally proposed were replaced by UWB and SDR technologies. Furthermore, due to technological improvements, two AGT prototype ietrations were developed. The first one was based on a pushcart data acquisition system, while the second was based on a backpack configuration.

Two AGT prototype systems have been tested, and while even the second one was not fully optimized for normal operations, the system worked well and imposed very little extra effort and attention on the field crew; note that the AGT system was operated by the developers, so their understanding was significantly higher than that of a typical technician. It is important to mention that with a moderate effort engineering, the AGT system can be almost entirely integrated to the existing TEMTADS 2x2 system; GNSS, recording, power, sharing the tablet for user interface, etc., can be shared. The only extra element is the UWB network. The current configuration of the network consists of four surveying poles, placed at the four corners of the site. Each pole has two UWB transmitters mounted at different heights. Note that the vertical separation of the UWB units allows for increased observability of the rover's vertical position (Z coordinate). Since these sensors are small, they can be easily integrated into a standard surveying pole. The use of these sensor poles increase the preparation time by about 30%. Since the AGT data processing is an additional step, there is a small increase in the processing time.

*Page Intentionally Left Blank*

# EXECUTIVE SUMMARY

## UXO DETECTION

Detection and removal of buried, unexploded ordnance (UXO) from past military activities are necessary to protect human lives and the environment. A key objective of the munition response program within the ESTCP portfolio is to demonstrate the capabilities of various technologies related to UXO detection and classification. EMI-based detection of UXO has been successfully demonstrated in the recent past; for example, the US Naval Research Laboratory's (NRL) TEMTADS 2x2. The quality of the modeling results from the post-processing of EMI observations is directly related to the quality of the position and attitude information used to merge these observations into one anomaly map.

The lack of practical navigation technologies for use in Global Navigation Satellite System (GNSS)-challenged areas has long hindered UXO remediation efforts; particularly for densely canopied areas. The developed geolocation solution demonstrated is based on a quadruple sensor integration, including GNSS PPK (post-processed kinematic), SDR (Software Defined Radio), Inertial Measurement Unit (IMU), and UWB (ultra-wideband) sensor technologies. The high-level description of the developed advanced navigation technology (AGT), including the sensor data streams, preprocessing modules and navigation filter is shown below. The potential benefits are enormous, as it provides the missing technology component to perform routine EMI surveys in GNSS-challenged areas.

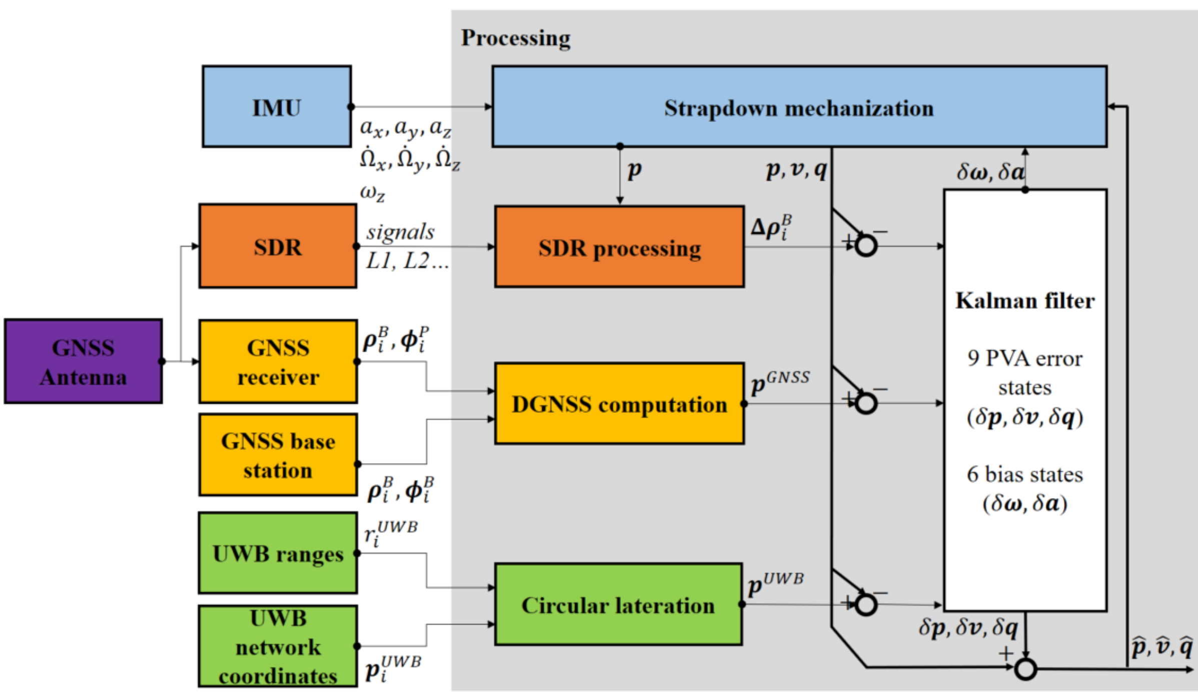


**Schematic Diagram for Quadruple Sensor Integration Used in AGT**

## AGT PROTOTYPE

The technology development achieved in SERDP MM-1564 project, titled *Novel Geolocation Technology for Geophysical Sensors for Detection and Discrimination of Unexploded Ordnance*, formed the basis for the prototype systems developed for the demonstrations in this project. As technology has advanced, the original sensor integration concept was updated to reflect the state-of-the-art in sensing, and consequently, in the data processing workflow. In short, the pseudolight and laser sensor sensors were replaced by UWB and SDR technologies. Furthermore, due to technological improvements, the first AGT prototype system was significantly upgraded for the main demonstration. The first one was based on a pushcart data acquisition system, while the second was based on a backpack configuration. Images below show the two systems.

**TEMTADS 2x2**

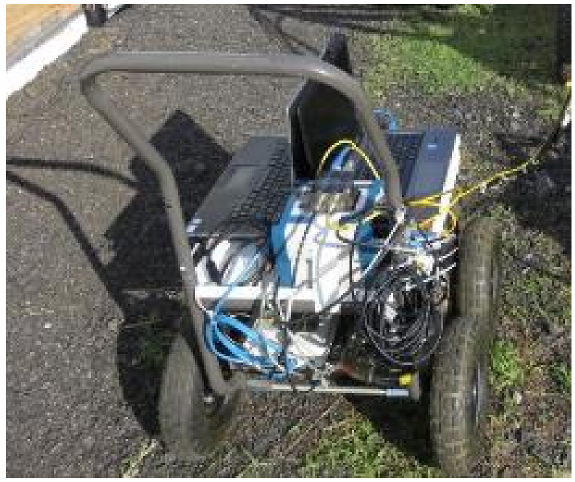

**AGT First Prototype (2016)**

**Configuration used in the Demonstration in 2018**

In GNSS-denied areas, such as forested areas, the UWB subsystem provides positioning, which is based on using a set of UWB radios with known local or global coordinates, installed around the surveyed areas. In our tests, UWB sensors were installed on four poles, which were placed at the corners of the test site. The setup and positioning of the pole required about 10-15 minutes per site.

**SITE SELECTION**

ARL - Blossom Point was jointly selected by ESTCP and NRL as the demonstration site. It provides the obvious benefit of being where NRL's equipment, tools, offices, etc. are located so thus strong support facilitated the development of the EMI and AGT system integration, establishing survey procedures and creating standards for testing. Beyond that, however, the environment provides many of the features one would look for in a "typical" survey site in the Eastern United States.

The actual test areas were selected in cooperation with BP personnel. The decision was based on:

- Canopy thickness in the area
- Density of ground vegetation should allow for pushcart operation
- Ability to tie survey control into area
- Ease of emplacing targets

To assure that the performance evaluation is unbiased, the development of the seed plan and the ground truth was held by a firewalled member of the NRL team, the team QC member, and specifically held from the EMI data analyst. The location of the detected anomalies was provided to the team QC by the EMI data analyst once the measurements were finished for evaluation.

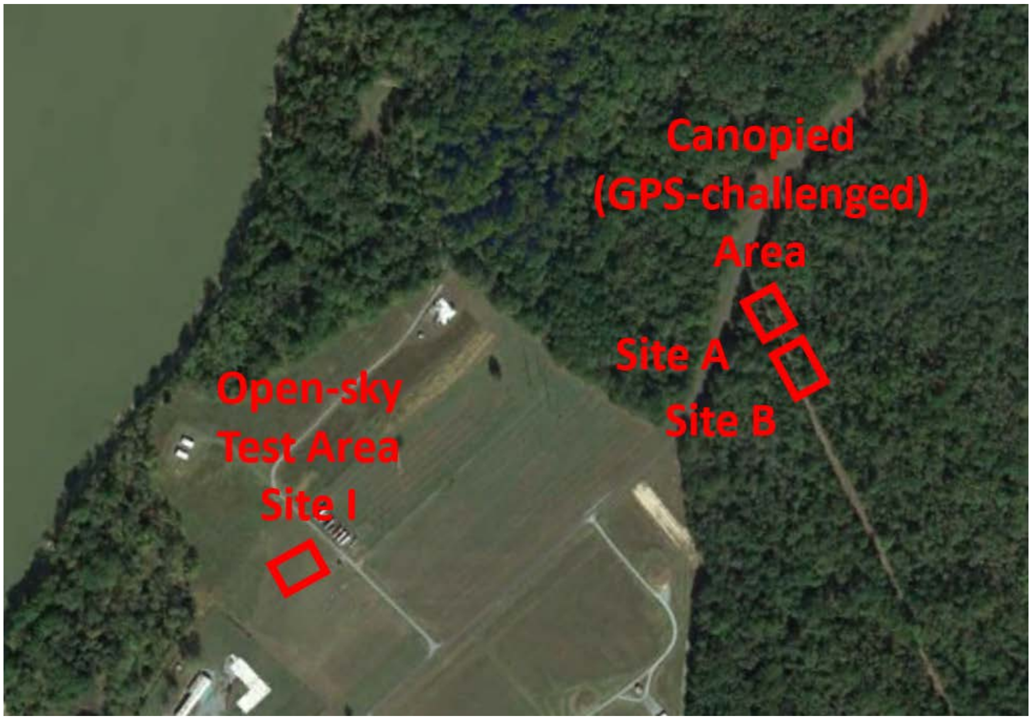


**Test Sites at the aARL - Blossom Point Facility**

## DATA ACQUISITION SESSIONS

During a four-day period, 19 measurement sessions were carried out, including 7 IVS-style measurements for the TEMTADS 2x2 sensor at the open-sky area, 11 performance tests at the two forested test sites, and one reacquisition test at site B. Typical trajectories at the open-sky and forested test sites are shown below.

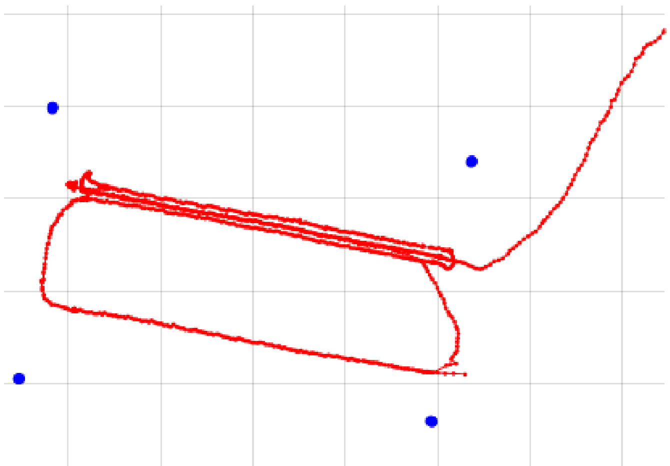

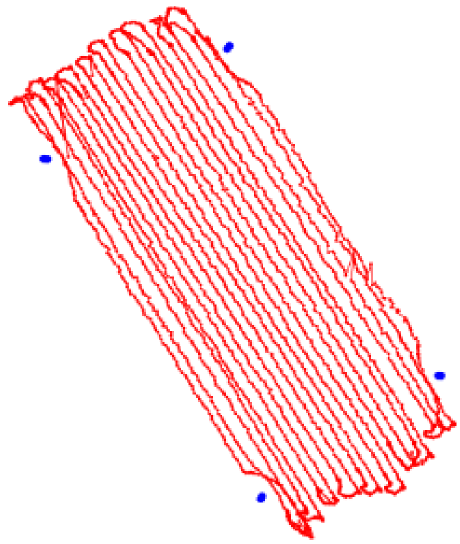

**Open-sky Area** **Canopied Area**

One data acquisition session, excluding site and system preparation, lasted about 25-30 minutes. Switching between test sites required repositioning of the UWB poles and downloading data acquired in the previous session, and typically took 15-30 minutes. Data acquisition in progress is shown below.

## PERFORMANCE RESULTS

The processing of the data sessions included data integrity check, preprocessing, creating the refined AGT solution, and applying the AGT georeferencing to the EMI processing to position the detected targets. Then, the performance evaluation included the comparison of the results to the ground truth and the statistical evaluation. The visualization of TEMTADS 2x2 system results based on AGT georeferencing is shown below.

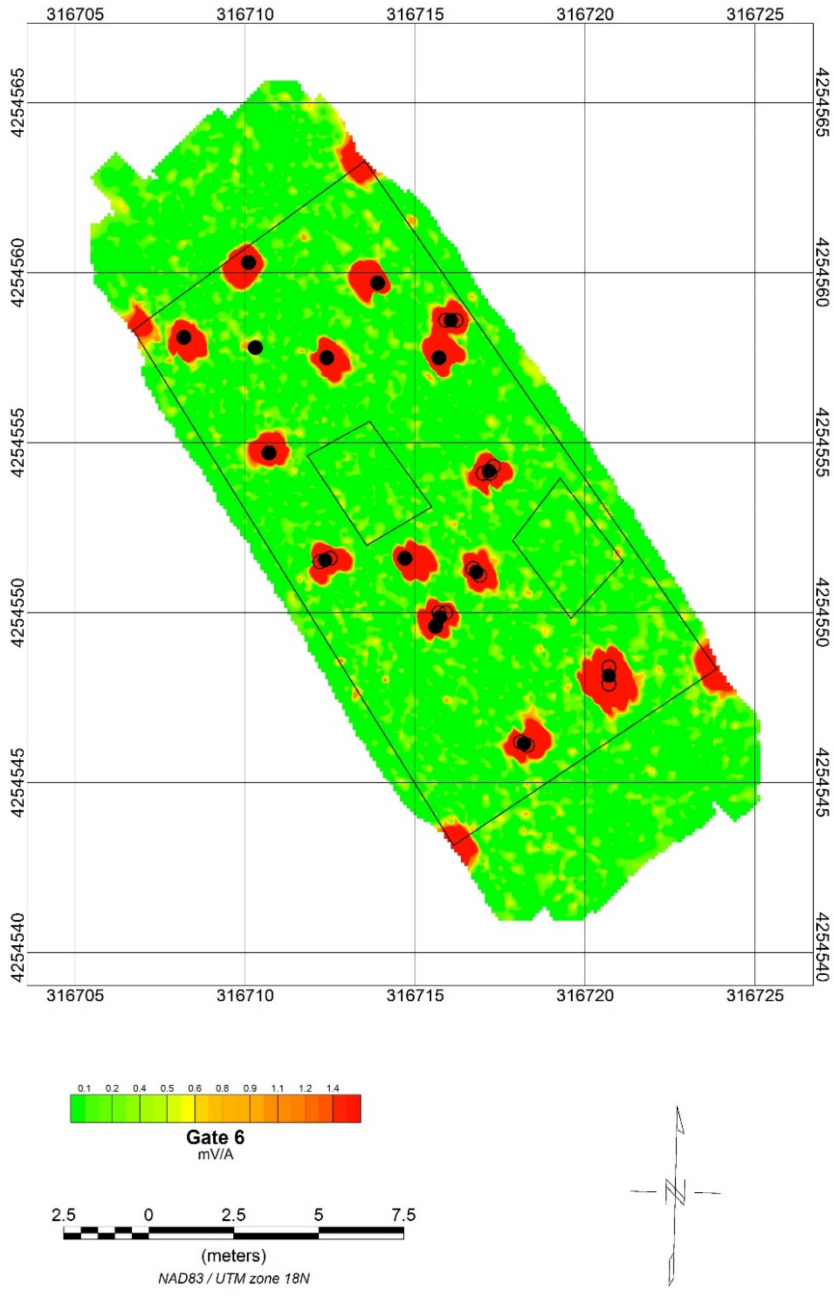


**Located and Leveled Dynamic Data from the TEMTADS 2x2 System, Site A; Black Circles Mark Target Locations Obtained by Clustering.**

Target localization errors localization errors are listed in the table below. Except for sessions A5, B3 and B4 the performance criterion of 30 cm at 95% CEP was achieved. The overall performance including all sessions was 32.4 cm, slightly above the required performance; note that the 30 cm localization accuracy for all sessions was achieved at P = 94.0%.

| Session | Average [cm] | STD [cm] | Median [cm] | 95$^{th}$ Percentile [cm] | Max [cm] |
|---|---|---|---|---|---|
| A3 | 12.1 | 3.5 | 11.0 | 17.0 | 18.0 |
| A4 | 15.3 | 7.7 | 13.0 | 28.5 | 30.0 |
| A5 | 20.7 | 11.8 | 19.0 | 41.5 | 48.0 |
| B3 | 17.8 | 12.1 | 13.0 | 37.8 | 45.0 |
| B4 | 13.8 | 10.8 | 11.0 | 30.6 | 39.0 |
| B5 | 12.7 | 6.4 | 12.0 | 22.8 | 27.0 |
| B6 | 16.9 | 7.8 | 16.0 | 26.0 | 26.0 |
| **Total** | **15.6** | **9.2** | **14.0** | **32.4** | **48.0** |

## REACQUISITION PERFORMANCE

The reacquisition was an optional item in the original objective, and only one session was carried out at Site B. During the test, the known target coordinates were provided to prototype software that provided real-time positioning, thus by moving the UWB antenna, the target location was flagged. Note that this software was used for the first time, yet provided an easy and accurate way to stake out the target location. The positioning accuracy was assessed by carefully excavating the targets, and then comparing the distance between the target center and the flag positioned by the AGT system. The results of the evaluation are listed in the table below.

| | |
|---|---|
| **# of targets** | 12 |
| **# of detected targets** | 11 |
| **Average** | 8.6 cm |
| **STD** | 6.3 cm |
| **Median** | 6.6 cm |
| **95$^{th}$ percentile** | 20.4 cm |

Two sample images show the reacquisition measurements.


**SUMMARY**

The ESTCP project, titled *Demonstration of Advanced Geolocation Technology to Support Dynamic Classification of EMI Data Collect in GPS-challenged Areas* has delivered consistent performance during the demonstration session at ARL - Blossom Point. The quadruple sensor integration-based system was able to accurately geolocate the EMI platform in forested areas, where GNSS reception was not available or of poor quality. In general, all relevant project objectives, such as detection and acquisition accuracies are achieved or are within a small margin. Furthermore, the reacquisition test has also shown excellent results.

Two AGT prototype systems have been tested, and while even the second one was not fully optimized for normal operations, the system worked well and imposed very little extra effort and attention on the field crew; note that the AGT system was operated by the developers, so their understanding was significantly higher than that of a typical technician. It is important to mention that with a moderate effort engineering, the AGT system can be almost entirely integrated to the existing TEMTADS 2x2 system; GNSS, recording, power, sharing the tablet for user interface, etc., can be shared. The only extra element is the UWB network, which is based on poles with the two UWB transmitters placed at the site corners. Since these sensors are small, they can be easily integrated into a standard surveying pole. The use of these sensor poles increase the preparation time by about 30%. Since the AGT data processing is an additional step, there is a small increase in the processing time.

*Page Intentionally Left Blank*

# 1.0 INTRODUCTION

## 1.1 INTRODUCTION

Global Navigation Satellite System (GNSS) / Inertial Measurement Unit (IMU) integrated systems provide high accuracy six degree of freedom (6-DOF) navigation solutions when good GNSS signals, such as good satellite geometry (PDOP) and high SNR are available. However, in several land-based applications, such as navigation in canopied or highly vegetated areas and indoors, GNSS is unable to position accurately or not at all. The goal of this project is to assess the performance of the navigation solution using advanced geolocation technologies (AGT), developed to aid the georeferencing of geophysical measurements made to detect buried unexploded ordnance (UXO) in GNSS-challenged/denied environments. The geophysical instrument used in this study is an advanced electromagnetic induction (EMI) sensor, installed on a cart-style platform. In a dynamic survey, buried metal objects can be identified by acquiring multiple EMI observations at various positions over the object and modeling the ensemble of data collectively. The generated anomaly map of the surveyed area can be used to derive the object locations. The aggregation process requires precise position and attitude data of the EMI platform. The desired accuracy can be easily achieved with GNSS/IMU integration in open-sky conditions, but in densely canopied or forested areas, integration with non-GNSS navigation systems is the only option to approach the open-sky accuracy of the navigation solution.

## 1.2 BACKGROUND

Detection and removal of buried, unexploded ordnance (UXO) from past military activities are necessary to protect human lives and the environment. A key objective of the munition response program within the ESTCP portfolio is to demonstrate the capabilities of various technologies related to UXO detection and classification. EMI-based detection of UXO has been successfully demonstrated in the recent past; for example, the US Naval Research Laboratory’s (NRL) TEMTADS 2x2 (see [1] and the links contained within). The quality of the modeling results from the post-processing of EMI observations is directly related to the quality of the position and attitude information used to merge these observations into one anomaly map.

The lack of practical navigation technologies for use in GNSS-challenged areas has long hindered UXO remediation efforts; particularly for densely canopied areas. The developed geolocation solution demonstrated is based on a quadruple sensor integration, including GNSS PPK (post-processed kinematic), SDR (Software Defined Radio), IMU, and UWB (ultra-wideband) sensor technologies; the technical details are discussed in Section 2. The potential benefits are enormous, as it provides the missing technology component to perform routine EMI surveys in GNSS-challenged areas.

## 1.3 OBJECTIVE OF THE DEMONSTRATION

The joint team from The Ohio State University (OSU) and NRL conducted a dynamic, detection survey at NRL's facility at the US Army Research Laboratory - Blossom Point Facility (BP), July 23-26, 2018. First, an appropriate survey area was identified in cooperation with BP staff to conduct the demonstration. The area is located in a wooded area to provide for GNSS-challenged conditions. Consideration was given to selecting an area where the TEMTADS 2x2 can be operated with no more than modest difficulty. Munitions surrogates were emplaced throughout the area to allow for quantitative assessment of the system's performance. During this demonstration, the location of these seed targets were firewalled from the EMI data analyst.

The integrated EMI/AGT system was used to conduct a dynamic survey of the demonstration area. The EMI and geolocation data streams were combined into a single data set. The combined data was processed using standard tools (Oasis montaj) to identify and select anomaly locations. The results were then compared to the firewalled ground truth by the quality control (QC) team member. The evaluation provided an absolute assessment of the achieved geolocation accuracy, namely the difference between the estimated and reference locations. This document describes the entire process of the demonstration.

## 1.4 REGULATORY DRIVERS

DoD's formation of the Advanced Geophysical Classification (AGC) Accreditation Program (DAGCAP), see [2], signals a strong commitment of the DoD to AGC. To perform AGC in the more challenging areas in which it will be required, technologies of this sort are clearly needed.

Stakeholder acceptance of the use of this navigation technology on real sites will require demonstration that the technology can be deployed efficiently and provide benefit to the AGC process. The first step in this process is to demonstrate that the AGT technology can be blended with an advanced EMI sensor system and exhibit satisfactory detection on a seeded site. Future steps in acceptance would involve integration into the full AGC pipeline and evaluation of the performance gains versus associated costs.

# 2.0 TECHNOLOGY

## 2.1 TECHNOLOGY DESCRIPTION

The system validated during the demonstration has two essential components: the TEMTADS 2x2, a proven AGC EMI sensor system installed on a pushcart, see Figure 1a, and the OSU AGT georeferencing/geolocating system specifically developed for under canopy (GNSS-challenged) applications, see Figure 1b and 1c. The overview of the main system components and their relationship is shown in Figure 2.

**(a)**

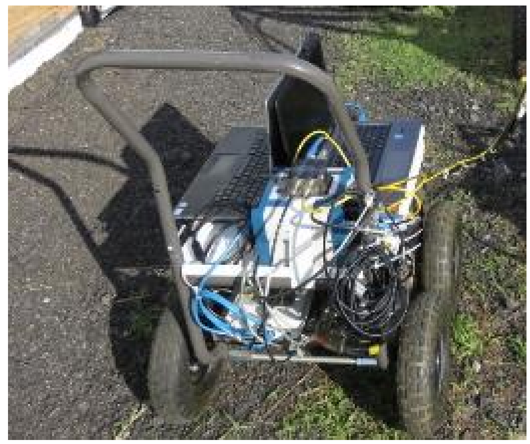

**(b)**

**(c)**

**Figure 1. (a) TEMTADS 2x2 Platform with the EMI Sensor (bottom) as Well as GNSS Antenna, UWB, IMU Sensors Installed on the Top Part; (b) First Pushcart Prototype for Data Logging, Used in 2016; and (c) Refined Backpack AGT Prototype, Used in 2018.**

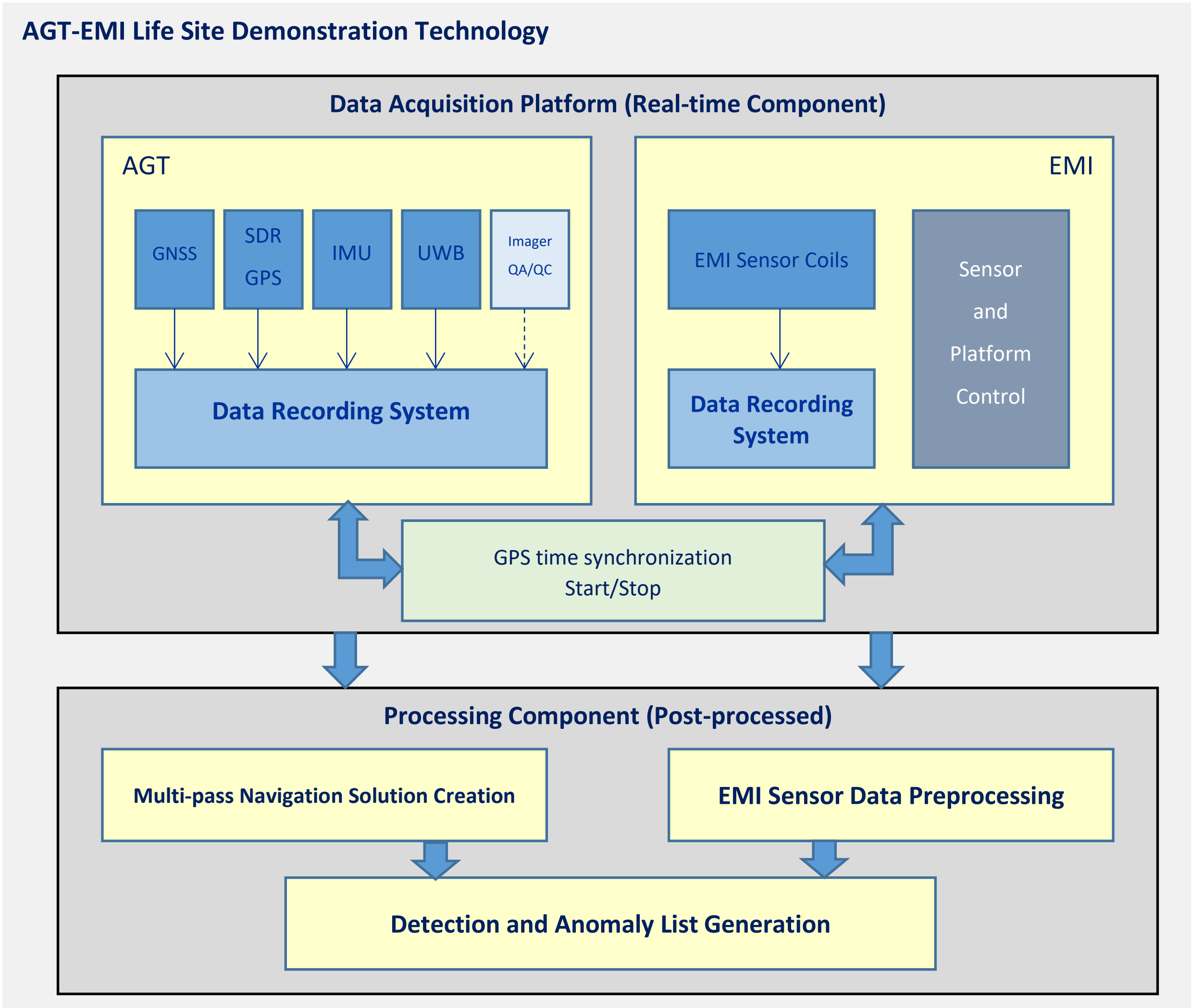


**Figure 2. System Architecture of the Demonstration System.**

### 2.1.1 Conventional Navigation Components: GNSS and IMU Sensors

The general principle of GNSS/IMU navigation systems is that the IMU measures the acceleration and the delta rotation angles of the platform, which are used to derive the platform's trajectory, while the GNSS subsystem provides the essential position updates to estimate and mitigate the IMU-related errors. The two measurement streams are fed into a navigation filter that is typically an Extended Kalman Filter (EKF). Using this framework allows for forward-backward filtering that provides a more reliable and accurate navigation solution during post-processing.

For the final demonstration, the OSU AGT prototype has been significantly upgraded from the early configuration used at the previous demonstration test. The main changes included Novatel's latest SPAN solution, the company's OEM7 (PW7700) GNSS receiver [3] and the STIM300 IMU sensor [4].

The new GNSS receiver is able to acquire and process signals from all the current GNSS systems, including GPS, GLONASS, Beidou and Galileo. The STIM300 IMU is a higher grade MEMS IMU, compared to the Epson MEMS IMU used in earlier tests; the performance parameters are listed in Table 1, for more information, please see the product sheet (https://www.sensonor.com/media/1132/ts1524r9-datasheet-stim300.pdf).

**Table 1. STIM300 IMU Performance.**

| Parameter | Specs | Epson |
|---|---|---|
| Weight | < 0.12 lbs | 0.02 lbs |
| Gyroscope bias in-run stability | 0.5 °/hr | 3 °/hr |
| Angular random walk | 0.15 °/$\sqrt{\text{h}}$ | 0.15 °/$\sqrt{\text{h}}$ |
| Accelerometer bias in-run stability | 0.05 mG | 0.1 mG |
| Velocity random walk | 0.06 m/s/$\sqrt{\text{h}}$ | 0.04 m/s/$\sqrt{\text{h}}$ |
| Max data rate | 2000 Hz | 180 Hz |

The GNSS/IMU data was processed using the Novatel's Waypoint software [5]. The entire traditional GNSS/IMU data acquisition and processing workflow relies on Novatel's off-the-shelf products; note that these systems are already tested and proved in various applications.

The SDR system shares the same GNSS antenna signal with the Novatel GNSS receiver, but processes only the GPS signal. Using SDR allows positioning solutions to be obtained at lower SNRs, where the conventional GNSS receivers are unable to detect/track signals. In addition, the SDR can provide relative position solutions when only a small number of satellites are tracked; in other words, it can constrain the platform motion, and thus improve the navigation solution. The same SDR system, including the Universal Software Radio Peripheral N200 from Ettus Research [6] and the Low-Noise Chip Scale Atomic Clock (LN-CSAC) with Evaluation Board GPS-2700/2750 from Microsemi [7] were used in all the demonstrations.

### 2.1.2 Ultra-wideband Ranging and Positioning (UWB)

Ultra-wideband signals have been used in radar applications by the military since the WWII. In 2002, the FCC allowed restricted use of UWB signals for civilians, and thus, opened the way for commercial UWB applications. For regulation, see 47 CFR Part 15, see [8], "Subpart F – Ultra-Wideband Operation", or for more details, see FCC's "Revision of Part 15 of the Commission's Rules Regarding Ultra-Wideband Transmission Systems" [9].

The main advantages of using UWB signals for positioning are that these signals are capable of propagating through objects and obstacles to certain extent, and they are fairly resistant against jamming [10]. Therefore, this technology represents an alternative positioning technique in GNSS-denied/challenged areas. One implementation of the UWB ranging technology for high accuracy applications is the impulse radio ultra-wideband approach (IR-UWB). A typical IR-UWB ranging system consists of transmitters that can both emit and receive signals.

To obtain a range measurement, a transmitter emits a very short pulse (high bandwidth) of low energy, and then on the other side, a receiver detects this signal. In general, the first peak from the received signal represents the shortest path between the transmitter and receiver. If the clocks at both ends are synchronized, the range can be calculated based on the speed of light. This ranging concept is similar to other RF based ranging techniques, but, as opposed to UWB signals, the conventional RF signal pulses are longer in time, and thus, more susceptible to signal corruption due to multipath propagation, see Figure 3. Clearly, due to the short pulse characteristics, UWB ranging allows for more accurate and reliable range estimation.

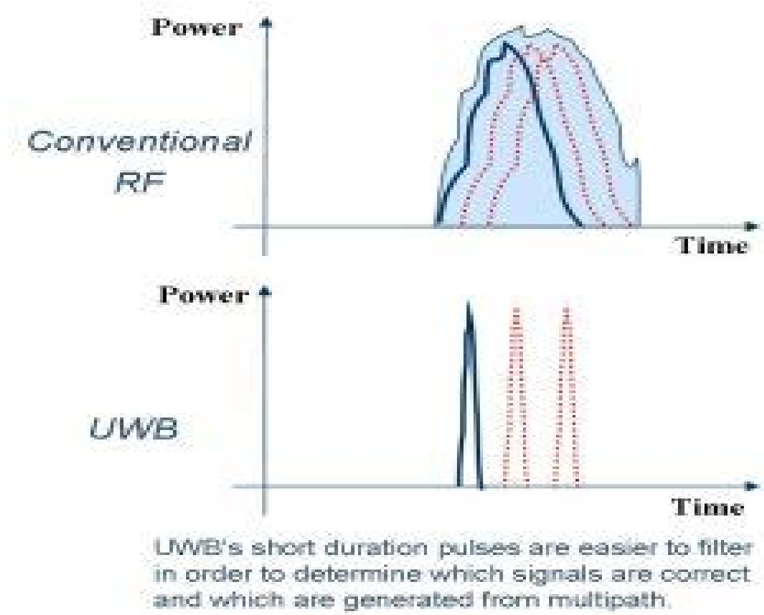


**Figure 3. Conventional and UWB Signals in Time Domain.**

TimeDomain's PulseON P440 and P410 series UWB units were used for all the tests and demonstrations, see [11]; note that only the P410 units were available for the Integrated Shakedown Testing in 2016 [12]. These units utilize two-way time of arrival (TW-ToA) ranging in order to eliminate/mitigate the receiver clock error. The TW-ToA transmitter emits a signal towards the receiver, which detects it and sends a response signal back to the transmitter. Since the receiver needs time to process and generate the response signal, there is a hardware delay at the receiver side. This delay can be measured by the receiver, and then included into the response signal. Then, the transmitter calculates the range between the two units based on the speed of light with considering the known hardware delay.

UWB positioning in an area relies on a set of UWB units or nodes that form a UWB network, where the coordinates of the static UWB units are known in a global or local coordinate system [13]. A rover, moving inside the network, measures the ranges from the nodes, and then the rover position can be obtained by circular lateration [14]. The 2D case of the circular lateration is shown in Figure 4, illustrating a network of three stations; the solid line circles represent the range measurements, and the dotted lines show the error envelope of each measurement. Note that at least three measurements are needed to find the unknown rover position in 2D; the point where all three circles intersect each other.

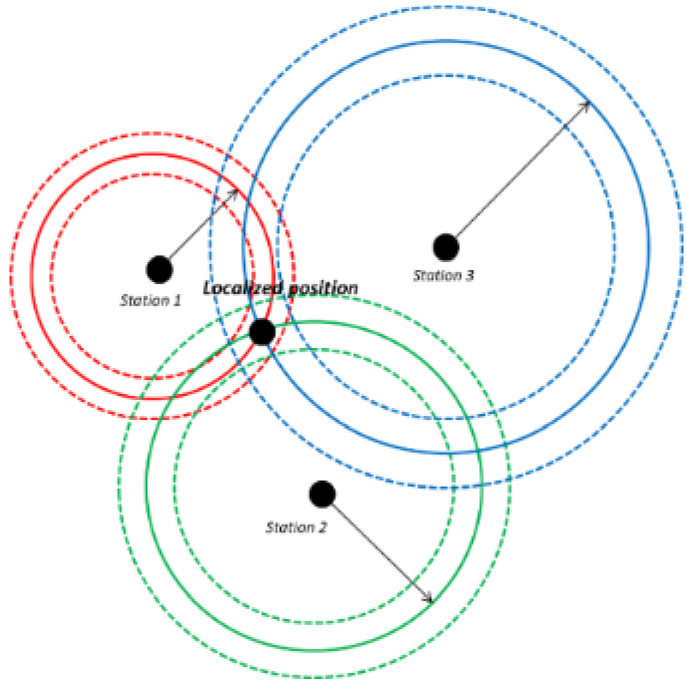


**Figure 4. The Principle of Circular Lateration with Three Stations.**

### 2.1.3 Software Defined Radio (SDR)

SDR fused GPS and inertial data at the signal processing level to extend GPS signal accumulation enable recovery of weak signals attenuated by the tree canopy. This extended accumulation is implemented in a form of deeply integrated GPS/INS navigation (DIGINAV) system. Figure 5 shows the high-level architecture of DIGINAV. It consists of (i) a high sensitivity GPS baseband signal processor, (ii) an inertial navigation system, (iii) an integration Kalman filter, and (iv) mutual aiding pathways among these system components that enable deep integration and offer the desired anti-jam capability. Modularized functionalities implemented either on reprogrammable hardware or as software modules lead to an open architecture with flexibility to integrate with new aiding sources and adaptability to new platforms and mission requirements.

As shown in Figure 5, incoming GPS signals are received by an antenna and down-converted to baseband by an RF front-end. Digitized GPS signals are processed by correlators that multiply incoming signals by internally generated replicas and initially accumulate the results over a 20-ms interval. Following the initial accumulation, Is and Qs are coherently accumulated over an extended period of time (such as 1 second) in order to suppress jamming signals. During the extended accumulation, parameters of replica signals generated by NCOs are adjusted for motion dynamics using aiding from the inertial navigation system (part of the deep integration) thus allowing for long integration. Long signal accumulation results are then applied to estimate GPS signal parameters that include code phase, carrier Doppler frequency shift, and carrier phase. The estimated GPS signal parameters are then used by the Kalman filter to estimate INS error states in order to maintain full system performance. The Kalman filter can readily accommodate measurements from other aiding sources (such as video-camera) using a reconfigurable integration filtering engine.

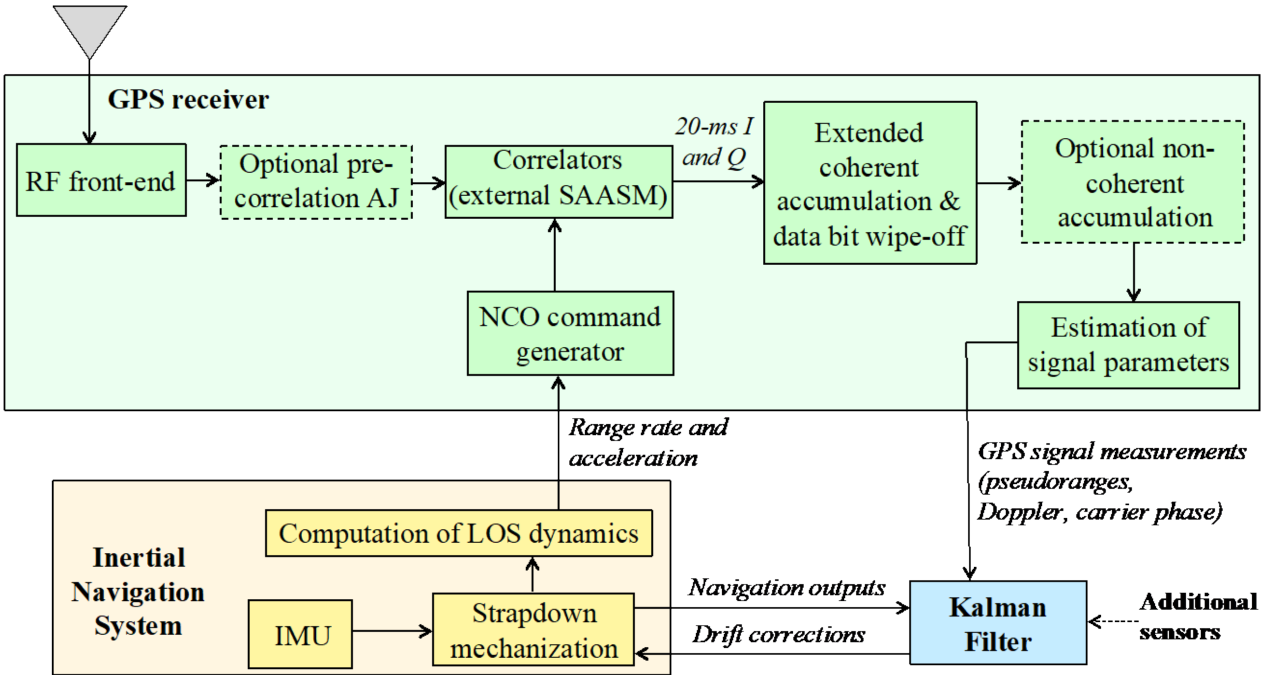


**Figure 5. Deeply Integrated GPS Inertial Navigation (DIGINAV) System.**

The extraordinary signal recovery capability of DIGINAV stems from extremely long coherent integration (LCI) of received GPS signals. Existing approaches limit coherent signal accumulation to 20-ms, which is followed by a Costas discriminator. An inertially-aided loop filter or an inertially-aided Kalman filter is then applied to discriminator outputs for narrowing the loop bandwidth for weak signal recovery and jamming suppression. In the ultra-tight coupling case, the use of Costas discriminator does not allow continuing the coherent signal integration beyond the 20-ms interval. In particular, a Costas discriminator divides or multiplies the 20 ms-accumulated in-phase and quadrature signals (I and Q, respectively); e.g., arctan(I/Q) or 0.5arcsin(IQ) discriminator functions are generally implemented. The use of these non-linear operations multiplies I and Q noise components before they are smoothed by the loop or Kalman filter. As a result, a squaring loss is introduced to the signal energy accumulation process, which limits anti-jam capabilities. The carrier phase tracking threshold of the ultra-tight coupling approach is derived as 22 dB-Hz carrier-to-noise (C/No) ratio. Moreover, a navigation-grade inertial navigation system (INS) is required to achieve this threshold. In contrast, DIGINAV is capable of maintaining carrier phase processing and continuous navigation capabilities at a 13 dB-Hz level (with unknown data bits) and at a 3 dB-Hz level when navigation data message is known (or pre-stored). A consumer-grade inertial unit can be used instead of navigation-grade IMU thus enabling significant cost reduction.

Another key feature of the deeply integrated architecture is that it supports independent tracking of individual satellite channels. This is illustrated in Figure 6.

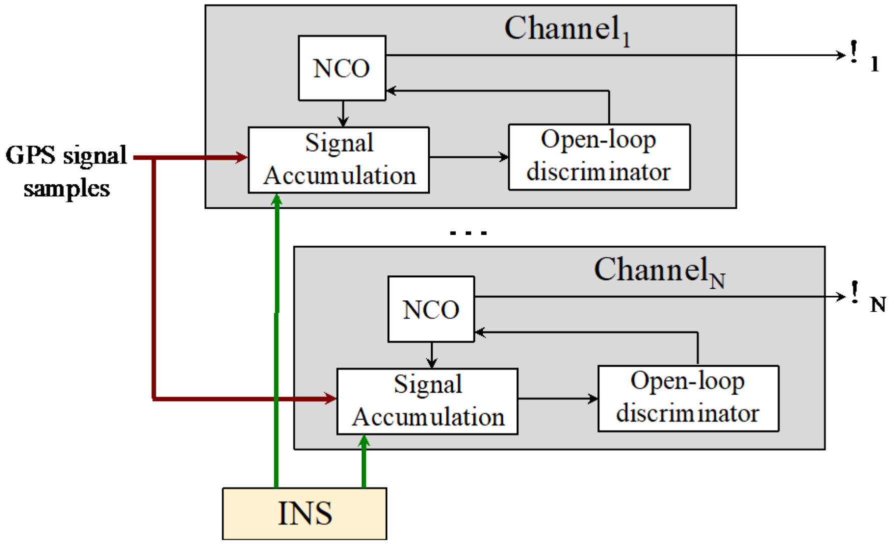


**Figure 6. Independent Tracking of Individual Satellite Channels.**

Satellite signals are accumulated independently for each tracking channel over the entire accumulation period. Signal accumulation results are utilized by open-loop discriminators to compute adjustments to signal parameters that are generated by numerically controlled oscillators (NCOs). For example, adjustment to the carrier phase is calculated based on a four-quadrant arctangent function of the inphase (I) and quadrature (Q) accumulation results. GPS measurements are then derived from NCO signal parameters for each satellite channel that is being tracked. This approach is different from the vector-tracking implementation, where signal accumulation results are generally sampled at a 20-ms accumulation point and are then fed into the joint filter that computes the overall navigation and clock solution. Independent signal tracking for individual satellites maintains stochastically independent signal measurements for different satellite channels. The main benefit is that these measurements can be exploited for data quality monitoring, for example, by using Receiver Autonomous Integrity Monitoring (RAIM) techniques, or GPS/INS integrity check, which is especially beneficial in canopied environments where large outliers can be present due to multipath errors.

## 2.2 TECHNOLOGY DEVELOPMENT

The technology development achieved in SERDP MM-1564 project, titled *Novel Geolocation Technology for Geophysical Sensors for Detection and Discrimination of Unexploded Ordnance*, see [15], formed the basis for the prototype systems developed for the demonstrations. As technology has advanced, the original sensor integration concept was updated to reflect the state-of-the-art in sensing, and consequently, in the data processing workflow. In short, the pseudolight and laser sensor sensors were replaced by UWB and SDR technologies.

The concept of the quadruple sensor integration is shown in Figure 7. The boxes on the left side of the figure represent the raw measurement streams from the four sensors. The IMU, the main navigation sensor, provides accelerometer, gyroscope and magnetometer data for the navigation filter.

The strapdown IMU mechanization algorithm calculates the position, velocity and attitude from the raw IMU observations considering the bias and drift error corrections estimated by the Kalman filter. Depending on signal conditions, the SDR system could be used to derive GPS style position or IMU style relative position fixes for the Kalman filter. The UWB and GNSS systems provide solutions for the position fixes. The main difference between the UWB and GNSS signals is the availability, which is severely limited for GNSS but can be always assumed for the UWB system. Consequently, the quality of the fixes from these sensors could range from good to medium to poor or no solution.

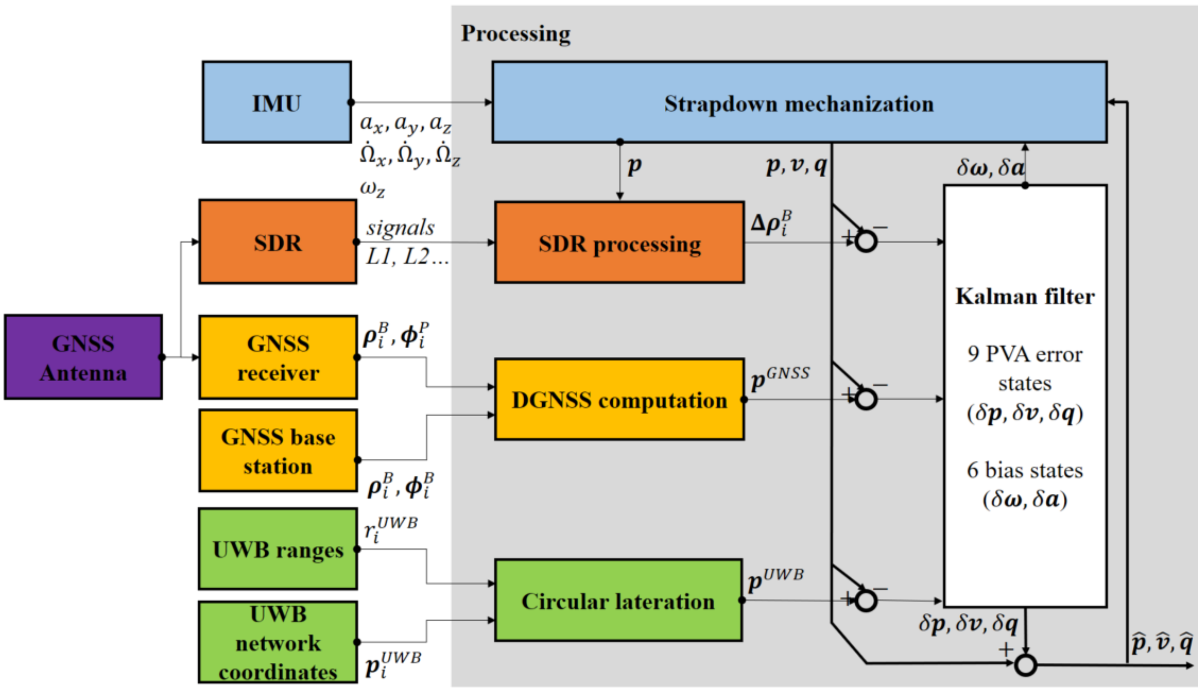


**Figure 7. Schematic Diagram for Sensor Integration.**

The UWB unit installed on the rover performs two-way time of flight (TW-TOF) ranging to all available UWB network nodes, and calculates its position based on circular lateration. The coordinates of the UWB network nodes in a local coordinate system can be derived using total station. For global coordinates, if they are required, control points might be established in open-sky conditions, near to the survey area, where their global coordinates are derived from GNSS. Measuring these control points with the total station allows for transforming the local coordinates to a global reference frame, such as WGS84 or UTM.

For the GNSS subsystem, a base station may be set up over a known point for allowing differential GNSS (DGNSS) solution, or network-based correction can be used, such as CORS-based solution. In this effort, we used Novatel Waypoint software that implements a closed-loop tightly-coupled Kalman filter for IMU/GNSS and loosely-coupled Kalman filter for IMU/UWB sensor integration. The Extended Kalman filter estimates the IMU bias and scale errors based on the GNSS or UWB observations. Under canopied or GNSS-denied areas, GNSS signal is not available, and thus, only UWB positions are used in the estimation.

Since the motion of the EMI sensor in pushcart configuration follows a simple pattern, parallel lines with overlap in sensing areas, this limited dynamic specific motion can be used as an object space constrain in the navigation filter. When GNSS and/or UWB data available, the IMU drift error is properly modeled and applied to the measurement data stream before the EKF processing. However, when neither GNSS nor UWB data is available or of poor quality, using motion constrains can bound the IMU drift error during short GNSS and UWB outages to improve the positioning, and the navigation solution, in general. The idea is that we consider the unique dynamics of the UXO mapping platform. During the geophysical survey, the platform moves along straight lines, makes turns and stops, representing three characteristics platform's dynamic states. This knowledge can be built in the navigation filter as adaptive motion constraint. The adaptivity was realized through two neural networks. The details of the investigation on the classification performance of two neural networks for dynamic state detection for this particular motion pattern, and the accuracy assessment of the navigation solution is discussed in [17]. For a backpack or pushbroom style EMI sensor configuration, such as Man Portable Vector (https://www.serdp-estcp.org/Program-Areas/Munitions-Response/Land/Live-Site-Demonstrations/MR-201228/(language)/eng-US), the motion constraint model cannot be applied due to the variability of the platform, caused by human motion. This only means that in these situation, the system has less tolerance to bridge gaps in the data. Obviously, using a higher grade IMU can offset the need for object space constraint.

## 2.3 ADVANTAGES AND LIMITATIONS OF THE TECHNOLOGY

Since GNSS reception is not available or severely limited in the target application environment, UWB technology provides the positing fixes for the IMU-based navigation solution. Therefore, only the pros and cons of UWB technology are discussed here.

As with all RF based ranging systems, the accuracy and reliability of the system depends on the signal propagation characteristics of the environment. In an unobstructed environment, the accuracy only degrades with range, as the signal strength decreases with the distance. This phenomenon can be quite accurately modeled. Ranging in complex environments, however, is hindered by obstructions, where the signal suffers significant attenuation, and then from multipath, which is caused by signal reflection from objects, resulting in receiving a cumulative signal of the multiple reflections. The multipath issue is significantly mitigated by the UWB signal structure, while obstructions equally effect all RF systems. In addition to the general propagation aspect, the geometry of the objects and the RF system components plays an important role in the ultimately achievable accuracy. In our case, the canopy is the critical obstruction for GNSS signal reception, while the ground vegetation and tree trunks represent the main obstruction for UWB signals.

UWB systems are able to provide cm-level accuracy within short ranges and under unobstructed signal path conditions, and then dm-level accuracy can be generally achieved in moderately complex environments. For the main demonstration, the maximum unit-to-unit distance was set to 15 m based on the difficulty of the test areas, such as limited pushcart maneuverability and adverse RF signal conditions. Note that similar grid dimensions are used for standard munitions response work in dense foliage and GPS-challenged conditions, rather than the typical 30m x 30m used in open-sky conditions. In such an area, the signal attenuation is limited in line-of-sight (LOS) conditions, and the signal time delay, caused by smaller obstacles, such as tree trunks, bushes, etc., introduces moderate, and thus acceptable corruption in the ranging distance [12][16].

For UWB positioning, it is important to note that the geometric configuration of the network could have relevant influence on the archived accuracies. If the network geometry is not favorable and the measurement error is large, obtaining a reliable solution is difficult. For instance, the case, depicted in Figure 8, demonstrates the existence of two possible solutions, which is due to the uncertainty of the range measurements. Note that this figure represents a 2D case, and this problem may also happen in three dimensions, such as three nodes at the same height can have ambiguous solutions in Z. If two solutions are relatively close to each other, then the impact can be partially mitigated by smoothing the derived trajectory with a kernel function or applying Kalman filtering [14][17].

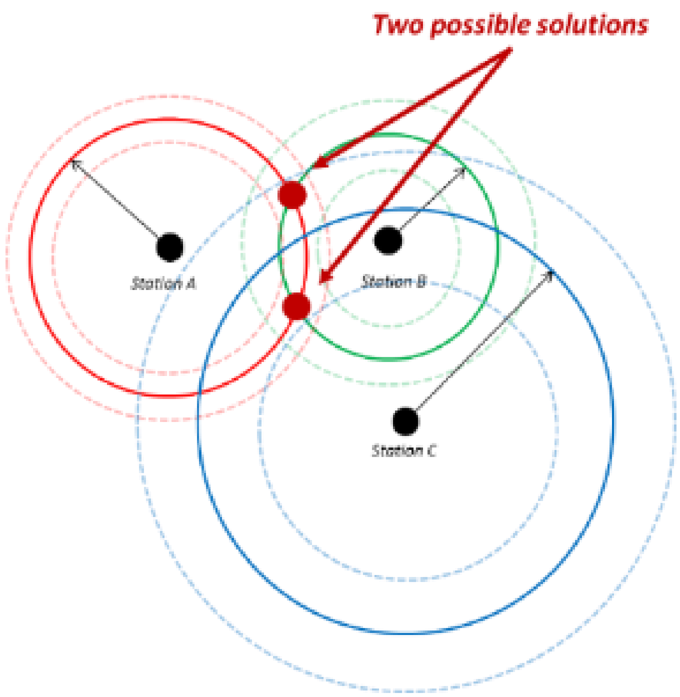


**Figure 8. Illustration of Ambiguity in Lateration for the Case of Unfavorable Network Geometry and Large Ranging Errors.**

# 3.0 PERFORMANCE OBJECTIVES

Performance objectives for the demonstration are given in Table 2 to provide a basis for evaluating the performance and costs of the demonstrated technology. These objectives are for the technologies being demonstrated only. The objectives are divided into four parts, data acquisition, AGT-unique, and overall seed detection quantitative performance objectives, and qualitative performance objectives.

Compared to the Demonstration Plan, there are minor changes in the Performance Objectives:

- There are minor changes in terminology to better express the objectives.
- The success criteria have been changed to CEP to be more in line with practice.
- The reacquisition performance, an optional item in the proposed effort, was added as it was tested during the demonstration.

The results and statistical analysis are described in Sections 6 and 7.

The entries in the Results column of Table 2 are color-coded to describe the success in meeting the individual performance objectives. Dark green indicates that the performance objective was exceeded. A lighter shade of green indicates that the performance level was very close, but the sample was too small and thus it is not statistically representative, and thus we feel the performance objective was still achieved. Yellow indicates the target performance level was not achieved, but it is close, say within about 1%, and therefore, from a practical perspective, we feel that it is acceptable. Finally, orange indicates that the achieved performance level was significantly different from the success criterion.

## Table 2. Performance Objectives for Demonstration

| Performance Objective | Metric | Data Required | Success Criteria | Results |
|---|---|---|---|---|
| **Quantitative Data Acquisition Performance Objectives** | | | | |
| Consistent data logging of the AGT system | Consistent data streams, no gaps, reliable time synchronization | IMU raw data<br>SDR raw data<br>GNSS raw data<br>UWB raw data | No missing records,<br>time tagging error is less than 1 ms | No missing records, 0.3 ms tagging error |
| Interference between the EMI and AGT sensors | Interference | Interference can be detected during data processing | No interference | No inference was found |
| **Quantitative Geolocation Performance Objectives of AGT System** | | | | |
| Reliability of the UWB ranging | The ratio of epochs with less than four ranges and all epochs | Raw UWB observations | < 1% | 0.21% |
| UWB positioning accuracy | 2D RMSE with respect to the ground truth for open-sky area | IMU/GNSS reference solution, UWB positioning solution | 2D RMSE < 15 cm (1σ) | 4.9 cm (1σ) |
| Accuracy of the IMU/UWB with and without SDR positioning solution | RMSE with respect to the ground truth for open-sky area | IMU/UWB position solution, IMU/GNSS position solution | ΔXY < 15 cm (95% CEP) | 13.1 cm |
| Heading accuracy of the platform attitude solution | Average error and standard deviations of the roll, pitch and heading angles | IMU/UWB attitude data, IMU/GNSS attitude data (reference solution) | Heading < 0.5° (1σ) | 1.4° (1σ) |
| **Quantitative Performance Objectives of Seed Detection** | | | | |
| Detection Rate | Ratio of detected and all targets | AGT navigation solution; processed EMI data; location of seed items, surveyed at accuracy of 1-2 cm | 95% | 100% (85/85, true positive) |
| Detection Accuracy | Localization accuracy of the targets in RMSE | AGT navigation solution; processed EMI data; location of seed items, surveyed at accuracy of 1-2 cm | ΔX, ΔY < 30 cm (95% CEP) | 32.4 cm (95% CEP)<br>30.0 cm (94% CEP) |
| Reacquisition Rate | Ratio of detected and all targets during reacquisition | UWB network node coordinates; location of seed items, surveyed at accuracy of 1-2 cm | 95% | 91.6% (11/12) |
| Reacquisition Accuracy | Localization accuracy of the targets in RMSE | UWB network node coordinates; Location of seed items, surveyed at accuracy of 1-2 cm | ΔXY < 30 cm (95% CEP) | ΔXY < 20 cm (95% CEP) |
| **Qualitative Performance Objectives** | | | | |
| Ease of use | Difficulty scale (1-3)<br>Time of data acquisition | Feedback from operators on usability of technology and time required | Difficulty is below than 2<br>Data acquisition is shorter than 1 hour | Difficulty: 2<br>Time: 45 min |

## 3.1 OBJECTIVE: CONSISTENT DATA LOGGING OF THE AGT SYSTEM

The performance objective describes whether the navigation system is able to provide reliable data for further processing. Issues might be associated with hardware connections, logging device, memory capacity, signal inference, etc. This objective does not include accuracy assessment.

### *Metric*

The metric is based on the preprocessing of the data streams. This analysis includes consistency check of the data records for all streams and the time synchronization error, expressed in seconds.

### *Data Requirements*

The evaluation requires the raw data from the GNSS, UWB, IMU, and SDR sensors.

### *Success Criteria*

The data records acquired by the GNSS, UWB, IMU, and SDR sensors have to be continuous; i.e., no gaps. The time synchronization error must be under 1ms. There must be no critical system failure during the acquisition.

The requirement for the time synchronization accuracy is primarily defined by the platform motion characteristics. Since the pushcart moves slowly, less than 2 m/s, the maximum traveled distance is about 2 mm during 1 ms. This is significantly below the best positioning accuracy achievable by GNSS, and required for EMI geolocation, thus no positioning error is introduced if the time synchronization error is l ms or less.

The data streams fall into two categories depending on whether GNSS is directly integrated into a sensor system or not. For example, GNSS data is internally time tagged at ns level. Some IMUs have simple built-in GNSS receivers, providing microsecond level time tagging. IMUs without internal GNSS and UWB transmitters need external time-tagging, which is generally established at the data recording system; the records, broadcast by the sensor are time-tagged when they are arrive to the logging device. The timing in the data recording system is accomplished by synchronizing the logging device internal clock to GPS time. This is the approach implemented in the AGT prototype, where 1PPS and NMEA messages are used to connect the internal system clock to GPS time.

### *Results*

Various tests conducted at OSU during the prototype development confirmed that better than 1 ms time-tagging accuracy can be achieved. The estimated average time-tagging error was 0.3 ms for the 2018 demonstration test, and consequently, the objective is satisfied.

## 3.2 OBJECTIVE: INTERFERENCE BETWEEN THE EMI AND AGT SENSOR

Previous tests indicated intermittent electromagnetic interference between the EMI sensor and the time synchronization signal of the AGT system. In addition, there was some concern on the interference between the EMI and UWB sensors. This performance objective is evaluated in conjunction with the performance objective presented in section 3.1.

***Metric***

The metric is based on the preprocessing of the UWB/GNSS data streams, as interference can be detected during data processing.

***Data Requirements***

The collected UWB/GNSS data streams.

***Success Criteria***

No interference is detected.

***Results***

No interference was detected during the 2018 demonstration tests.

## 3.3 OBJECTIVE: RELIABILITY OF THE UWB RANGING

The number of ranges captured by the UWB rover depends on the distance from the UWB network nodes and the LOS conditions. Clearly, larger number of ranges allows to account for and to describe the uncertainties associated with the ranging.

***Metric***

To compute a 2D/3D position, at least 3/4 range measurements are needed. Since the spatial distribution of UWB transmitters has a strong impact on the accuracy, more range measurements are preferred as well as good spatial distribution of the nodes. Given the slow motion of the platform and the 30 Hz polling rate of UWB transmitters, 0.25 s represents a good measurement sampling rate.

***Success Criteria***

At least four range measurements have to be observed in each 0.25 s measurement time window during 99% of the whole trajectory (1% fault rate).

***Results***

During the demonstration test, 99.7% of the data contained four or more ranges. The objective is satisfied.

## 3.4 OBJECTIVE: UWB POSITIONING ACCURACY

This performance metric describes the accuracy of the UWB positioning subsystem. The uncertainties associated with the UWB positioning was assessed in open-sky areas.

***Metric***

For open-sky areas, where reliable GNSS solution is available, the differences between the GNSS and UWB positions were used as performance metric.

***Data Requirements***

The evaluation requires the GNSS trajectory solution where it is available, and the computed UWB positions.

***Success Criteria***

The horizontal X, Y positioning errors are expected to be lower than 0.15 m (1σ).

***Results***

The achieved 0.049 m (1σ) accuracy is significantly lower than the 0.15 m success criterion. The objective is satisfied.

## 3.5 OBJECTIVE: ACCURACY OF THE PLATFORM POSITIONING SOLUTION

This performance metric describes the accuracy of the overall positioning solution provided by the navigation filter. Similarly to the previous, the performance is defined for open-sky areas.

***Metric***

The absolute accuracy is defined by 95% circular error probability using the IMU/GNSS solution as ground truth for open-sky test areas.

***Data Requirements***

The evaluation requires the IMU/UWB/SDR position solution, and the IMU/GNSS trajectory solution, if it is available.

***Success Criteria***

The horizontal X, Y errors are expected to be lower than 0.15 m at 95% probability level.

***Results***

The achieved 13.1 cm (P=95%) accuracy is lower than the success criterion. The objective is satisfied.

## 3.6 OBJECTIVE: ACCURACY OF THE PLATFORM HEADING SOLUTION

This performance metric describes the accuracy of the combined IMU/UWB/SDR/GNSS attitude solution provided by the navigation filter. Similarly to the previous cases, the performance is defined for open-sky area.

*Metric*

The absolute accuracy is defined as the error of the heading angle with respect to the IMU/GNSS solution for the open-sky test areas.

*Data Requirements*

The evaluation requires the IMU/UWB/SDR heading solution and the IMU/GNSS heading solution.

*Success Criteria*

The heading error is expected to be lower than 0.5° (1σ).

*Results*

The detected 1.4° (1σ) heading error is above the success criterion. The objective is not satisfied. However, the qualitative and quantitative results of the derived solutions suggest that the success criterion is probably too strict, as reliable anomaly map can be derived at the detected heading accuracy level.

## 3.7 OBJECTIVE: DETECTION RATE

The performance objective examines the entire navigation system using all available data streams for EMI munition detection. The performance metric describes all errors associated with not only the navigation system, but with the EMI subsystem as well. This performance objective measures the detection rate of the entire system to localize buried targets. Note that blind seeded targets were used for the performance evaluation.

*Metric*

The ratio of undetected and the sum of undetected and detected targets.

*Data Requirements*

The evaluation requires the detected targets derived from the EMI data using the IMU/UWB/SDR/GNSS navigation solution as well as the number of the buried targets installed on the test site.

*Success Criteria*

The ratio of the detected and total number of targets has to be higher than 95%. All 85 targets were identified during the test.

*Results*

All 85 targets were identified during the test. The success criterion is satisfied.

## 3.8 OBJECTIVE: DETECTION ACCURACY

This performance objective examines the entire EMI/AGT system using all available data streams for munition detection. Therefore, the performance metric considers all errors associated with not only the navigation system, but with the EMI subsystem as well. This performance objective measures the detection and localization accuracy of the entire system to localize buried targets. Note that blind seeded targets were used for the performance evaluation.

***Metric***

The metric is the 95% horizontal circular error probability measured between the precisely surveyed coordinates of the seed targets, and the estimated coordinates derived from the EMI sensor processing using the IMU/UWB/SDR navigation solution.

***Data Requirements***

The evaluation requires the coordinates of the targets derived from the EMI data processing when the IMU/UWB/SDR navigation solution was used for georeferencing as well as the pre-surveyed ground truth coordinates of the targets in the UTM 18N coordinate system (reference frame).

***Success Criteria***

The 95% horizontal circular error is expected to be lower than 0.30 m.

***Results***

The average of this metric for all sessions was 0.32 cm at the given probability level, which is slightly worse than the performance criterion. Note that the 0.30 m performance objective is achieved at 94.0% level. The success criterion is nearly satisfied with a very small margin.

## 3.9 OBJECTIVE: REACQUISITION RATE

The goal of the target reacquisition was to assess the UWB system performance to stake out the target locations in the GNSS-challenged environment. Note that this element of the testing was optional, and was carried out on the last day in relatively short time. This performance objective measures the capability of the UWB positioning system to localize buried targets. Note that no EMI functionality was considered in this effort.

***Metric***

This performance objective measures the detection rate of the system to localize buried targets during reacquisition.

***Data Requirements***

The evaluation requires the number of targets buried at the test site.

*Success Criteria*

The ratio of the detected and total number of targets has to be higher than 95%.

*Results*

The UWB system was capable of finding 11 targets during the test out of 12, resulting in 91.6% success rate. The success criterion is nearly satisfied with a small margin. One target was not localized within 40 cm due to our inexperience with the recently developed and not yet field-tested reacquisition system. In addition, the sample size is small that allows for no rigorous comparison between the detection rate and the success criterion. Note that this element of the testing was optional, and was carried out in a short time on the last day.

## 3.10 OBJECTIVE: REACQUISITION ACCURACY

The reacquisition accuracy is an essential performance parameter, which shows how closely the targets can be reacquired. Practically, this is the measure of the UWB system performance; similar to Section 3.6.

*Metric*

This performance objective measures the distance between the known/actual location of a target and the reacquired location, which was flagged during the reacquisition session. The simple 2D distance was considered for evaluation.

*Data Requirements*

The evaluation requires the location coordinates of all targets buried at the test site, and the flags, used to stake out the reacquired locations; more precisely, the coordinates of know target locations and the coordinates of the flags are needed in a local or global frame.

*Success Criteria*

The 95% horizontal circular error is expected to be lower than 0.30 m.

*Results*

0.21 m is achieved at the 95% probability level, which is significantly better than the performance criterion. The objective is satisfied with a large margin.

## 3.11 OBJECTIVE: EASY OF USE

The performance objective describes the difficulty level of the system usability.

*Metric*

The performance objective is evaluated on a 1-3 scale, where

1. Easy to use: no special expertise is required and/or short training that is not longer than 1 hour.

2. Medium difficulty: technician has to present and/or training longer than 1 hour is needed.

3. Difficult to use special expertise of the field is required.

The metric is applied to the data acquisition as well as data processing. Finally, the time required for data acquisition is an additional metric to this performance objective.

***Data Requirements***

The main source for the evaluation of this metric is the feedback from the operators, obtained during and after the tests.

***Success Criteria***

The difficulty level of the data acquisition and processing was judged to be well below 2. The data acquisition is shorter than 1 hour for a grid.

***Results***

The AGT system could be operated by a technician after a 1-day training, and if no data gap or any fault are present, the data processing can be also done by that technician. Note that optimizing the software tools may decrease training time and reduce the complexity of data processing.

In the 2018 demonstration tests, the acquisition time was less than 1 hour for all the test sites at Blossom Point (18 × 10 m or 59 × 33 ft.), including the UWB network installation and EMI survey; the typical UWB network setup required 15 minutes and the EMI dynamic survey took about 30 min.

*Page Intentionally Left Blank*

# 4.0 SITE DESCRIPTION

## 4.1 SITE SELECTION

Blossom Point was jointly selected by ESTCP and NRL as the demonstration site. It provides the obvious benefit of being where NRL's equipment, tools, offices, etc. are located so thus strong support facilitated the development of the EMI and AGT system integration, establishing survey procedures and creating standards for testing. Beyond that, however, the environment provides many of the features one would look for in a "typical" survey site in the Eastern United States.

The actual test areas were selected in cooperation with BP personnel. The decision was based on:

- Canopy thickness in the area
- Density of ground vegetation should allow for pushcart operation
- Ability to tie survey control into area
- Ease of emplacing targets

To assure that the performance evaluation is unbiased, the development of the seed plan and the ground truth was held by a firewalled member of the NRL team, the team QC member, and specifically held from the EMI data analyst. The location of the detected anomalies was provided to the team QC by the EMI data analyst once the measurements were finished for evaluation.

## 4.2 SITE HISTORY

The Army Research Laboratory - Blossom Point Facility is comprised of 1,600 acres, approximately 50 miles south of Washington DC, in rural Charles County, Maryland, see Figure 9. The facility is located on Cedar Point Neck, between the Nanjemoy Creek and the Port Tobacco River on the northern shore of the Potomac River. Open, grassy fields, as well as areas of deciduous and mixed deciduous and coniferous forest are found on the property. Low elevation, swampy areas are present in the central and eastern portions of the property, and along the southern edge, adjacent to the Potomac River.

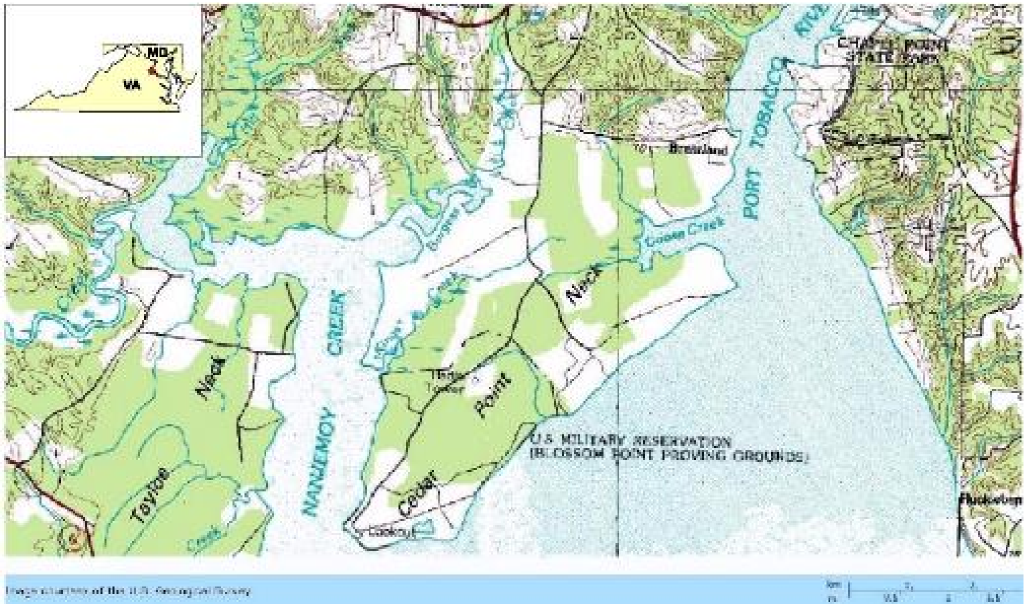


**Figure 9. Location of Army Research Laboratory Blossom Point Facility.**

## 4.3 SITE GEOLOGY

Charles County, MD is situated within the Coastal Plain Province. This province is underlain by an eastward thickening wedge of unconsolidated marine sediments including gravel, sand, silt, and clay. Cedar Neck Point is mapped in the 1989 Maryland Geological Survey Charles County Geologic Map, see Figure 10, almost entirely in the Upper Pleistocene-aged Maryland Point Formation (Qm). The Maryland Point Formation is described as fine to coarse grained sand, well to poorly sorted in the upper third, with poorly sorted silty clay in the lower part, with a pebbly sand at the base

Two other mapped units occur on Cedar Point Neck, Qk, and Qh, each occupying small areas. On Cedar Point Neck, the Upper Pleistocene-aged Kent Island Formation (Qk) occurs only on a peninsula south of Goose Creek. This unit overlies the Maryland Point Formation, and consists of fine to medium grained, moderate to poorly sorted silty sand. Minor silty to sandy clay is also present. The most recent mapped unit is Holocene deposits, undivided, which occur only in low lying areas adjacent to swamps and drainages at Blossom Point. These deposits include poorly sorted sand and gravel, as well as well sorted sand, silt and clay.

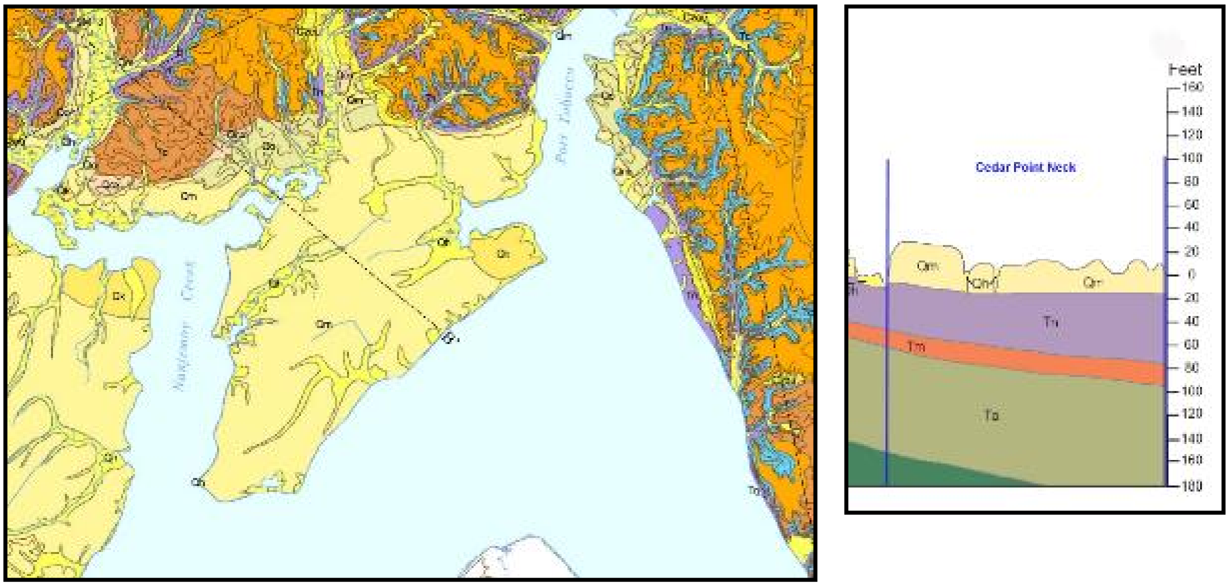


**Figure 10. Geologic Map and Cross Section (McCartan, 1989) showing Cedar Point Neck.**

The cross section presented in Figure 10 shows a maximum thickness of the Maryland Point Formation on Cedar Point Neck of approximately 40 feet. The formation is absent where the cross section traverses two small streams, filled with Holocene sediments.

Geologic responses observed in electromagnetic surveys are often caused by magnetic minerals, primarily magnetite and maghemite. These minerals are very likely present in the marine sediments at Blossom Point, though it is expected that they are generally dispersed, and that concentrations high enough to affect EM response are limited in area.

## 4.4 MUNITIONS CONTAMINATIONS

The Army Research Laboratory – Blossom Point Facility is a field testing location for fuzes, ordnance, and pyrotechnic devices, electronic telemetry systems, and production lot acceptance testing of contractor manufactured fuze components. The Facility occupies approximately 1,600 acres (2.5 square miles) of US Army-owned land in southern Charles County, MD, see [19]. The proposed demonstration area is located within the former range fan of an 81mm mortar firing range. Any *in situ* munitions would therefore likely be 81mm mortars.

*Page Intentionally Left Blank*

# 5.0 TEST DESIGN

The AGT prototype system evolved during the project, and various versions were used at different stages for performance testing at OSU and then at Blossom Point. Here the discussion is focused on the final version of the system and the last demonstration tests performed at Blossom Point in 2018.

UXO detection system, shown in Figure 11, consists of the EMI and AGT subsystems. OSU's AGT system provides the essential geolocation/navigation information; mainly, the coordinates and heading for the EMI data processing. The EMI sensor, discussed and evaluated in several pervious ESTCP projects, see [1][12][23], is installed on the bottom of a pushcart, and the data is recorded by a backpack recording system, carried by the operator. AGT's navigation sensors were also installed on the EMI pushcart; the Septentrio GNSS antenna, STIM300 IMU and TimeDomain's P410/P440 UWB radio were placed on top of the pushcart. A second operator, see Figure 11, carried the AGT logging unit in a backpack configuration. The sensors on the pushcart are connected to the logging units of the backpack systems. The hardware elements of the AGT backpack were a Novatel PowerPack 7 GPS receiver, which also logged the STIM300 IMU data, the SDR unit and two data logging laptop computers. In addition, the AGT system included a UWB network, consisting of field-deployed poles with attached UWB transmitters. Note that the coordinates of the UWB network were surveyed in a global coordinate system.

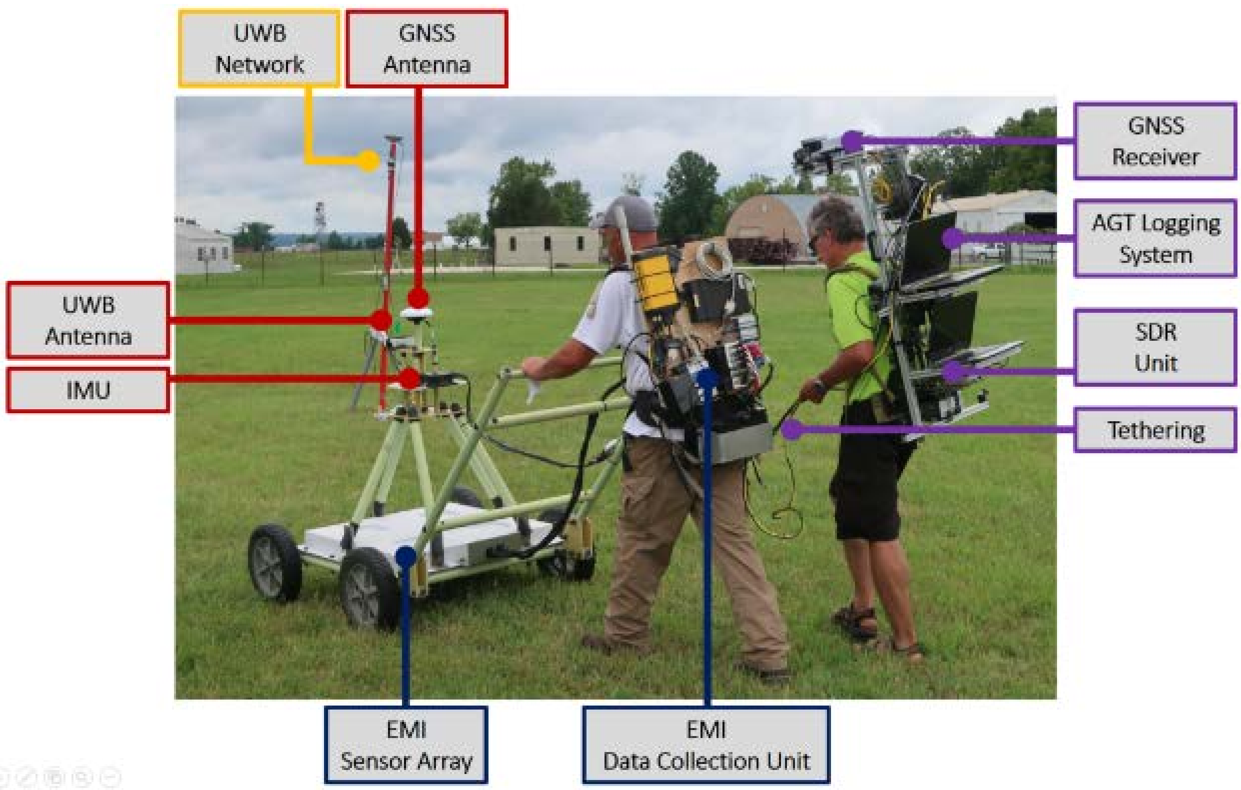


**Figure 11. The EMI and AGT Systems, Use in 2018.**

## 5.1 CONCEPTUEL EXPERIMENTAL DESIGN

The demonstration consisted of the following steps:

- **Site selection:** The site selection at Blossom Point was selected by NRL personnel, and included three test areas. The first one, a 14 × 27 m (46 × 89 ft.) open-sky area, was used for EMI sensor calibration, and general performance assessment of the AGT system. The second and third areas, referenced as Sites A and B, were selected in a forested region with an approximate size of 18 × 10 m (59 × 33 ft.), roughly the size of a typical MR survey grid under such conditions (15m x 15m).
- **Site development:** Targets were buried at the two forested sites, and their location was accurately surveyed. Based on input from the USACoE, a grid size of roughly 15x x 15 m was used to define the two survey sites. Two dozen small ISO80 munitions surrogates were seeded into the area, carefully located using total station and then covered. The details of the demonstration area preparation and seeding plan was kept firewalled from the EMI data analyst.
- **Site preparation:** For every measurement session at the three sites, the UWB network nodes were installed at the four corners of each area. The precise location of the site corners was surveyed during the target emplacement process, and the site corners were used for the UWB poles deployment. Knowing the coordinates of these points provides an easy connection between the local and global coordinates systems.
- **Data acquisition**: During the data acquisition, the EMI platform equipped with the AGT navigation sensors performed typical dynamic surveys of the test areas. The measurement were repeated 5-6 times, as time allowed. Three measurement sessions were planned as a minimum.
- **Data processing**: Once a data acquisition session was completed, the data was processing started at the Blossom Point facility and then was completed offsite. First, the IMU/SDR/GNSS/UWB navigation solution was calculated, and then merged with the EMI measurement stream, so the standard EMI processing workflow could be used.
- **Performance evaluation**: Based on final results of data processing, comparison and statistical evaluation were performed using the target location and type reference information.

## 5.2 SITE PREPARATION

Three test sites were selected for the demonstration tests at the NRL's Blossom Point Facility. The first test site is a 14 × 27 m (46 × 89 ft.) open-sky area that allows for GNSS positioning. At this test site, GNSS/IMU solution was used as ground truth for assessing the accuracy and performance of the AGT system. The second and third test sites of an area of 18 × 10 m (59 × 33 ft.) were selected in a forested area. The data collected at these last two test sites provided the main data to demonstrate the AGT system performance for UXO detection in GNSS-challenged environment. The overview of test sites at the ARL - Blossom Point Facility is shown in Figure 12.

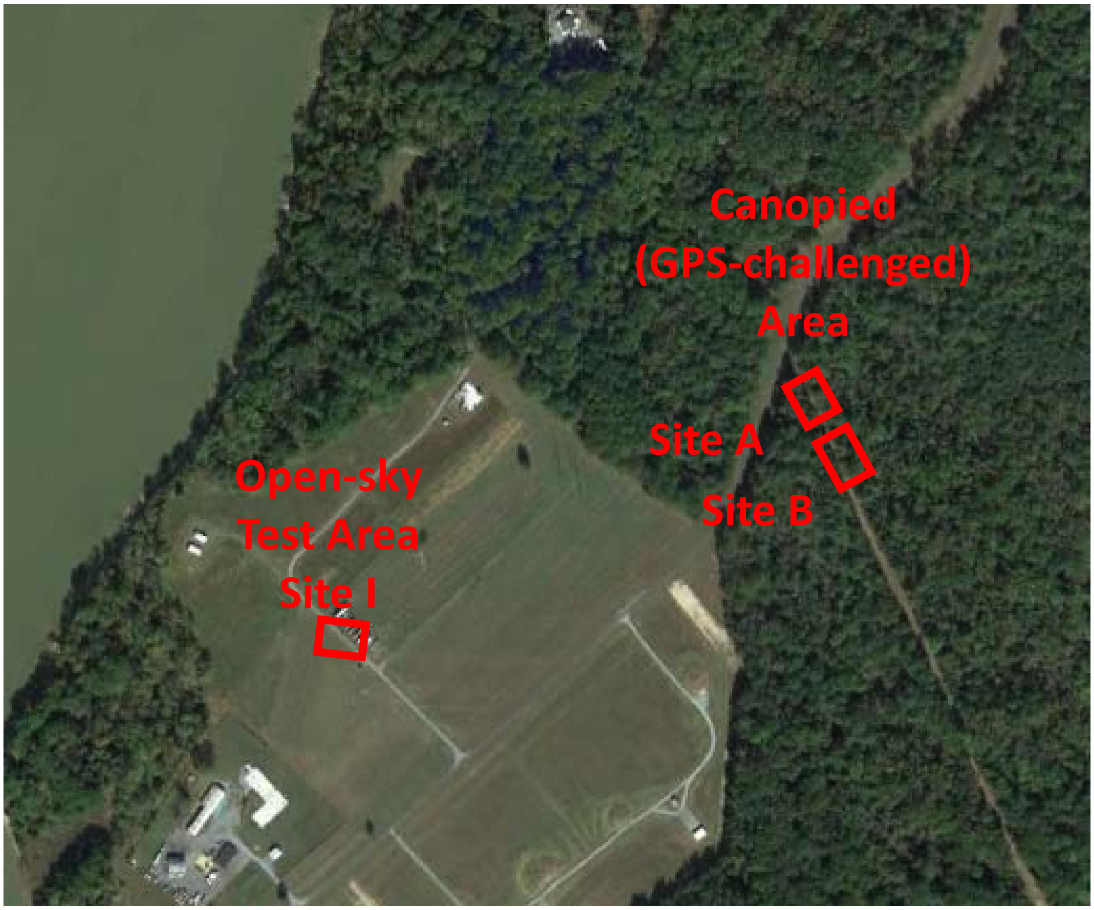


**Figure 12.  Test Sites at the ARL - Blossom Point Facility.**

The demonstration at the open-sky test site included two main steps:

> **Site preparation:** For the UWB network installation, the four poles, equipped with two UWB radios and one GNSS antenna, were installed at the corners of the area. All the four corner locations were measured by GNSS as well as total station. The second measurement was not needed, and it mainly served as a rehearsal and also as a check for the GNSS-based geolocation.
>
> **Open-sky data acquisition**: The data acquisition, including sensor function tests, replaced the standard IVS daily EMI QC checks, though the AGT system also collected data. This allowed for quality control and performance evaluation of the IMU/UWB system by comparing it to the IMU/GNSS reference solution. The tests were conducted in the beginning and end of each day. Note the GNSS on the UWB network poles were constantly recording, and the data served as base station observations for IMU/GPS integration.

The main demonstration took place at the canopied test site. The site preparation and data acquisition consisted of the following main steps:

**Site development:** The two approximately 18 × 10 m (59 × 33 ft.) test sites, referenced as A and B, were prepared by burying 24 blind targets by NRL personnel. The targets were buried about 2 inches below ground level. Since GNSS signal is blocked by trees around the test site, the position of the EMI sensor could be only derived from the IMU/UWB system. During the target emplacement process, the accurate target locations were measured by total station. To derive WGS84 and UTM (zone 18N) coordinates of the targets, the total station was georeferenced using control points, which were established in the nearby open area and measured by GNSS. The accuracy of the final target coordinates was estimated to be about 3-4 cm. These coordinates were used during the evaluation and target reacquisition. Note that the locations of the targets were not shared with the EMI data process (blind targets).

**Site preparation:** To establish the UWB network, poles with the UWB units were installed at the four corners of each test site. The poles were swapped between test sites as the measurements alternated between the two sites. At each time, when the poles were moved, the coordinates of the network nodes were measured with a total station. The coordinates were also converted to WGS84 using the control points, created during the site development.

**Data acquisition:** Several data acquisition sessions were carried out at the two test sites using the EMI and AGT system, 5-6 for Sites A and B.

**Target reacquisition**: In a real operating situation, the processed EMI data first detects and then using the geolocation solution estimates the possible UXO locations, which have to be marked ("stake-out") at the site for the excavation team. The goal of the target reacquisition was to assess the UWB system performance to stake out the target locations in the GNSS-challenged environment. The reacquisition test was based on using the reference data; the coordinates measured during the site development. This way, the reacquisition performance was accurately assessed. Note that this element of the testing was optional, and was carried out on the last day in a short time. Consequently, only the 12 targets buried at site B were reacquired, and the results analyzed.

### 5.2.1 Open-sky Area

The goal of the tests conducted at the open-sky area was to assess the AGT IMU/UWB system performance by comparing it to the reference IMU/GNSS solution. Additionally, the EMI system performance was quality controlled in a known environment. A typical IVS pattern of three objects was laid out on the surface in the test area. The installation of the UWB network and the survey of the UWB radios were the only preparations needed prior conducting EMI surveys. The UWB network poles were set up at the corners of the 14 × 27 m (46 × 89 ft.) area, see Figure 13. The stands of the poles were fixed to the ground by stakes. The positions of the UWB antennas were measured with total station by directly aiming at the antenna center. We used the total station in reflectorless mode which allowed measuring the distances without prism. In this mode, the distance measurement accuracy is about 5 mm. We also used the GNSS antennas attached to the poles to georeference the total station and compute the WGS84 coordinates of the antennas centers.

In addition, these static GNSS receivers were constantly recording during the data acquisition sessions in order to provide base station data for the IMU/GNSS integration.

**Figure 13. Open-sky Area with the Installed UWB Network.**

### 5.2.2 Canopied Area

Two, approximately 18 × 10 m (60 × 30 feet) test sites in close proximity to each other were prepared, see Figure 14, where 11 and 13 targets were buried at Sites A and B, respectively. The targets were buried about 2 inches below the ground, see Figure 15. The target locations could not be identified by sight after they were buried. The site preparation was made by NRL personnel. OSU personnel measured the locations of the seed ideas via total station. The coordinates of the targets were not shared with the EMI data analyst (blind targets).


**Figure 14. The Two 18 x 10 m (60 x 30 feet) Test Areas Marked by "A" and "B"; Red and White Circles Show UWB Network Nodes and Target Locations, Respectively.**

**Figure 15. Unburied Target.**

### 5.2.3 Surveying

The seed item locations were precisely measured by total station for the canopied area. The following surveying activities were performed:

1. Two control points were established around a nearby service road, located about 20 m from Site A, where GNSS signal reception was available, see Figure 16 and Figure 17. The two control points were observed by GNSS for approximately one hour. The RINEX data files were processed with OPUS. The GNSS measurement and processing allowed us to derive WGS84 and UTM coordinates of the control points at 0.5 inch (1-1.5 cm) accuracy. These control points were subsequently used to georeference the total station measurements for the Site A and B surveys later, see the red arrows in Figure 17.

2. The four corners of each of the two sites were marked with stakes, and measured with total station. Figure 17 shows the layout of the surveying, where the black arrows depict the measurements towards the stakes. The locations of the seed items were also measured after emplacement, but prior to being covered with soil during the site preparation phase. All total station measurements were performed with a prism (reflector mode) which allows for mm-level distance measurement. The target coordinates were determined in UTM projection; the accuracy of these coordinates is about 4 cm; this was due to the lack of clear reference point on the targets. These coordinates were used during the evaluation and target reacquisition.

3. The poles with UWB transmitters were installed at the stakes (at the four corners of Sites A and B). During the measurement sessions, the poles were several times swapped between the two test sites. Therefore, each time the poles were moved, the coordinates of the UWB network nodes (antennas) were measured again. The sketch of the survey layout is shown in Figure 18. First, the total station was georeferenced with measuring the angle and distance of two stakes at the opposite corners, using a prism, and then, the UWB antenna coordinates were measured by directly aiming the antenna phase center using the total station in reflector-less mode. The coordinates were always converted to the global reference frame using the UTM coordinates of the stakes measured in (2).

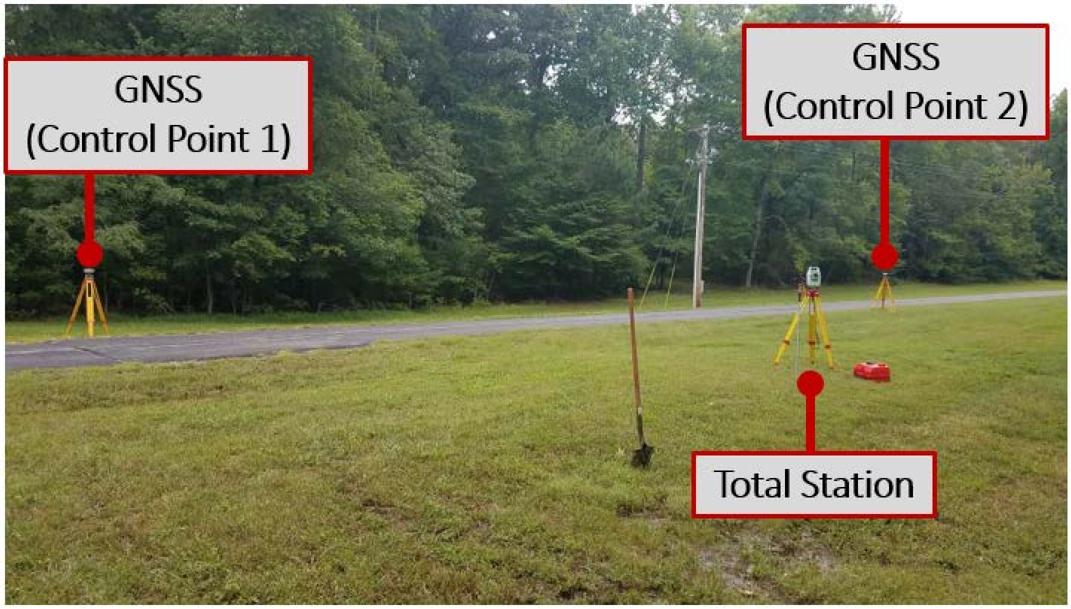


**Figure 16  Total Station Survey Setup.**

*Note the two tripods in the background equipped with GNSS receivers, which served as ground controls for tying the surveying to the global system.*

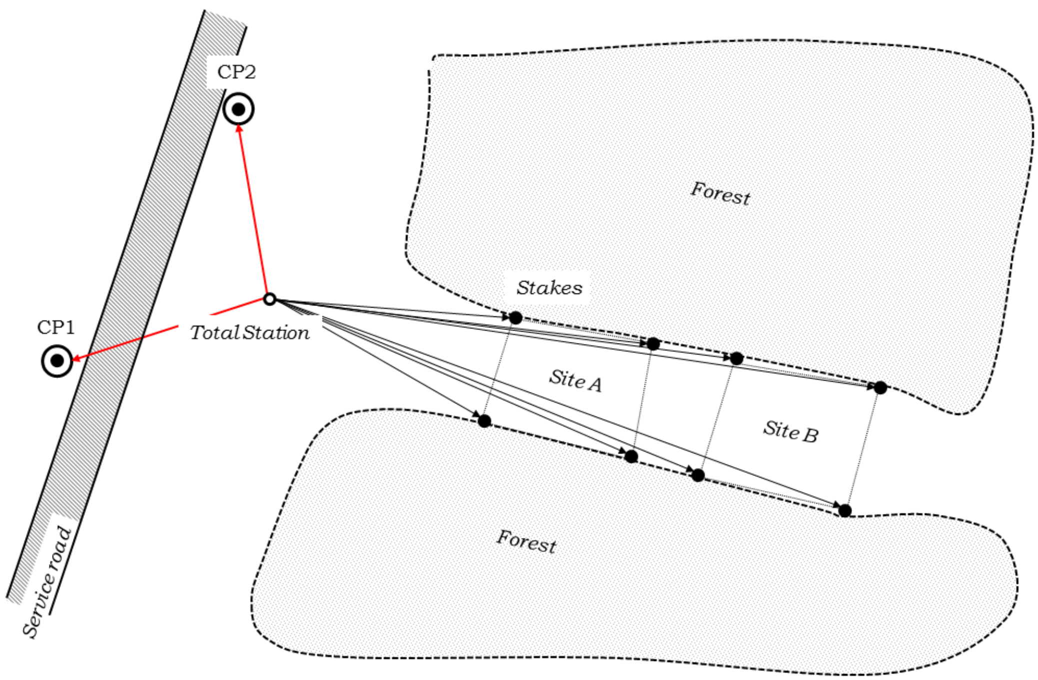


**Figure 17. Sketch of Surveying Layout for the Targets and Stakes.**

*Red arrows depict the measurements for total station georeferencing and black arrows are the measurements of points with unknown coordinates.*

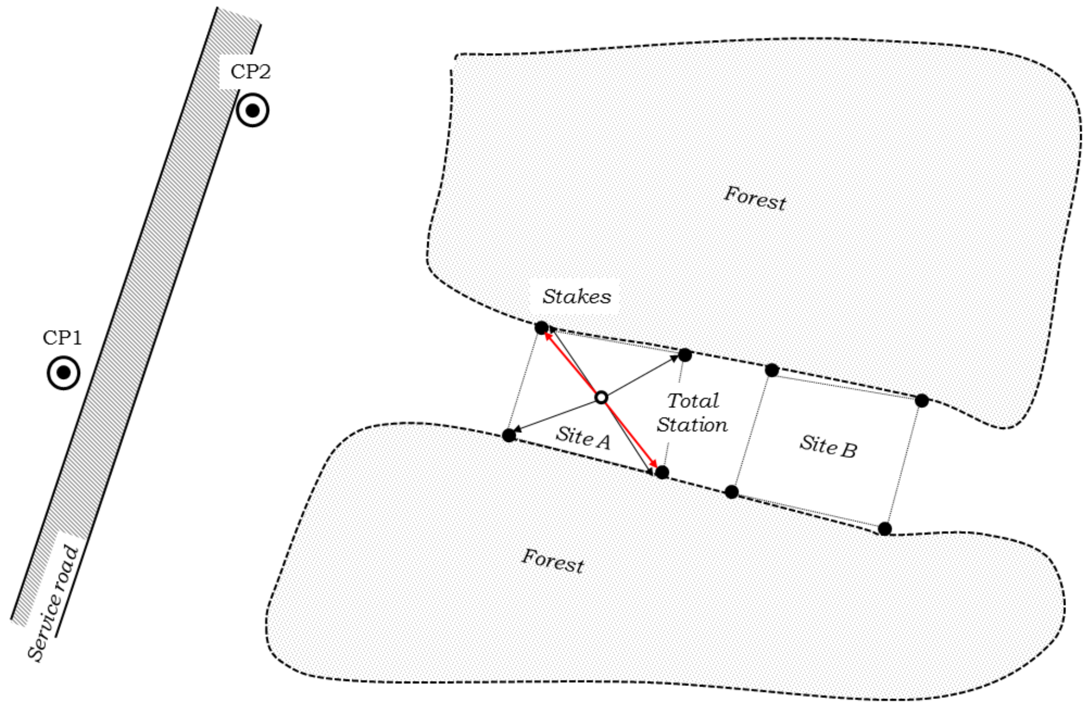


**Figure 18. Sketch of Surveying Layout for the UWB Network.**

*This survey was conducted every time after the network had been moved; red arrows depict the measurements for total station georeferencing and black arrows are the measurements of points with unknown coordinates.*

## 5.3 SYSTEM SPECIFICATION

The overview of the system used in the demonstration in 2018 is shown in Figure 11, here the main components are discussed.

### 5.3.1 TEMTADS 2x2

The TEMTADS 2x2 is a man-portable system comprised of four of the TEMTADS/3D EMI sensors arranged in a 2x2 array as shown in Figure 19. The orientation of the sensor cubes is also noted. The TEMTADS 2x2, shown in Figure 20 (left) at Fort Rucker, AL, is fabricated from PVC plastic and fiberglass. The center-to-center distance is 40 cm yielding an 80 cm x 80 cm array. The array is typically deployed on a set of wheels resulting in a sensor-to-ground offset of approximately 20 cm. The transmitter electronics and the data acquisition computer are mounted in the operator backpack, as shown in Figure 21 . The TEMTADS 2x2 can be operated in two modes; dynamic or survey mode and cued mode. A Global Positioning System (GPS) antenna and an inertial measurement unit (IMU) are mounted above the TEM array as shown in Figure 20 (right).

Data collection is controlled in dynamic mode using G&G Science's *EM3D* application suite, the same software that is used for the Geometrics MetalMapper systems. In cued mode, the locations of the anomalies must already be known and flagged for reacquisition. Custom software written by NRL provides cued data acquisition functionality, see left Figure 21

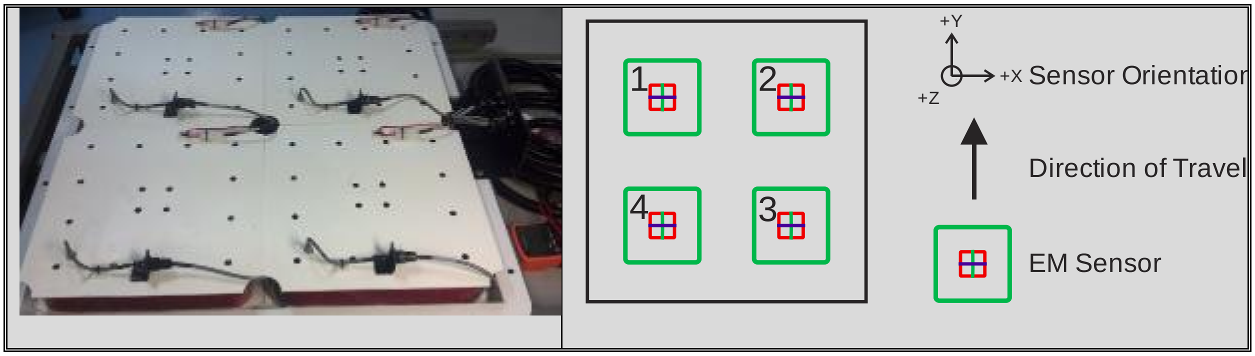


**Figure 19. TEMTADS/3D EMI Sensor Array with Weather Cover Removed (left). Sketch of the EMI Sensor Array Showing the Position of the Four Sensors (right).**

*The Tri-axial Revised EMI Sensors Are Shown Schematically. The Direction of Travel for the Array and the Orientation of the Sensor Cubes Are Indicated.*

**Figure 20. The NRL TEMTADS 2x2 (left) and TEMTADS 2x2 with GPS Antenna Tripod (right).**


**Figure 21. TEMTADS 2x2 Electronics Backpack (left); Screenshot of Cued Mode Interface (right).**

In dynamic mode, a series of lane markers (*e.g.*, beanbags) are placed over the survey area to provide a visual guide for maintaining lane spacing. Data are then collected to cover the area by pushing the TEMTADS 2x2 along the indicted lanes at a slow walking speed (0.75 m/s). The status of the TEM sensors is indicated on the operator screen. The operator is able to review positioning and orientation data for the platform during data collection.

In cued mode, the operators position the cart over each anomaly location in turn and collect a set of TEM data. Geolocation and cart orientation are monitored and recorded. Functionality to record field notes is provided. If anomaly flagging is unavailable or undesirable, it is possible to load a list of virtual flag locations into the vendor-provided survey controller for the GPS unit and use the provided interface for anomaly-to-anomaly navigation.

For this demonstration, the AGT's main GPS antenna feed will be amplified and broadcast to several GPS receivers, including the TEMTADS 2x2 standard RTK GPS receiver and the Trimble Thunderbolt E GPS timing receiver which synchronizes the EMI data acquisition electronics with the GPS 1PPS signal.

### 5.3.2 AGT System

The OSU AGT system contains four sensors, described below, and references are provided in Table 3.

**Novatel PwrPak7-E1** is an integrated navigation product from Novatel. Under the shell, the PwrPak7 contains the latest Novatel GPS OEM7 chipset that supports multiple GNSS constellations and frequencies. The product also allows for sustained data collection, as it has 4 GB memory storage capacity. Users can access to the data via Wi-Fi or USB communication. PwrPak7 support IMU data acquisition and recording; either by using a built-in Epson IMU or connecting to an external IMU sensor, such as the STIM300. The advantage of using an IMU/ GNSS product solution is that the time synchronization of the IMU and GNSS sensors is very reliable and accurate.

**Novatel SPAN-IGM-S1** and **STIM300** provide an interface between the STIM300 IMU and the PwrPak7 for seamless data collection and time synchronization. The STIM300 IMU is a small tactical grade IMU sensor. The specification of the IMU can be found in Table 1.

**PolaNt MC GNSS** antenna is manufactured by Septentrio, and supports all major GNSS signals and constellations.

**TimeDomain P440** and **P410** UWB units are members of the TimeDomain IR-UWB PulseOn radio family that constantly developed and improved during the time of the project. For the demonstration test, both the older P410 and the newer P440 models were used. The transmitters are self-contained for network formation, but the rover radio unit requires laptop connection via USB for data logging. An in-house developed logging software was used during the tests, as the original TimeDomain software interface did not support recording multiple range measurements. It is noteworthy that the latest interface does support this type of data collection; obviously, laptop connection is still required.

**Ettus Research USRP N200** SDR receiver, supported by a stable **GPS-2700/2750, Microsemi, Chip Scale Atomic Clock** is able to digitize the GNSS antenna signals. The data stream is logged in a dedicate laptop, as the data rate is high, about 18 MB/s.

**Table 3. AGT Sensor References.**

| Sensor | Website |
|---|---|
| Novatel PwrPak7-E1 receiver | https://www.novatel.com/products/span-gnss-inertial-systems/span-combined-systems/pwrpak7-e1/ |
| Novatel SPAN-IGM-S1 (STIM300) | https://www.novatel.com/products/span-gnss-inertial-systems/span-combined-systems/span-igm-s1/ |
| Sensonor STIM300 IMU sensor | https://www.sensonor.com/media/1132/ts1524r9-datasheet-stim300.pdf |
| PolaNt MC GNSS antenna | https://www.septentrio.com/products/antennas-field-controllers/antennas/polantmc |
| TimeDomain P440 and P410 UWB | https://www.humatics.com [1] |
| Ettus Research USRP N200 SDR | https://www.ettus.com/product/details/UN200-KIT |

Note that the OSU AGT system was significantly upgraded since the Integrated Shakedown Tests in 2016. The changes were motivated by the lessons learnt from that testing, and to some extent to advancement in sensing technologies. The major changes are:

- The Novatel OEM4 GPS receiver was replaced with a Novatel PwrPak7 GNSS receiver that can acquire data from all the current GNSS constellations, including GPS, COMPASS, Beidou, Galileo.

[1] TimeDomain was acquired by Humatics during the project.

- The Epson IMU has been replaced with an STIM300 IMU, representing about an order increase in performance, and improved time tagging capabilities.

- The pushcart configuration of the data logging subsystem was replaced by a backpack configuration.

The high-level system diagram with changes marked by red ellipses is shown in Figure 22. The navigation sensors installed on the EMI pushcart are shown in Figure 23. The Septentrio GNSS antenna signal cable is connected to a splitter installed on the AGT back. The four outgoing GNSS signals feed to the Novatel PwrPak7 GNSS receiver, the USRP N200 SDR receiver, the laptop interfaced with the UWB data recording (time-tagging), and then to the EMI system, where it serves two purposes: input to the local Trimble GPS receiver and then provides for time synchronization. The UWB transmitter is placed below the GNSS antenna in the forward direction, and is directly connected by a USB cable to the data logging laptop on the AGT backpack. Finally, the STIM300 IMU is mounted closer to EMI sensor in the backward direction, and similarly, the interface cable directly connects it to the PwrPak7 GNSS receiver on the AGT backpack.

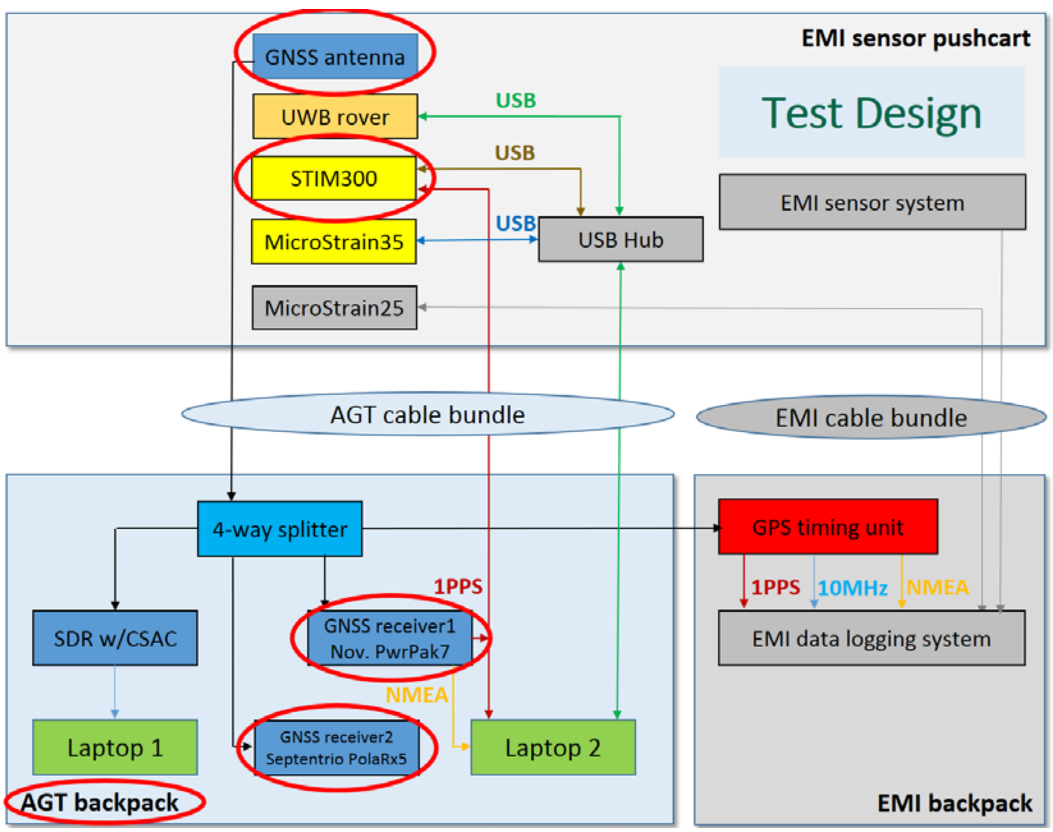


**Figure 22. System Configuration for the Live Site Demonstration in 2018.**

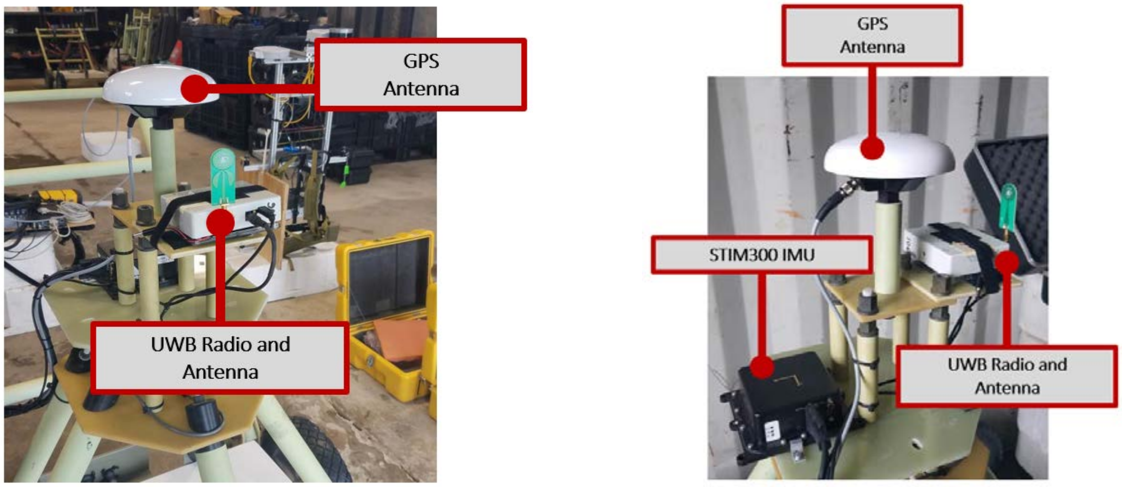


**(a)** **(b)**

**Figure 23. GNSS Antennas, UWB Transmitter and IMU Installed on the Pushcart.**

The spatial relationship of the navigation sensors is of high importance to achieve accurate sensor integration. Figure 24 presents the sensor arrangement and offsets, which can be measured at mm-level accuracy that is more than sufficient. The position of the GNSS and UWB antenna in the IMU frame was determined by tape measurements. Since the antennas are omnidirectional, there is no need to establish the rotational relationship of the sensors.

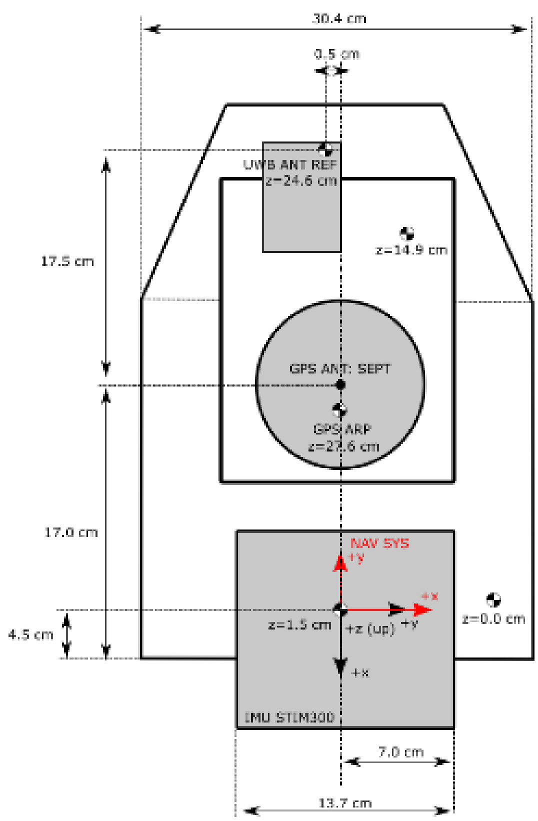


**Figure 24. Sensor Arrangement on the Pushcart; the Platform Coordinate System in Red.**

To form the UWB network, eight UWB transmitters were rigidly attached to four poles, see Figure 25. This construction allows for fast deployment and moving of the UWB network. Each pole was equipped with two UWB units. Based on our earlier tests, the optimal vertical location of the UWB units is at the top and lower third of the pole. This way, the vertical separation allows for better Z coordinate estimation of the rover and yet the signal absorbing effect of the ground is still less severe. A medium-sized battery provided power for the UWB units and for the GNSS receiver. Note that GNSS was only available for the open-sky test area. After the poles were installed at a site, their positions had to be measured. The positions were obtained from long GNSS observations in open-sky areas, and were surveyed with total station in canopied areas.

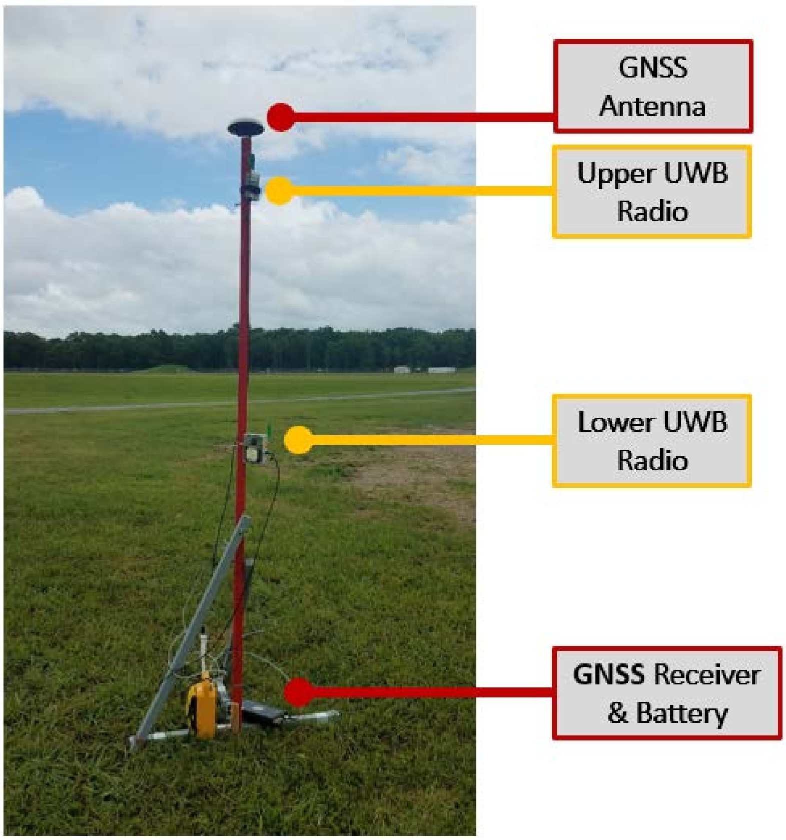


**Figure 25. Pole Configuration with Two UWB Units, GNSS Antenna and Receiver.**

*Note that GNSS is optional and was only used for open-sky area tests.*

## 5.4 QUALTIY CONTROL ACTIVITIES

Given the complicated nature of interpreting multi-static TEM data from systems like the TEMTADS 2x2, a common question is "How can I tell the system is working?" To help answer that question, a Sensor Function Test functionality was implemented for the TEMTADS 2x2's standard data acquisition software. This test allows the operator to get a non-ambiguous, first-order Yes/No answer for this question. There still remain a large number of caveats that must be explored by the QC data analysis chain. Since dynamic and cued data collection use different data acquisition parameters, this test should be run for each relevant set of conditions.

In preparation for each sensor function test, the operator uses the [Setup] tab in *TEM DataLogger* or *TEM Tablet* applications to set the correct data acquisition parameters for the survey planned. The easiest way to accomplish this is to use the [Standard Cued] or [Standard Dynamic] buttons, Figure 26. The standard parameters are listed in Table 4.

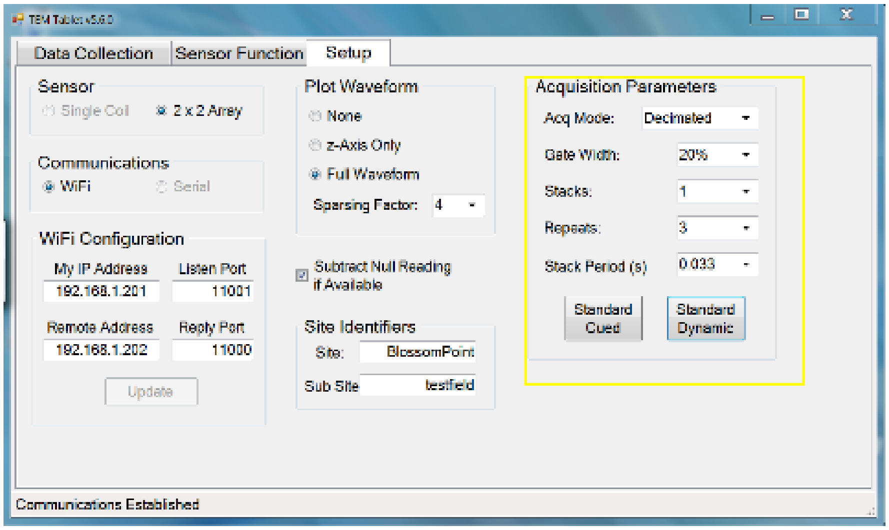


**Figure 26. Standard Acquisition Parameters for Dynamic Surveys.**

**Table 4. Standard Data Acquisition Parameters.**

| Parameter | Cued Survey | Dynamic Survey |
|---|---|---|
| Acquisition Mode | Decimated | Decimated |
| Gate Width | 5% | 20% |
| Stacks | 18 | 1 |
| Repeats | 9 | 3 |
| Stack Period | 0.9 | 0.033 |
| Hold Off Time | 50 µs | 50 µs |

The sensor function test compares the background-subtracted TEM response for a known target against a reference response recorded with the same combination of hardware and data acquisition parameters. To conduct a sensor function test, the operator positions the sensor in a spot known to be clear of buried metal collects a background measurement from [Sensor Function] tab of the data acquisition software by pressing the “Collect Null” button. The data acquisition cycle will commence and when completed, the display will look similar to the one shown in Figure 27. Without moving the sensor, the operator places the chosen test item in same location as was used for the reference measurement. For example, the small ISO80 shown in Figure 28 (right) is placed in the hole on the top of the sensor housing.

The operator then collects the sensor function data by pressing the “Sensor Function” button, shown highlighted in Figure 27. If the results agree with the reference values, a green LED is displayed as shown in Figure 28 (upper right). If they do not agree, a red LED is displayed and a summary of the incorrect results is displayed as shown in Figure 28 (lower right).

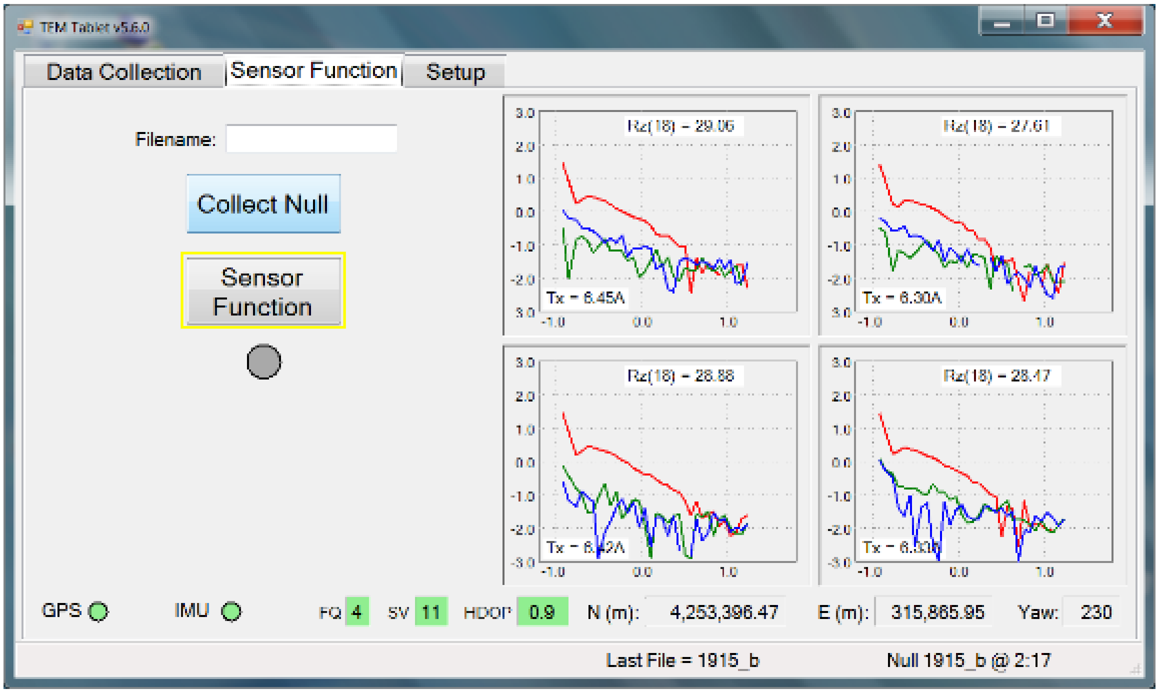


**Figure 27. TEM Tablet Sensor Function Tab, Ready to Conduct a Sensor Function Test.**

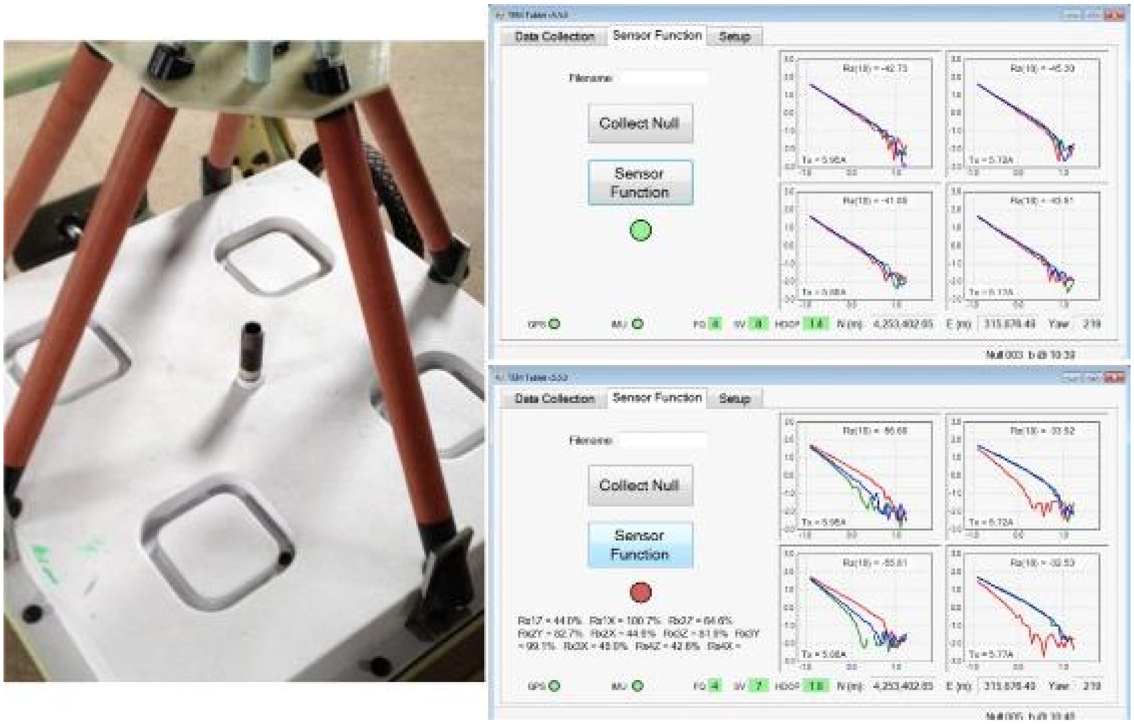

**Figure 28. Test Item Positioned for a Sensor Function Test (Left Panel) and Examples of the Test Results (Right Panels).**

For the TEMTADS 2x2 system integrated with the AGT, a different version of the National Instruments data acquisition hardware is required to perform the synchronization to the GPS 1PPS pulse, which is incompatible with the standard TEMTADS 2x2 TEM_DataLogger software. The SFT functionality was provided using IDL routines developed from the standard analysis used by the TEM_Datalogger and UX-Analyze software packages.

The AGT system requires no specific calibration besides routine power-on check in open-sky condition, including GNSS signal reception and logging, IMU recording integrity check, UWB positioning check, and SDR logging check. These checks assure that GNSS signals and timing are provided to the sensors and all data streams are properly recorded.

## 5.5 DATA COLLECTION PROCEDURES

### 5.5.1 Scale of Demonstration

The OSU NRL team conducted about 20 EMI/AGT measurement surveys in the open-sky and GNSS-challenged environment. The focus of the testing was the two about 18 m x 10 m canopied sites, where two dozen munitions surrogates (sISO80) were emplaced in the area prior to the demonstration. Table 5 lists the data collection sessions. The EMI sensor was quality controlled for proper operation at the beginning and end of each day in the open-sky test area, tagged with "I" in the table. The AGT system is not used for all "I" sessions, as indicated in the last column of the table. All the other sessions were conducted at the canopied Sites A and B. For repeatability assessment, two consecutive data collections were performed at each site before moving the UWB network and pushcart to the other site. Purposely, the platform's moving direction was different between these consecutive tests.

The standard procedure during EMI data collection was that the pushcart moved over the investigation area along parallel lines. The pushcart turned back at the end of each line, after stopping data acquisition for the current line and starting it again for the next line. Figure 29 shows the schematic pattern of the pushcart's trajectory. Note that the figure is not scaled for the sake of visualization, as in reality the parallel lines were only separated by 40-50 cm. At the beginning and end of each session, the platform was stationary for 1-2 min that allowed for static alignment of the IMU sensor. Following standard recommendations, the initial heading of the platform at each start and end was logged for using as initial value for the processing software. Note that the heading can be easily obtained with the required 10-degree accuracy using mobile phone apps or simple mechanical compass. Figure 30 and Figure 31 show photos of the data acquisition sessions, conducted at the open-sky and canopied areas, respectively. Figure 32 shows sample platform trajectories from open-sky and canopied areas.

The production rate was six sessions per day during the demonstration tests, which was better than planned, as the demonstration plan called for four missions per day. Furthermore, this rate can be probably further improved for an experienced field crew.

**Table 5. Data Acquisition Sessions.**

| Date | Session | Area | Start time | End time | Duration | AGT |
|---|---|---|---|---|---|---|
| 07/23/2018 | I1 | Open-sky | 13:12 | 13:32 | 0:20 | Yes |
| 07/24/2018 | I2 | Open-sky | 9:50 | 10:04 | 0:14 | No |
| 07/24/2018 | A1 | Canopied | 11:45 | 12:35 | 0:50 | Yes |
| 07/24/2018 | A2 | Canopied | 13:16 | 13:47 | 0:31 | No |
| 07/24/2018 | B1 | Canopied | 14:58 | 15:20 | 0:22 | No |
| 07/24/2018 | B2 | Canopied | 15:20 | 15:47 | 0:27 | No |
| 07/24/2018 | I3 | Open-sky | 15:57 | 16:07 | 0:10 | No |
| 07/25/2018 | I4 | Open-sky | 8:10 | 8:21 | 0:11 | No |
| 07/25/2018 | A3 | Canopied | 8:46 | 9:10 | 0:24 | Yes |
| 07/25/2018 | A4 | Canopied | 9:11 | 9:40 | 0:29 | Yes |
| 07/25/2018 | B3 | Canopied | 9:41 | 9:52 | 0:11 | Yes |
| 07/25/2018 | B4 | Canopied | 11:18 | 12:14 | 0:56 | Yes |
| 07/25/2018 | I5 | Open-sky | 13:55 | 14:12 | 0:17 | Yes |
| 07/26/2018 | I6 | Open-sky | 10:05 | 10:31 | 0:26 | No |
| 07/26/2018 | A5 | Canopied | 11:05 | 11:35 | 0:30 | Yes |
| 07/26/2018 | B5 | Canopied | 12:15 | 12:38 | 0:23 | Yes |
| 07/26/2018 | B6 | Canopied | 12:38 | 13:15 | 0:37 | Yes |
| 07/26/2018 | Reacquisition | Canopied | 14:11 | 14:40 | 0:29 | Yes |
| 07/26/2018 | I7 | Open-sky | 15:11 | 15:26 | 0:15 | No |

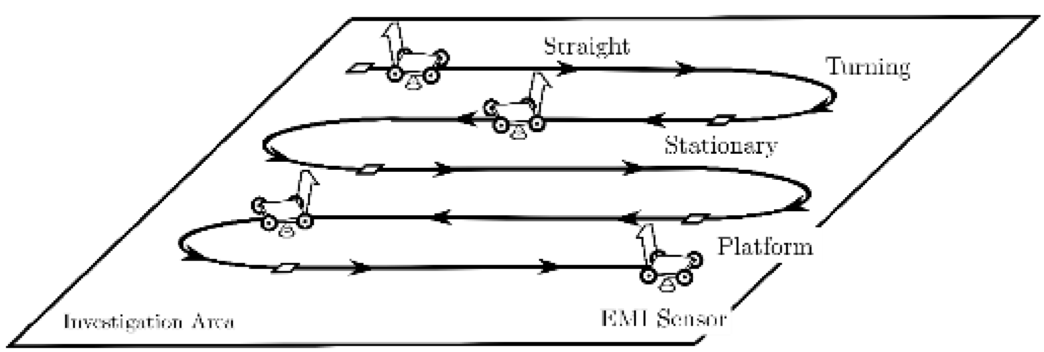


**Figure 29. Data Collection Pattern at the Demonstration.**

**Figure 30. Data Acquisition at the Open-sky Area.**

**Figure 31. Data Acquisition at the Canopied Area.**

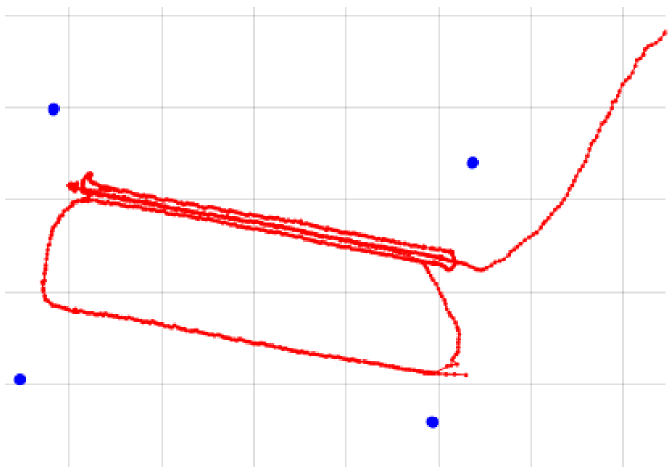

**(a) open-sky area**

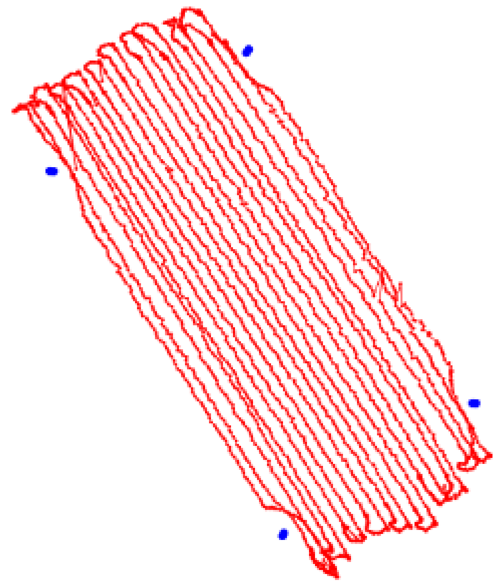

**(b) canopied area**

**Figure 32. Typical Pattern of the Pushcart Trajectory for (a) Open-sky and (b) Canopied Site Tests.**

*UWB network nodes are depicted by blue dots.*

### 5.5.2 Sample Density

The EMI data spacing for the TEMTADS 2x2 in dynamic mode was typically less than 50 cm along track and less than 70 cm cross track between successive measurements. Exceptions were made for avoidance of obstacles. The sensor streams were acquired at different data rates, see Table 6. Considering the low dynamics of the TEMTADS platform, the GNSS signals was acquired at 5 Hz and UWB operated at 30 Hz polling rate. Note that the rover UWB radio can measure ranges at 30 Hz, and since eight network nodes are used, the rate to acquire all the eight ranges is 30/8 Hz, resulting in a positioning frequency of 3.75 Hz. The IMU operated at 125 Hz; clearly, above the required sampling rate.

**Table 6. Sensor Data Rates.**

| Sensor | Data rates |
|---|---|
| PwrPak7-E1 GNSS receiver | 5 Hz |
| STIM300 IMU sensor | 125 Hz |
| TimeDomain's UWB (one range) | 30 Hz |
| Ettus Research USRP N200 SDR receiver | 1575.42 MHz |

### 5.5.3 Quality Checks

Preventative maintenance inspections were conducted at least once a day by all team members, focusing particularly on the sensor cart and cabling. The AGT system was checked for connections, such as antenna and interface cabling, and then data acquisition was checked every time the system was powered on. This was straightforward and quick, as each sensor has monitoring tools available on the data logging laptops. No hardware problems occurred during the demonstration tests in 2018.

For the TEMTADS 2x2 operating in dynamic mode, the data QC process was applied to lines of data rather than single data points. The TEM response for data points associated with both background locations and over targets were inspected for reasonable values and variation. A TEM data profile along survey line is shown in Figure 33. The recorded transmitter current for each transmit period was inspected to insure a good transmit cycle. A transmitter misfire typically did not reach the average peak value and had a non-standard waveform. An example is shown in Figure 34, where transmitter Tx2 misfired. As this demonstration was intentionally being conducted in a GNSS-challenged area, the GNSS and IMU status was monitored, though poor conditions for either TEMTADS 2x2-specific systems did not stop data collection nor invalidate collected EMI data.

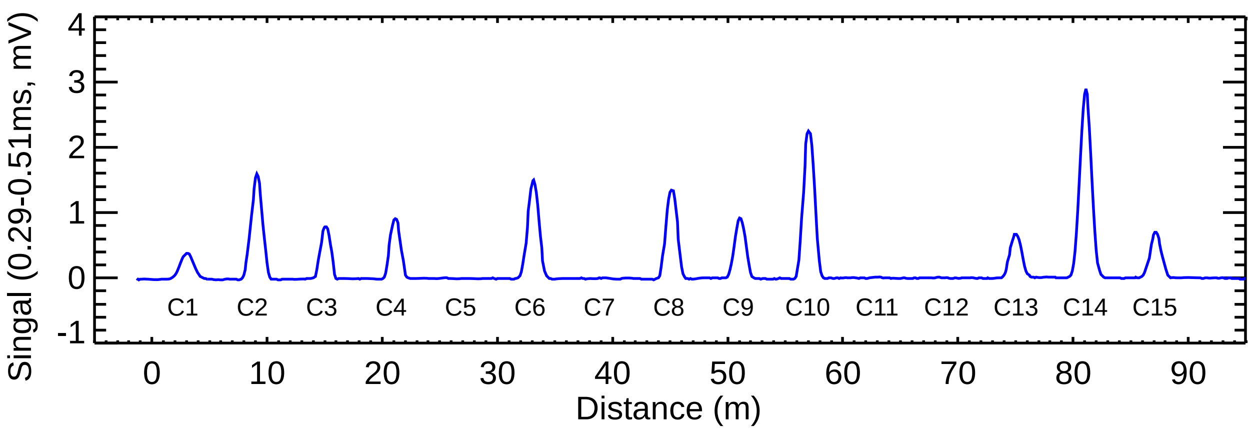


**Figure 33. TEMTADS 2x2 System TEM Data Profile Along a Survey Line Over Line C in the NRL Blossom Point Test Field.**

*The signal is the sum of the monostatic TEM decays for all four sensors summed over the time bins centered from 0.29 to 0.51 msec.*

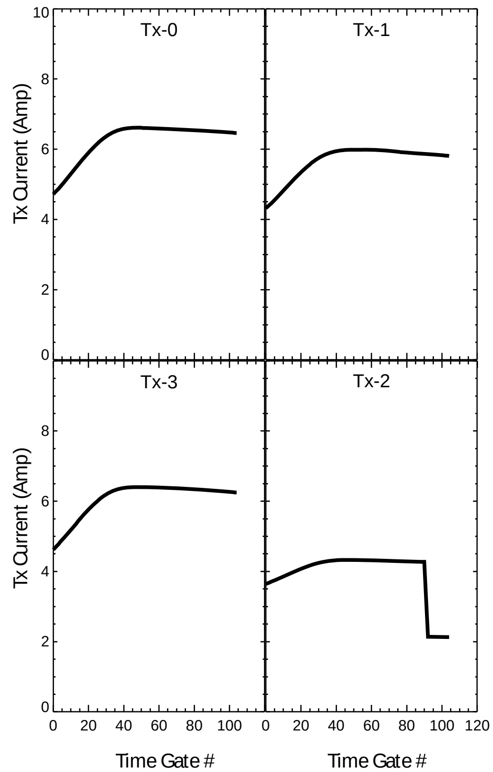


**Figure 34. TEMTADS 2x2 Transmit Current Waveforms for a Bad Transmit Cycle.**

*In this case, transmitter Tx2 misfired.*

During data acquisition, the QC process of the AGT system mainly included frequent data checks on the recorded data streams, including:

- stability of UWB range measurements
- continuity of the IMU measurements
- observed satellites for GNSS and SDR (not a check rather monitoring data availability)
- interference check between the AGT and EMI modules

These checks were periodically done during data acquisition, and if any of the checks failed, the data acquisition was stopped until the issue was resolved. No serious problem occurred during the surveys, except for running out of disk space on the laptops that were quickly corrected by downloading the data to free up space.

### 5.5.4 Data Handling

TEMTADS data were stored electronically as collected on the backpack data acquisition computer hard drive. Approximately every two survey hours, the collected data were copied onto removable media. At least once daily, the data was transferred to the data analyst for QC/analysis. Raw data and analysis results were backed up from the data analyst's computer to external hard disks daily. These results were archived on an internal file servers at OSU and NRL at the end of the survey.

Examples of the TEMTADS file formats are provided in Appendix C of Reference 21. All field notes / activity logs are written in ink and stored in archival laboratory notebooks. These notebooks are archived at OSU and NRL. Relevant sections are reproduced in demonstration reports. Dr. Charles Toth was the Point of Contact (POC) for obtaining data and other information. His contact information is provided in Appendix B of this report.

## 5.6 VALIDATION

At the conclusion of data collection activities, the recovered positions of all detected anomalies were compared to the firewalled ground truth. These results were used to validate the objectives listed in Section 3. The buried target location in UTM Zone 18N coordinate system, the reference, are listed in Table 7.

There was one reacquisition session with the goal to assess the AGT system capability to flag any given location on the ground, such targets' position provided by the EMI processing. Note that accurate staking out the target locations identified by the EMI processing is essential for the excavation work. Since during the testing, there was no time to process data, we used the coordinates of the targets measured during the site preparation. Consequently, this approach provided a better assessment for the positioning accuracy, as the reference was very accurate; the EMI processing may have introduce location error. During the reacquisition session, the targets were still buried, and thus, the operator could not see the physical location of the targets. The target locations were flagged based on the UWB measurements, and then subsequently, excavated, see Figure 35. The difference of the flag and the target center is measured by surveying tape.

**Figure 35. Target Locations Flagged after Reacquisition.**

**Table 7. Coordinates of Target Locations.**

| Site | Target ID | UTM Zone 18N | | Ellipsoidal Height |
|---|---|---|---|---|
| | | X [m] | Y [m] | (WGS84) [m] |
| A | 1 | 316709.957 | 4254560.067 | -28.195 |
| A | 2 | 316713.605 | 4254559.720 | -28.256 |
| A | 3 | 316712.491 | 4254557.399 | -28.126 |
| A | 4 | 316715.960 | 4254558.516 | -28.368 |
| A | 5 | 316710.766 | 4254554.817 | -28.195 |
| A | 6 | 316712.475 | 4254551.522 | -28.198 |
| A | 7 | 316717.107 | 4254554.046 | -28.185 |
| A | 8 | 316716.817 | 4254551.169 | -28.147 |
| A | 9 | 316715.634 | 4254549.825 | -28.134 |
| A | 10 | 316720.717 | 4254548.363 | -28.280 |
| A | 11 | 316718.282 | 4254546.180 | -28.223 |
| B | 1 | 316723.827 | 4254537.097 | -28.412 |
| B | 2 | 316728.778 | 4254540.176 | -28.661 |
| B | 3 | 316727.429 | 4254537.862 | -28.465 |
| B | 4 | 316726.100 | 4254535.515 | -28.467 |
| B | 5 | 316723.444 | 4254533.298 | -28.520 |
| B | 6 | 316731.073 | 4254535.862 | -28.652 |
| B | 7 | 316730.010 | 4254532.442 | -28.495 |
| B | 8 | 316727.755 | 4254529.336 | -28.541 |
| B | 9 | 316733.043 | 4254530.606 | -28.538 |
| B | 10 | 316728.751 | 4254525.120 | -28.580 |
| B | 11 | 316735.374 | 4254528.835 | -28.686 |
| B | 12 | 316733.162 | 4254526.707 | -28.505 |
| B | 13 | 316732.450 | 4254523.162 | -28.576 |

*Page Intentionally Left Blank*

# 6.0 DATA ANALYSIS AND PRODUCTS

## 6.1 PREPROCESSING

The AGT system recorded multiple data streams, including GNSS, SDR, IMU and UWB data, which were processed in several steps. In addition, geodetic surveying was done prior to the data collection sessions to provide ground control and reference for the precise performance evaluation of the entire system. The AGT system produced files with format description are listed in Table 8.

**Table 8. File Formats of AGT Data Streams.**

| Data stream | Format | File type | Format type |
|---|---|---|---|
| GNSS and IMU | Novatel's internal (*.LOG) | binary | raw |
| GNSS extracted | RINEX (*.*O, *.*N) | text | converted |
| IMU extracted | CSV (*.csv) | text | converted |
| SDR | Software internal (*.DAT) | binary | raw |
| UWB | Text (*.txt) | text | raw |
| UWB Time Synch | Text (*.txt) | text | raw |
| Total Station | Text (*.txt) | text | raw |

### 6.1.1 Ground Control Surveying

In both areas, two temporary geodetic reference points were established by long-term GNSS measurements. At each point, GNSS receivers acquired about two-hour long observations, and the RINEX files were processed by the NGS OPUS service (https://www.ngs.noaa.gov/OPUS/). The reported accuracy is 2-3 cm. OPUS provides the WGS84 and UTM 18N coordinates of the control points. Using the two control points at each site, total station measurements provided the coordinates of the corner stakes for the three sites with the help of Helmert transformation, see Equation 5.1. The four corner stakes at each site stayed in position for the entire duration of the testing, and were used as reference to locate the UWB antennas.

The poles with the UWB radios were generally deployed before each measurement session, and the location of the UWB antennas, two per pole, was measured by total station with respect to the corner stakes. The conversion between the local horizontal coordinates and UTM 18N was computed with a 2D Helmert transformation using the corner stakes as control:

$$\text{minimize} \sum_{i=1}^{n} \left\| \begin{bmatrix} cos\alpha & -sin\alpha \\ sin\alpha & cos\alpha \end{bmatrix} \begin{bmatrix} x_{i,l} \\ y_{i,l} \end{bmatrix} + \begin{bmatrix} \Delta x \\ \Delta y \end{bmatrix} - \begin{bmatrix} x_{i,UTM} \\ y_{i,UTM} \end{bmatrix} \right\|_2 \tag{5.1}$$

where $x_{i,l}, y_{i,l}$ are coordinates in the local, and $x_{i,UTM}, y_{i,UTM}$ are coordinates in the UTM system, and the unknowns are the $\alpha$ the rotation angle and $\Delta x$, $\Delta$y translations between the two systems. Two control points, i.e., $n = 2$, are used in the transformation computation, and because the 2D Helmert transform has three unknowns, the transformation has one extra observation that allows for assessing the accuracy. These accuracies for each session are presented in Table 9.

The conversion of the vertical component is a simple translation between the two coordinate systems. Since two control points are known, there is also an extra observation allowing for estimating the error in the vertical transformation, see Table 9. The coordinate conversion between the local and UTM system is an optional step, because horizontal coordinates might be sufficient to identify possible target locations in the field.

**Table 9. Accuracy of the Transformation Between Local and UTM Coordinate Systems.**

| Session | Horizontal error [cm] | Vertical error [cm] |
|---|---|---|
| I1 | 1.5 | 8.6 |
| A1 | 2.7 | 5.3 |
| A2 | 5.4 | 0.2 |
| B1, B2 | 3.7 | 2.6 |
| A3, A4 | 4.7 | 0.5 |
| B3, B4 | 0.1 | 0.1 |
| I5 | 1.8 | 2.2 |
| A5 | 0.8 | 5.6 |
| B5, B6, Reacquisition | 0.0 | 0.2 |

### 6.1.2 UWB Positioning

The UWB transmitters are not synchronized; i.e., their clocks run independently from each other, and therefore, they use two-way TOF measurement approach to eliminate the clock error. This means that in any application when they are used for range measurement, time-tagging is required, as otherwise their measurements cannot be integrated to other sensor data, such as IMU measurements. The AGT UWB logging software uses the CPU time to tag the range records. Since GPS time is used predominantly for time synchronization for sensor streams, the CPU time must be connected to GPS time to convert the UWB time records to GPS time-tags. Therefore, PPS and NMEA signal from the GNSS receiver is sent to the UWB logging laptop and are stored along with the CPU time during the data acquisition. The logged data, GPS PPS and NMEA signals logged by the CPU time, allows for calculating the offset and drift between the CPU time and GPS time basis. Once the parameters are estimated, interpolation can be used to compute the GPS time-tag for all the UWB records, see Figure 43.

The EMI/AGT pushcart platform positions in the UWB network were computed based on the method discussed in Section 2.1.2 that can be done regardless of the time records used. In our implementation, the GPS time-tagged UWB data was used for the trajectory computation. Next the local UWB coordinates were converted to UTM 18N coordinates, as described above. In the final step, using Matlab code, the plain text trajectory data was formatted to Novatel PVA format that is required for sensor integration by the Waypoint software. During the processing, the lever-arm correction was applied, so the UWB trajectory solution was reduced to the IMU origin. IMU/UWB Integration

The Novatel Waypoint software is a widely used commercial navigation/georeferencing processing software that supports both loosely and tightly coupled IMU/GNSS integration. A screenshot of the user interface can be seen in Figure 38. The software allows for using other position updates, but only for loosely coupled integration. This software was used to derive integrated IMU\UWB navigation solution. The Waypoint allows for using other position updates in the loosely coupled integration, which approach was used to derive the integrated IMU/UWB trajectory solutions for all the measurement surveys.

During the processing, first, the logged binary IMU data stored in the Novatel receiver is imported to the Waypoint software. Then, the settings for the loosely coupled integration was specified, see left side of Figure 36, and the PVA file with UWB positions were provided, see right side of Figure 36. The loosely coupled integration requires about 1-2 minute initialization for static alignment of the IMU at the beginning and at the end of the survey. During initialization time intervals, the platform has to be static in order to allow the software to correctly initialize the heading of the platform. To facilitate easier initialization, an initial value of the heading with about better than 10º accuracy was provided in all sessions. These stationary periods and initial heading could be obtained by analyzing the UWB trajectory. Obviously, it is advisable that the initialization intervals are applied and logged on the field in any future measurements. Note that the initial heading of the platform might be also observed and recorded using a simple mobile app or compass, and this method was used a few times in the 2018 tests. We emphasize that proper static alignment is essential to achieve the required accuracy when using loosely coupled integration. Figure 37 shows the dialog windows where these settings are configured in Waypoint.

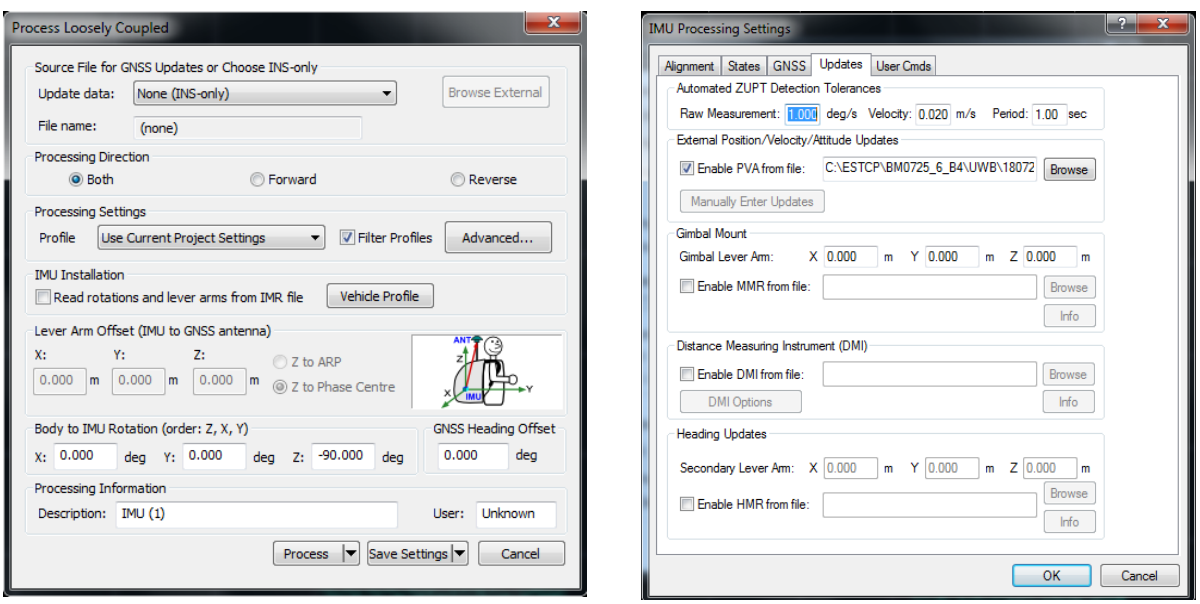


**Figure 36. Settings for the Loosely Coupled Integration (left) and Specifying the PVA File (right) in the Waypoint User Interface.**

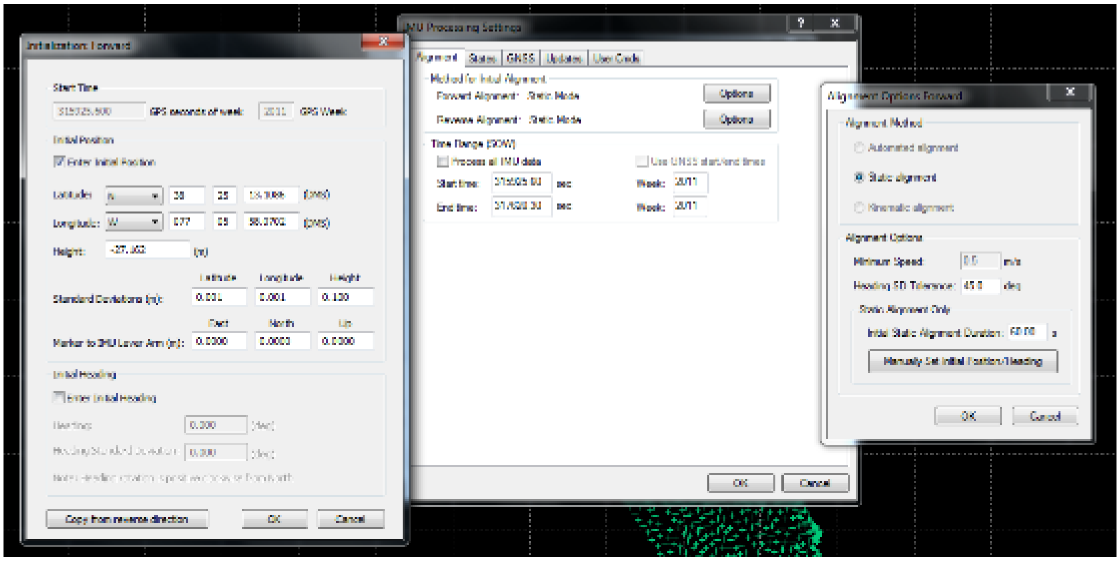

**Figure 37. Static Alignment Settings, Initial Coordinates (left), Dynamic Data Time Range (middle) and Static Time Interval (right)**

To obtain the highest accuracy possible, forward and backward loosely coupled integrated navigation solutions were computed and then combined, resulting in a smooth trajectory solution. It is noteworthy that this smoothed solution was not available for all sessions due to the lack of static initialization, and thus, the trajectory solution failed either for the forward or backward solution. In such cases, only one direction was computed. After completing the loosely coupled integration, the solutions were visually evaluated based on the height and heading profiles. Finally, the navigation solution is exported as a text file. Figure 38 shows a trajectory solution for session B4, where green indicating a consistently high accuracy.

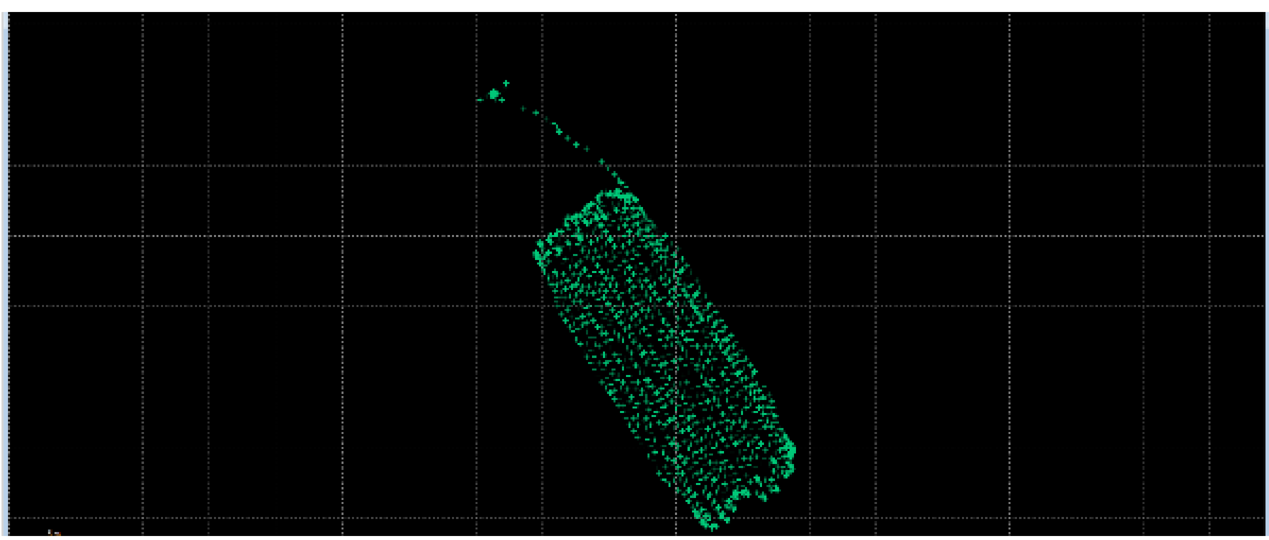

**Figure 38. Screenshot from the Waypoint Software with a Calculated Trajectory.**

### 6.1.3 Open-sky Reference Trajectory Computation

The computation of the open-sky reference trajectory followed the standard GNSS and IMU integration process. There were multiple GNSS base station data streams available from the receivers operating parallel at the geodetic control points and then on the poles used for the UWB sensors. The GNSS and IMU data processing is a basic capability of the Novatel SPAN software, and requires the RINEX format GNSS file and the IMU in the native logging format. The lever-arm was entered during configuration, and the smoothed solution was obtained based on forward and backward trajectory computation. Note that using tightly coupled integration, the Waypoint software is able to exploit dynamic alignment better, and therefore, initialization period may not be required. While this solution was tested for some sessions, the results in quality were similar to the loose integration model, so only the later ones were used for analyses. Given the ideal environment, good GNSS signal reception, the difference between tight and loose integration is expected to be negligible. The overall accuracy of the IMU/GNSS solution in the open-sky area was 1-2 cm per coordinate and 0.3-0.8° in attitude. Note that these are internally estimated performance numbers.

### 6.1.4 EMI Data Preprocessing

Preprocessing and quality control of the EMI data were conducted using IDL routines developed during the first demonstration to connect AGT-derived positions to the individual EMI sensor readings. The standard processing workflow found in Oasis montaj was used to grid and map the results.

The TEMTADS 2x2 has four sensor elements, each comprised of a transmitter coil and a triaxial receiver cube. For each transmit pulse, the responses at all of the receivers are recorded. This results in 48 possible transmitter/receiver combinations in the data set (4 transmitters x 4 receiver cubes x 3 receiver axes). In dynamic mode the data acquisition system records the signal over 19 logarithmically-spaced time gates, the measured responses over the first 5 gates including distortions due to transmitter ringing and related artifacts and are discarded. We further subtract 0.028 ms from the nominal gate times to account for time delay due to effects of the receive coil and electronics [20]. The delay was determined empirically by comparing measured responses for test spheres with theory. This leaves 14 gates spaced logarithmically between 0.109 ms and 2.472 ms. In preprocessing, the recorded signals are normalized by the peak transmitter current to account for any variation in the transmitter output. On average, the peak transmitter current is approximately 6 Amps.

The raw data files (*.tem) were converted to an ASCII format (*.csv) using built-in functionality of the EM3D software package used to collect dynamic data. This format was then imported into IDL and stored in an IDL save set. The data were then subjected to a QC assessment, in particular for the following were typically evaluated:

1. Transmit (Tx) current within limits
2. EMI response signal not saturated
3. Other data QC metrics such as unusual timing gaps

Data measurements that did not pass QC were flagged for no further use, but maintained for auditability. The OSU team then provided the AGT post-processed locations using the common GPS-clock time stamp.

The background response of the geology and the self-response of the system was modeled and subtracted from the data line by line. A site-specific de-median filter was applied to the raw monostatic, Z-component data to derive an estimate of the background model. This model was subtracted from the raw data to provide a background removed or “leveled” data set.

The AGT-updated data set was then exported as .csv file for import into Oasis montaj for mapping and target selection.

## 6.2 TARGET SELECTION FOR DETECTION

A similar anomaly detection procedure as the one described in [21] was used using the standard Oasis montaj tools. A preliminary detection threshold was selected based on the final burial depths of the munitions surrogates used. As the goals of this demonstration were not to exercise the detection limits of the TEMTADS 2x2, the surrogates were placed so as to allow robust detection (buried at about 2 in depth). A threshold of 1.5 mV/A (Gate 6) was selected as representative of a sISO80 buried horizontally at 30 cm. The site-specific background signal level was also considered and determined to be 0.3 mV/A. Two sub grids, free of anomalies were selected in both Sites A and B, shown in Figure 39. The results from each data set are shown in Table 10.

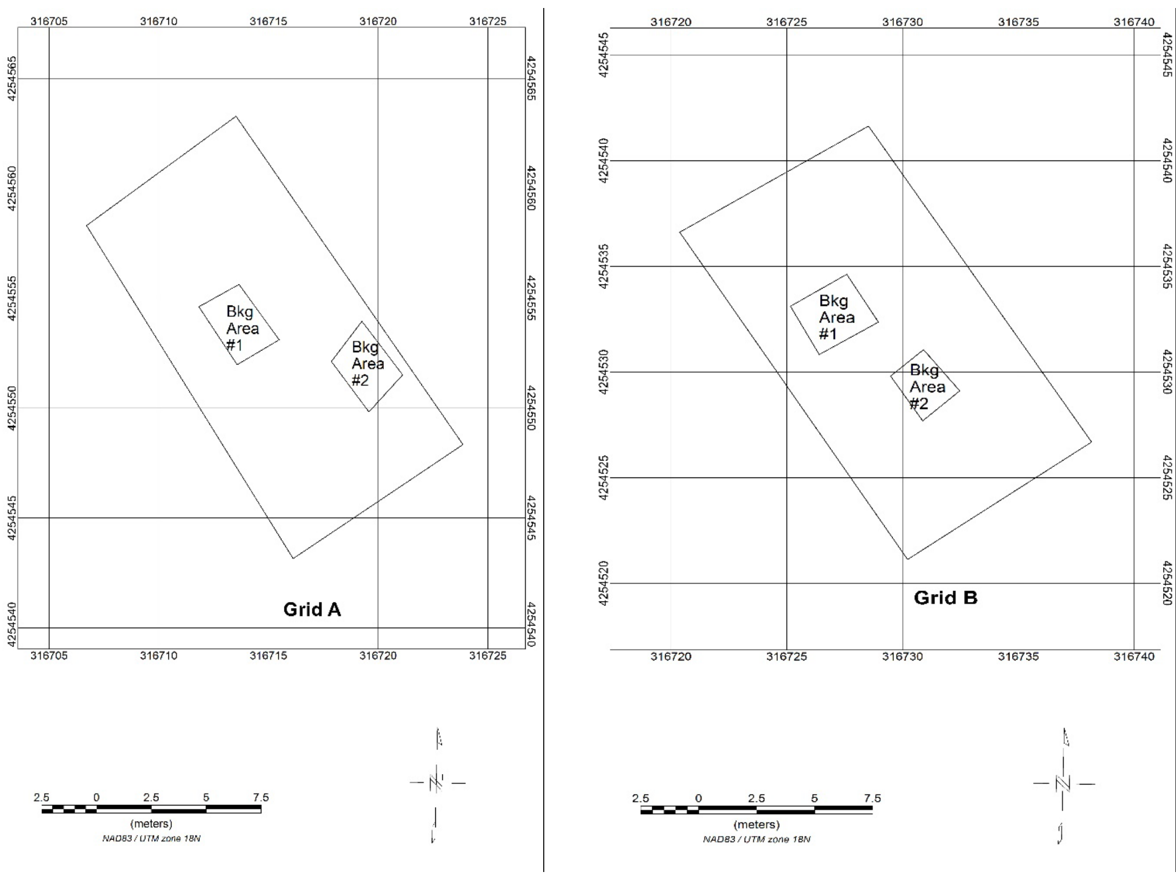


**Figure 39. Background Locations for Sites A and B.**

**Table 10. Background Statistics for Sites A and B**

| Grid | Dataset | Data Bkg 1 mV/A | Data Bkg 2 mV/A | Grid Bkg 1 mV/A | Grid Bkg 2 mV/A |
|---|---|---|---|---|---|
| Grid A | A3 | 0.42 | 0.42 | 0.32 | 0.28 |
| Grid A | A4 | 0.52 | 0.47 | 0.43 | 0.41 |
| Grid A | A5 | 0.44 | 0.43 | 0.27 | 0.27 |
| Grid B | B3 | 0.48 | 0.44 | 0.33 | 0.30 |
| Grid B | B4 | 0.43 | 0.44 | 0.24 | 0.25 |
| Grid B | B5 | 0.38 | 0.41 | 0.36 | 0.29 |
| Grid B | B6 | 0.34 | 0.37 | 0.25 | 0.31 |

Anomalies were picked from mapped data. An example mapped data file is shown in Figure 40. A manual clustering technique was used to evaluate multiple detections for the same object. A clustering radius of 0.25 m was used as a guide and each cluster was evaluated manually by the data analyst. Clustering is required because multiple local maxima, marked by black dots in Figure 41, can be above threshold on a given anomaly. This approach reduces the number of multiple picks on the final detection list.

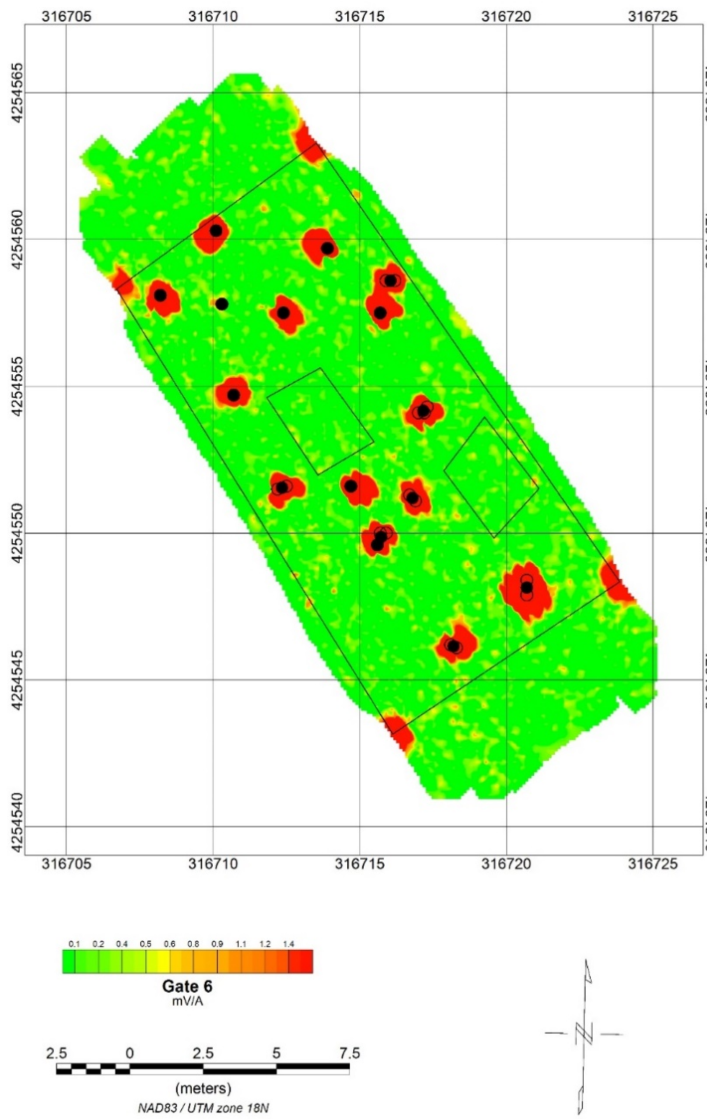


**Figure 40. Located and Leveled Dynamic Data from the TEMTADS 2x2 System, Site A; Black Circles Mark Target Locations Obtained by Clustering.**

## 6.3 PARAMETER ESTIMATES

Since the objective was to assess the geolocation performance of the EMI/AGT system, identical targets buried at the same depth were used for testing. Consequently, there was no parameter estimate done.

## 6.4 CLASSIFIER AND TRAINING

Since the objective was to assess the geolocation performance of the EMI/AGT system, identical targets buried at the same depth were used for testing. Consequently, there was no classification element of the testing.

### 6.5 DATA PRODUCTS

The EMI data products were generated using the standard formats used by Oasis montaj and the UX-Analyze Advanced module and ASCII, comma-delimited representations (*.csv).

The AGT post-processed data, the platform navigation solution was created in a text file format, containing UTC timestamp, position and attitude of the platform in the WGS84 system.

The results for each sortie are shown graphically in Section D of the Appendix. The final, processed data sets are stored as Oasis montaj databases (*.gdb) and are provided digitally. The detection results are stored as Oasis montaj databases (*.gdb) and are provided digitally. All raw and intermediate data files are also attached digitally.

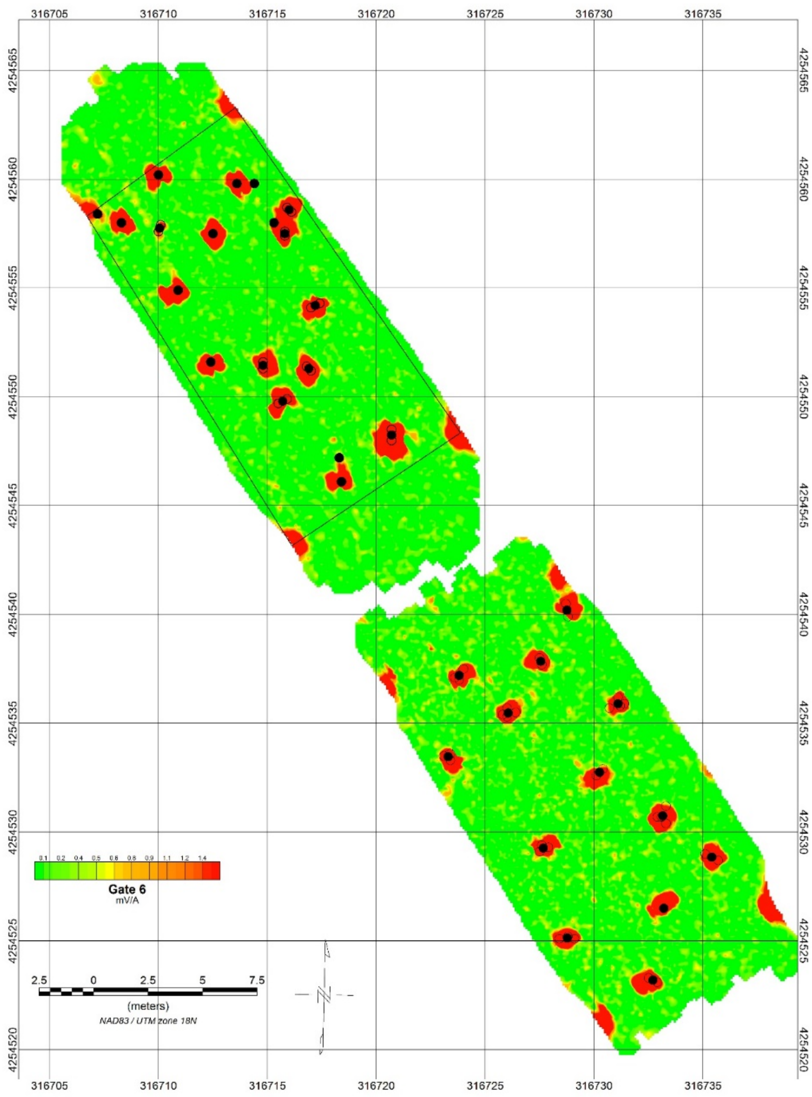


**Figure 41. The Map Shows the EMI Data, Sites A and B, and the Targets Picked.**

*The clusters are manually picked using a radius of 0.25 m as a guide. Clustering is required because multiple local maxima, marked by black circles, can be above threshold at a given anomaly.*

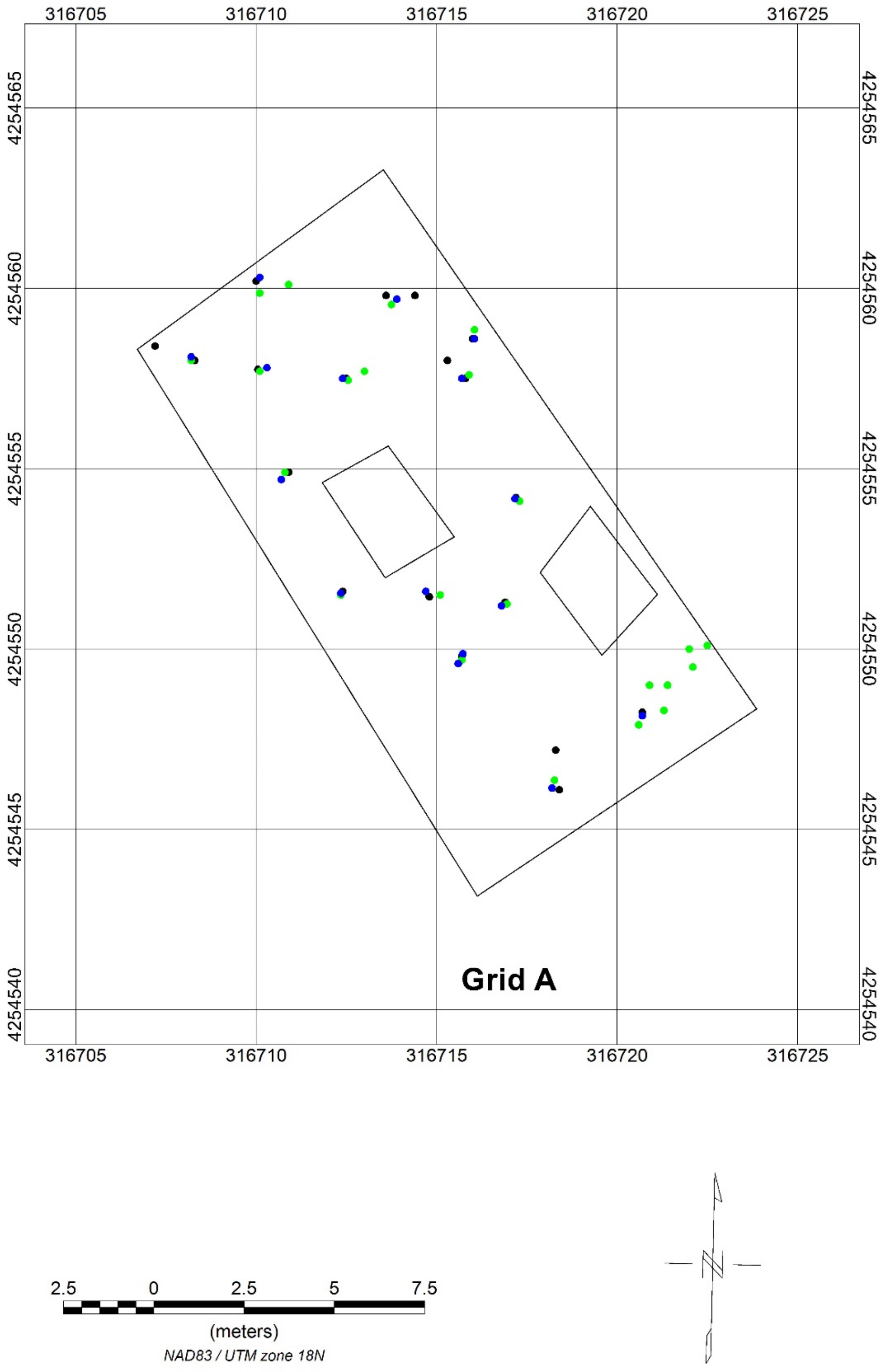


**Figure 42. All Clustered Picks for Site A (All Surveys); Colors Mark Different Surveys.**

*Note the clustering of the results from survey to survey.*

# 7.0 PERFORMANCE ASSESSMENT

## 7.1 CONSISTENT DATA LOGGING OF THE AGT SYSTEM

During the 2016 testing, there were data logging due to interference, see Section 7.2 below. The complete evaluation of all the data streams acquired in 2018 showed no data anomalies; there were no missing records, or incorrect time-tags. Since the IMU data records were internally time-tagged, the investigation mainly focused on the UWB sensor time-tagging, as it was implemented on the data logging laptop.

PPS signal and NMEA data from the GNSS receiver were fed to the logging laptop to connect the laptop CPU time base to GPS time during the data acquisition. The logged data allowed for estimating the offset and drift of the CPU time with respect to the GPS time, see Figure 43. The drift error was modeled as linear function, including scale and offset. The standard deviation for each session in milliseconds using the linear function is listed in Table 11. The standard deviation suggests less than 1 ms synchronization error for all sessions. Note that we use interpolation to convert CPU time to GPS time records for the UWB data rather than using a linear regression function. Therefore, the values presented in Table 11 has to be interpreted as an upper bound of time synchronization error, and the actual value is likely to be significantly smaller.

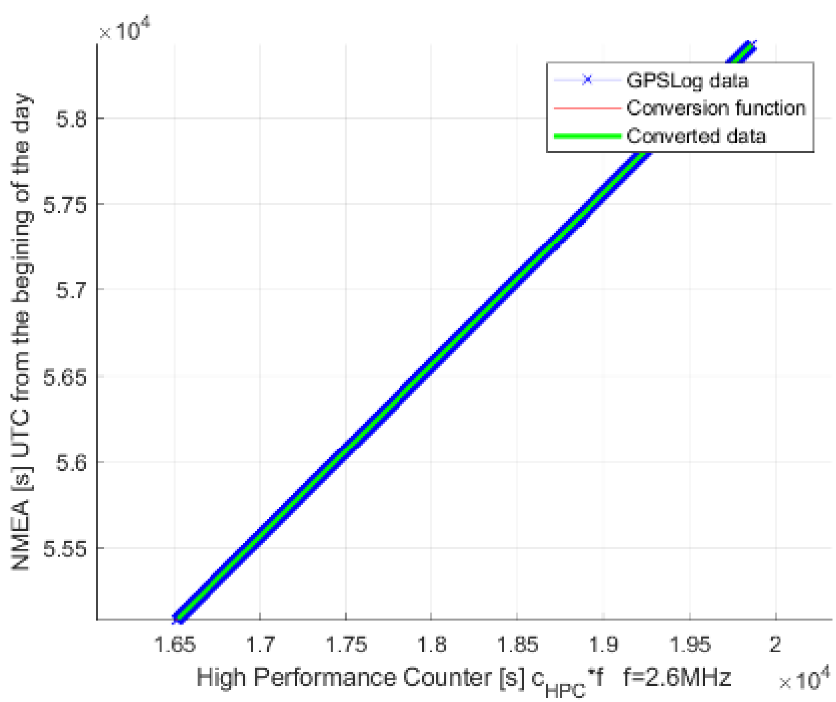


**Figure 43. Offset and Drift Estimation of Between CPU (X axis) and GPS (Y axis) Times.**

**Table 11. Standard Deviation of the Drift Error Between GPS and CPU Times in Milliseconds.**

| Session | Standard deviation [ms] |
|---|---|
| I1 | 0.31 |
| A3 | 0.30 |
| A4 | 0.30 |
| B3 | 0.30 |
| B4 | 0.30 |
| I5 | 0.30 |
| A5 | 0.29 |
| B5 | 0.38 |
| B6 | 0.37 |

## 7.2 INTERFERENCE BETWEEN THE AGT AND EMI SYSTEMS

During the 2016 testing, the time synchronization of the IMU to the GPS time showed intermittent anomalies, such as multiple PPS signal detection in a 1-sec period. Correcting of the data was feasible in most of the cases, yet this was unacceptable for an operational system. The new IMU procured after the 2016 test has a much better cabling, providing better isolation to electromagnetic waves, and equally importantly, the GPS time-tagging is implemented within the IMU unit. During the 2018 demonstration tests, no signal problem was found, and no sign of any interference was observed.

## 7.3 RELIABILITY OF UWB RANGING

At least three UWB ranges have to be known to calculate a 2D position, and thus, it is important to have at least three ranges for all network measurements, performed at around 3 Hz. Table 12 shows the number of epochs where this condition was not met as well as the failure rate, the ratio of unsuccessful and all epochs. Note that the failure rates are under 0.5% for all sessions and the total failure rate is 0.12%; clearly, an acceptable failure rate.

**Table 12. UWB Availability by Sessions.**

| Session | Epochs with less than 3 observations | Number of all epochs | Failure rate |
|---|---|---|---|
| I1 | 1 | 4377 | 0.02 % |
| A3 | 7 | 5251 | 0.13 % |
| A4 | 4 | 6341 | 0.06 % |
| B3 | 3 | 6149 | 0.05 % |
| B4 | 11 | 6138 | 0.18 % |
| I5 | 12 | 3789 | 0.32 % |
| A5 | 6 | 5316 | 0.11 % |
| B5 | 10 | 6358 | 0.16 % |
| B6 | 6 | 6245 | 0.09% |
| **Total** | **60** | **49964** | **0.12%** |

## 7.4 UWB POSITIONING ACCURACY

The UWB 2D positioning accuracy was validated in the open-sky I1, I5 tests. Using the GNSS trajectory as a reference, there was no bias found, and the standard deviation of the differences was 4.9 cm. This results matched the expectation, given the ideal environment (open-sky, and no signal obstruction) and the size of the UWB network.

## 7.5 IMU/UWB POSITIOING ACCURACY WITH AND WITHOUT SDR

### 7.5.1 IMU/UWB positioning

The integrated IMU and UWB trajectory solution was evaluated using the IMU/GNSS reference solution in the open-sky test area. In this case, the full 6-parameters trajectory solutions were compared and analyzed. Table 13 shows the statistical parameters of evaluation for sessions I1 and I5; note only the 2D distance and heading from the attitude parameters are listed. The empirical cumulative distribution functions of 2D positioning errors for both sessions are shown in Figure 44.

**Table 13. Comparison of IMU/UWB and IMU/GNSS Solutions.**

| | Abs. ΔX [cm] | Abs. ΔY [cm] | Abs. ΔZ [cm] | 2D difference [cm] | Heading [°] |
|---|---|---|---|---|---|
| **Session I1** | | | | | |
| Average | 3.8 | 2.8 | 61.8 | 5.2 | 1.73 |
| STD | 3.5 | 2.6 | 44.8 | 3.8 | 2.90 |
| Median | 3.1 | 2.0 | 52.9 | 4.3 | 1.00 |
| Abs. Max | 73.0 | 37.3 | 302.6 | 82.0 | 17.00 |
| 95$^{th}$ percentile | 10.1 | 8.2 | 142.1 | **11.6** | 10.39 |
| **Session I5** | | | | | |
| Average | 3.6 | 7.2 | 48.0 | 8.6 | 0.99 |
| STD | 3.4 | 3.5 | 17.4 | 3.7 | 3.44 |
| Median | 2.5 | 7.4 | 52.8 | 7.9 | 0.08 |
| Abs. Max | 24.2 | 17.8 | 74.8 | 24.3 | 16.00 |
| 95$^{th}$ percentile | 9.8 | 13.2 | 68.7 | **14.6** | 10.15 |
| **Combined at 95$^{th}$ percentile** | 10.0 | 10.7 | 105.4 | **13.1** | 10.27 |

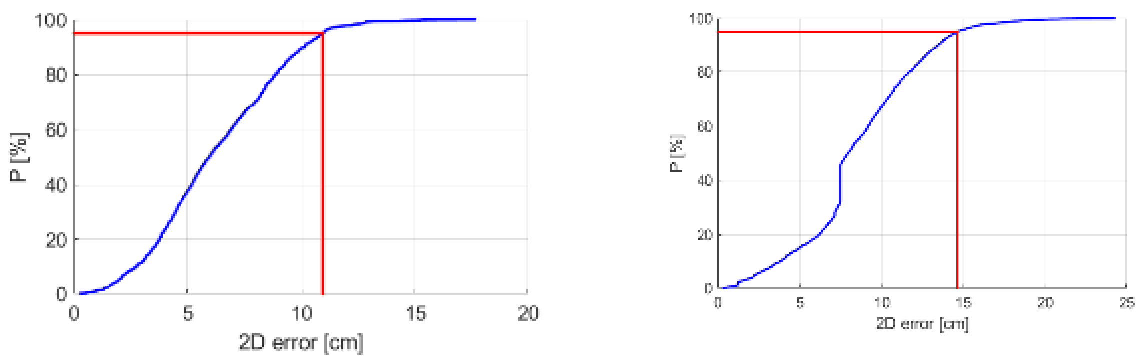


I1 I5

**Figure 44. Empirical Cumulative Distribution Functions of 2D Positioning Error for Session I1 and I5.**

*Red lines show 95% percentile reached at 11.6 cm and 14.6 cm, respectively.*

### 7.5.2 IMU/SDR/UWB positioning

As mentioned previously, SDR implementation fuses GPS and inertial data at the signal processing level. This enables extended signal accumulation, and thus recovering GPS signals attenuated by foliage and multiple layers of canopy.

Performance of the IMU/SDR/UWB system mechanization was assessed for the tree-covered test location, Session A5. Figure 45 shows its reconstructed test trajectory displayed in Google Earth. Reliable and continuous trajectory reconstruction capabilities are demonstrated.


**Figure 45. IMU/SDR/UWB Position Solution Displayed in Google Earth, Session A5.**

Horizontal position solution of the reference IMU/GNSS system is shown in Figure 46.

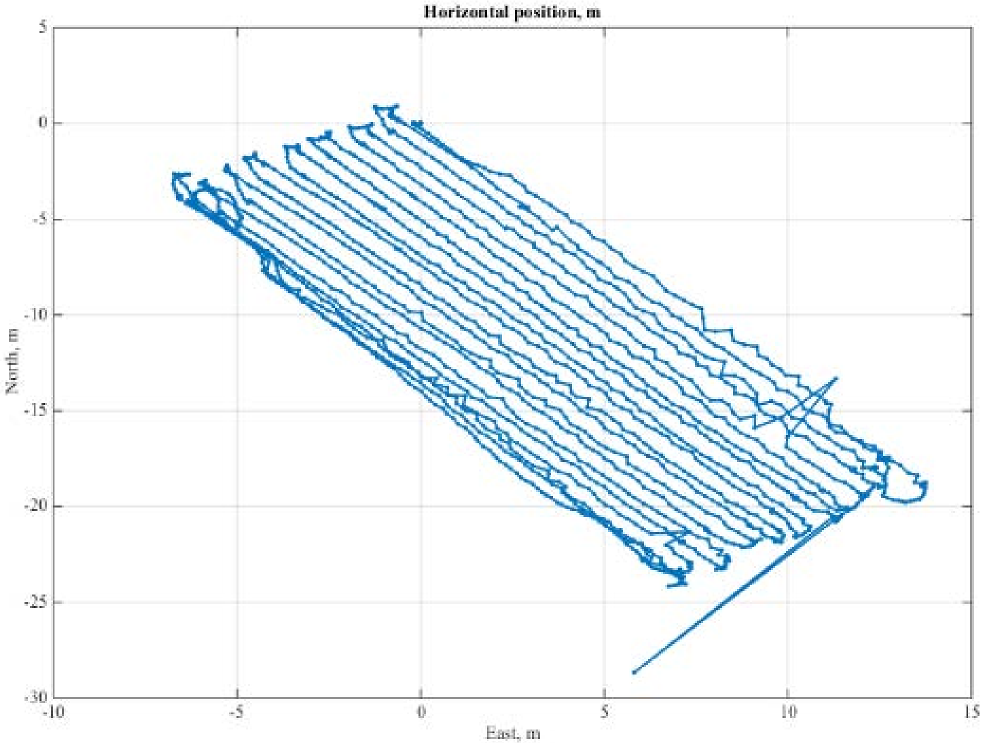


**Figure 46. Horizontal Position Solution of the Reference IMU/GNSS System**

*The reference solution clearly contains some discontinuities at a level from about 0.5 to 5 meters.*

Figure 47 shows IMU/SDR/UWB position estimates. The plot demonstrates that the use of SDR signal processing mitigates discontinuities in the reference position and enables reliable positioning capabilities under the foliage.

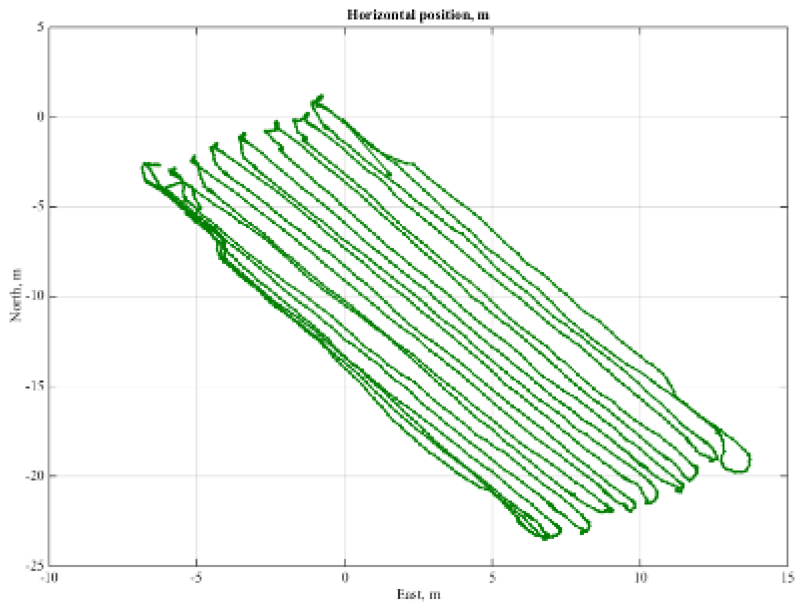


**Figure 47. Horizontal Position Solution of the IMU/SDR/UWB Implementation.**

The improved positioning performance is demonstrated more clearly when the IMU/SDR/UWB position estimates are overlapped over the reference solution as shown in Figure 48.

Figure 48 shows differences in position estimates of reference and SDR-based mechanizations. It is important to outline that large error spikes are due to errors in the reference IMU/GNSS solution whose performance is significantly degraded under the foliage.

Table 14 summarizes position test statistics. Increased differences between reference and SDR-based solutions (as compared to open-sky scenarios) are due to the decreased level of accuracy in the reference position outputs.

**Table 14. Comparison of IMU/GNSS and IMU/SDR/UWB Solutions.**

| | **Abs. ΔX [cm]** | **Abs. ΔY [cm]** | **2D difference [cm]** |
|---|---|---|---|
| **Session A5** | | | |
| Average | 11.6 | 13.8 | 18.0 |
| STD | 18.2 | 23.2 | 29.5 |
| Median | 9.81 | 11.58 | 15.18 |
| Abs. Max | 562.80 | 820.55 | 995.01 |
| $95^{th}$ percentile | 18.89 | 30.76 | **36.10** |

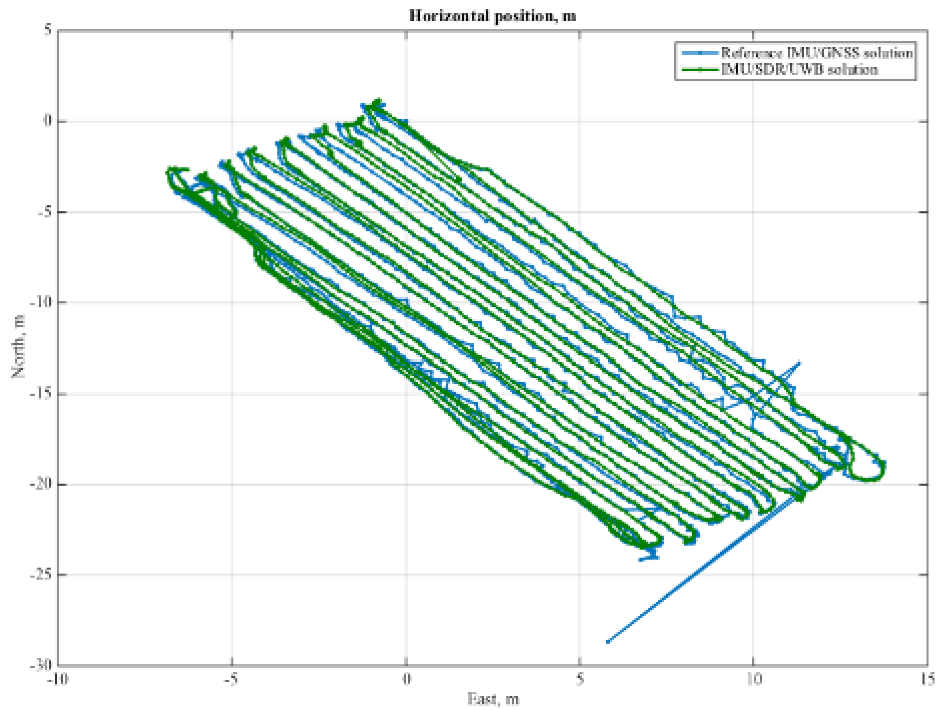


**Figure 48. Comparison of Horizontal Position Outputs of IMU/GNSS and IMU/SDR/UWB.**

## 7.6 HEADING ACCURACY

The heading estimation performance of the IMU/UWB solution was assessed based on the IMU/GNSS solution. Since the trajectory followed a parallel pattern, the visual interpretation is simple, see reference heading solution in Figure 49. For the straight trajectory segments the heading is alternating between 145º and 325º.

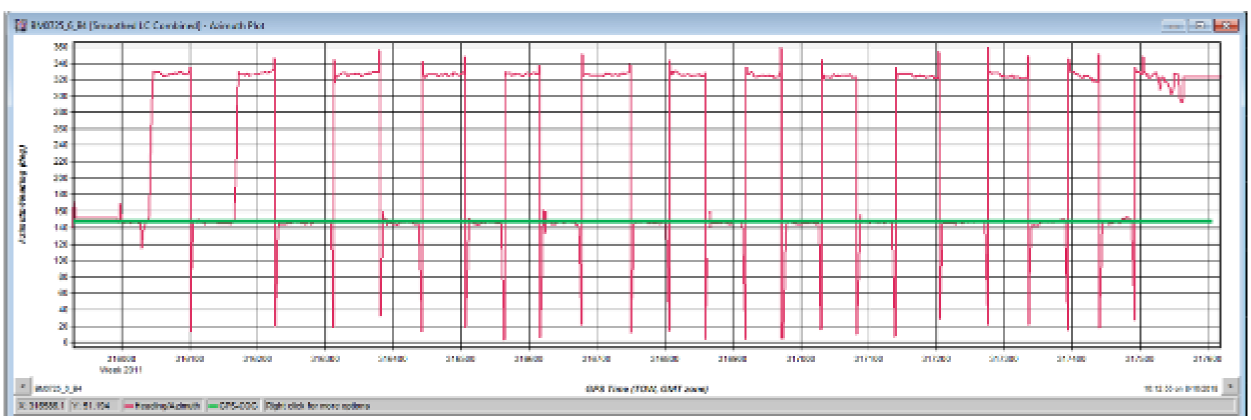

**Figure 49. Reference Heading Graph Based on IMU/GNSS Solution.**

Table 15 shows the statistics of the heading errors. Clearly, the performance objective of 0.5º was not achieved in these cases. There is an ongoing investigation on this subject. Note that heading information has minimal impact on the EMI data processing.

**Table 15. Statistics of Heading Errors.**

| | Heading error | |
|---|---|---|
| | **Session I1 [º]** | **Session I2 [º]** |
| Average | 0.99 | 1.73 |
| STD | 3.44 | 2.90 |
| Median | 0.08 | 1.00 |
| Abs. Max | 16.00 | 17.00 |
| $95^{th}$ percentile | 10.15 | 10.39 |
| Percentile of objective | **23.8%** | **89.1%** |

## 7.7 DETECTION RATE

Site A and B had 11 and 13 targets, respectively. Sessions A3, A4, A5, B3, B4, B5 and B6 were used for evaluation, and using the AGT geolocation information, the EMI processing resulted in correctly detecting all the 85 targets. In addition, the EMI system detected additional anomalies in each session, presumably due to existing cultural items as the area was not cleared prior to seeding. In summary, this performance criterion was fully satisfied.

## 7.8 DETECTION ACCURACY

The picked target locations and localization errors for all targets are listed in Section C of the Appendix. Note that the localization error is defined by the distance between the known target location and location of closest target pick. Table 16 shows the localization error statistics by sessions. Except for sessions A5, B3 and B4, the performance criterion of 30 cm at 95% CEP was achieved. The overall performance including all sessions was 32.4 cm, slightly above the required performance; note that the 30 cm localization accuracy for all sessions was achieved at P = 94.0%.

**Table 16. Target Localization Errors.**

| Session | Average [cm] | STD [cm] | Median [cm] | $95^{th}$ Percentile [cm] | Max [cm] |
|---|---|---|---|---|---|
| A3 | 12.1 | 3.5 | 11.0 | 17.0 | 18.0 |
| A4 | 15.3 | 7.7 | 13.0 | 28.5 | 30.0 |
| A5 | 20.7 | 11.8 | 19.0 | 41.5 | 48.0 |
| B3 | 17.8 | 12.1 | 13.0 | 37.8 | 45.0 |
| B4 | 13.8 | 10.8 | 11.0 | 30.6 | 39.0 |
| B5 | 12.7 | 6.4 | 12.0 | 22.8 | 27.0 |
| B6 | 16.9 | 7.8 | 16.0 | 26.0 | 26.0 |
| **Total** | **15.6** | **9.2** | **14.0** | **32.4** | **48.0** |

## 7.9 REACQUISITION RATE

There was only one test to assess the reacquisition performance; note that this was an optional item in the demonstration plan. In the target reacquisition test at Site B, the 11 out of 12 targets were successfully located well within the 30 cm range limit, as confirmed by subsequent removal of the targets by careful digging. The only out of range measurement, about 40 cm occurred at the first measurement, and is likely due to operator error, as it was the first time that the prototype software was used. In the midst of the session, decision was made to revisit that target at the end. Unfortunately, it could not be done due running out of power on the laptop used for the measurement. In fact, the 13$^{th}$ target was not measured at all, as the power failure happened when its localization started.

## 7.10 REACQUISITION ACCURACY

The assessment of reacquisition accuracy of targets included two field steps. First, using the UWB laptop system, the surveyed coordinates of the targets were fed into the OSU developed software system, and using an interactive interface, the operator was instructed to follow the motion suggested by the software. Once the UWB antenna was on the desired location, a flag was placed as closely as possible. In the second step, NRL personnel started to carefully dig the target area, and when the target became visible, a tape measurement was done between the flag and the center of the target, see Figure 49. The statistical results of the reacquisition accuracy are listed in Table 17.

The UWB system was capable of finding 11 targets during the test out of 12, resulting in 91.6% success rate. One target was not localized within 40 cm due to our inexperience with the recently developed and not yet field-tested reacquisition system. In addition, the sample size is small that allows for no rigorous comparison between the detection rate and the success criterion. Note that this element of the testing was optional, and was carried out in a short time on the last day.

Given all the circumstances, such dislocation of the target during burying and digging, and using an early prototype software, the reacquisition performance is truly excellent, as there is a high consistency in terms of accurate retracing the locations.

**Table 17. Reacquisition Accuracy.**

| | |
|---|---|
| **# of targets (measured)** | 12 |
| **# of located targets** | 11 |
| **Average** | 8.6 cm |
| **STD** | 6.3 cm |
| **Median** | 6.6 cm |
| **95$^{th}$ percentile** | 20.4 cm |

**Figure 50 Reacquisition Error Measured on the Field.**

## 7.11 EASE OF USE

The EMI sensor system was operated by skilled and very experienced NRL personnel. The AGT system in its new prototype configuration was used for the first time, so the OSU team was also somewhat learning on the job. Nevertheless, both teams got very familiar with the AGT system operation by the second day, including the setup of the UWB network and running the various data logging tools. Since the AGT was a prototype, the potential performance in terms of time and efficiency can be only coarsely approximated. So assuming that the AGT system has been reengineered to optimize both the hardware and software, so following statements can be made. It is fair to say that adding AGT to the existing EMI system would not impose a measurable load on the operator, and in fact, it could be easily integrated to the EMI workflow. Combining the two backpacks, and running the software tools from the same tablet would mean barely noticeable change compared to the current practice. The only extra imposition on the operator is the setup of the four corner poles with the UWB transmitters, which could be easy once the UWB units are permanently installed inside the poles. Consequently, the difficulty scale would be between 1 and 2.

The duration of each test is presented in Table 5. Some sessions were longer due to logging issues, but in most cases, the sessions were completed in 20-25 min. The UWB network setup typically required 15 min. The total setup and data acquisition time was about 45 min. Clearly, comparing the survey time to GNSS-based navigation for EMI sensor navigation, the network setup is the only additional time-consuming step that the AGT system requires. In summary, the AGT system may increase the survey time by 30%, a conservative estimate.

*Page Intentionally Left Blank*

# 8.0 COST ASSESSMENT

A cost model for the addition of the AGT system to an AGC system, the NRL TEMTADS 2x2 is included in Table 18. As the AGT system can replace the standard RTK GPS/IMU solution typically used for the TEMTADS 2x2, only the differences from the baseline implementation are discussed here.

## 8.1 COST MODEL

**Table 18. Cost/effort Breakdown for the AGT Component.**

| Cost Element | Data to be Tracked |
|---|---|
| **Instrument cost** | Component and integration costs:<br>• Engineering estimates based on current development: **$100K**<br>• GNSS unit: **$10K**<br>• IMU unit: **$2K/$6K**<br>• SDR unit: **$4K**<br>• UWB network: **$8K**<br>• Laptops: **$2K**<br>• Backpack: **$1K** |
| **Mobilization and demobilization** | Cost to mobilize to site<br>• Cost of normal field work: **$2K/day**<br>• The shipping of the poles represents a negligible extra effort compared to moving the EMI pushcart, so no additional cost is considered for it |
| **Site preparation** | Effort in hours per grid:<br>• AGT system installation: **15 mins**<br>• EMI survey: **30 mins** |
| **Instrument setup costs** | Unit: $ cost to set up and calibrate<br>Data requirements:<br>• Hours required: 15 mins<br>• Personnel required: **2 persons** (EMI) + **1 person** (AGT) that may be eliminated after training EMI personnel<br>• Frequency required: **every day** |
| **Survey costs** | Unit: $ cost per hectare<br>Data requirements:<br>• Number of grids per day: **8-10**<br>• Hours per hectare: **40**<br>• Personnel required: **3(2) persons**<br>• Cost per hectare: **40 hours/hectare x 3 people x $100/hour = $12K/hectare** |
| **Detection data processing costs** | Unit: $ per hectare as function of anomaly density<br>Data Requirements:<br>• Time required: **three hours per day** (may decrease as experience builds up); note anomaly density has no impact on the AGT processing<br>• Personnel required: **one person**<br>• Cost per hectare: **5 days/hectare x 3 hours/day x $100/hour = $1,500/hectare** |
| **Discrimination data processing** | • **N/A** |

## 8.2 COST DRIVERS

Cost drivers are mostly labor. For each grid, the UWB poles needs to be placed and surveyed in using a total station. Additionally, the data preprocessing is more involved that current GNSS and RTK solutions.

## 8.3 COST BENEFIT

Better positioning yields benefits twofold. First, better positioning results in a better reacquisition, meaning less time on an anomaly to find it. Additionally, the better positioning drives down one of the major noise sources in EMI data processing, the noise budget consumed by positioning error.

# 9.0 IMPLEMENTATION ISSUES

For the current iteration of equipment, the main issues are Size, Weight, and Power (SWaP) concerns. For a field technician already wearing a heavy pack and pushing a cart through the woods, any more weight or bulk is unwelcome. Additionally, a real-time version would enable reacquisition and would easy data collection. Otherwise, the technology requires nothing that is not already required for work in these challenging conditions.

*Page Intentionally Left Blank*

## 10.0 REFERENCES


[1] Final Report, MR-200807 / MR-200909, Handheld Electromagnetic Induction Sensor for Cued UXO Discrimination / Man-Portable Electromagnetic Induction Array for UXO Detection and Discrimination, URL: https://www.serdp-estcp.org/Program-Areas/Munitions-Response/Land/Sensors/MR-200807-MR-200909/, last accessed: 12/2018

[2] "Department of Defense Advanced Geophysical Classification Accreditation Program," dated April 11, 2016.

[3] Novatel's OEM7700 Product Website: https://www.novatel.com/products/gnss-receivers/oem-receiver-boards/oem7-receivers/oem7700/, last accessed: 04/2018

[4] Novatel's IGM-S1 Product Website: https://www.novatel.com/assets/Documents/Papers/IMU-IGM-S1-PS_2.pdf, last accessed: 04/2018

[5] Novatel's Waypoint Product Website: https://www.novatel.com/products/software/

[6] Ettus Research's USRP N200 Product Website: https://www.ettus.com/product/details/UN200-KIT, last accessed: 04/2018

[7] Microsemi's Low Noise CSAC: https://www.microsemi.com/product-directory/embedded-clocks-frequency-references/4518-low-noise-csac-ln-csac, last accessed: 04/2018

[8] 47 CFR Part 15, Subpart F – Ultra-Wideband Operation, link: https://www.law.cornell.edu/cfr/text/47/part-15/subpart-F?qt-ecfrmaster=0#qt-ecfrmaster, last accessed: 04/2018

[9] "Revision of Part 15 of the Commission's Rules Regarding Ultra-Wideband Transmission Systems", link: https://apps.fcc.gov/edocs_public/attachmatch/FCC-10-151A1_Rcd.pdf, last accessed: 04/2018

[10] Koppanyi Z., Toth C. K. and Grejner-Brzezinska D. A., Positioning in Challenging Environments Using Ultra-Wideband Sensor Networks, GPS World, Vol. 26, No. 3, pp. 44-49, March 2, 2015, Innovation Column, link: http://gpsworld.com/innovation-where-are-we/

[11] TimeDomain's PulsOn 440, link: https://timedomain.com/products/pulson-440/, last accessed: 04/2018

[12] Live Site Demonstration of Advanced Geolocation Technology to Support Dynamic Classification of EMI Data Collect in GPS-challenged Areas, MR-201418, In-Progress Review Meeting, September 20, 2016

[13] Koppanyi, Z., Toth, C.K. (2014): Indoor Ultra-Wide Band Network Adjustment using Maximum Likelihood Estimation, ISPRS Ann. Photogramm. Remote Sens. Spatial Inf. Sci., II-1, 31-35

[14] Toth, C. K.; Jozkow, G., Koppanyi, Z., Grejner-Brzezinska, D. (2016): Positioning Slow Moving Platforms by UWB technology in GPS-Challenged, Journal of Surveying Engineering (ASCE), Volume 143, Issue 4

[15] Final Report, SERDP MR-1564, Novel Geolocation Technology for Geophysical Sensors for Detection and Discrimination of Unexploded Ordnance, URL: https://www.serdp-estcp.org/content/download/16926/189819/file/MR-1564-FR%20(Phase%20II).pdf, last accessed: 12/2018

[16] Dierenbach, K., S. Ostrowski, Z. Koppanyi, G. Jozkow, C. Toth, and D. Grejner-Brzezinska (2015): UWB for Navigation in GNSS Compromised Environments, ION GNSS+ International Meeting, September 2015.

[17] Koppanyi, Z., Navratil, V., Xu, H., Toth, C. K., Grejner-Brzezinska, D., (2018): Using Adaptive Motion Constraints to Support UWB/IMU Based Navigation, Navigation: Journal of The Institute of Navigation, Volume 65, Issue 2, pp. 247-261

[18] Live Site Demonstration of Advanced Geolocation Technology to Support Dynamic Classification of EMI Data Collect in GPS-challenged Areas, MR-201418, In-Progress Report, June, 2015, p. 108

[19] “Environmental Assessment of the Blossom Point Field Test Facility, Charles County, Maryland,” US Army Laboratory Command, December 1990.

[20] “Design and Construction of the NRL Baseline Ordnance Classification Test Site at Blossom Point,” H.H. Nelson, J.R. McDonald, and R. Robertson, NRL Memorandum Report NRL/MR/6110—00-8437, US Naval Research Laboratory, Washington, DC, March 20, 2000.

[21] “User’s Guide, TEMTADS MP 2x2 Cart, v2.00,” MTADS Program, Chemistry Division, US Naval Research Laboratory, May 27, 2014.

[22] T. Bell, B. Barrow, J. Miller, and D. Keiswetter, Time and Frequency Domain Electromagnetic Induction Signatures of Unexploded Ordnance, (2001): Subsurface Sensing Technologies and Applications Vol. 2, No. 3, July 2001.

[23] “MTADS Demonstration at Camp Sibert Magnetometer / EM61 MkII / GEM-3 Arrays,” Demonstration Data Report, G.R. Harbaugh, D.A. Steinhurst, N. Khadr, August 21, 2008.

# APPENDIX A PAPERS PUBLISHED


1. Koppanyi, Z., Navratil, V., Xu, H., Toth, C. K., Grejner-Brzezinska, D. (2018), Using Adaptive Motion Constraints to Support UWB/IMU Based Navigation: ***ION Journal of Navigation***, Vol. 65, Issue 2, pp. 247-261, 10.1002/navi.227

2. D. A. Grejner-Brzezinska, C. K. Toth, Z. Koppanyi, D.A. Steinhurst, T. Bell, G. Harbaugh (2018): Demonstration of Advanced Geolocation Technology to Support Dynamic Classification of EMI Data Collect in GPS-challenged Areas, SERDP and ESTCP Symposium, November 27–29, 2018, Washington, DC.

3. Koppanyi, Z., Toth, C. K., Grejner-Brzezinska (2018): Scalable Ad-hoc UWB Network Adjustment, IEEE/ION PLANS, April 23-26, 2018, Monterey, California

4. Toth, C. K., Jozkow, G., Koppanyi, Z., Grejner-Brzezinska, D. (2017): Positioning Slow Moving Platforms by UWB technology in GPS-Challenged Areas, ***ASCE Journal of Surveying Engineering***, Vol 143, Issue 4, 2017, ISSN: 0733-9453

5. D. A. Grejner-Brzezinska, C. K. Toth, Z. Koppanyi, D.A. Steinhurst, T. Bell, G. Harbaugh (2018): Live Site Demonstration of Advanced Geolocation Technology at NRL's Blossom Point Test Field: Performance Assessment of EMI Data Acquisition in GPS-challenged Areas, SERDP and ESTCP Symposium, November 28–30, 2017, Washington, DC.

6. Koppanyi, Z., Navratil, V., Xu, H., Toth, C. K., Grejner-Brzezinska, D. (2017): UWB/IMU Integration with Adaptive Motion Constraints to Support UXO Mapping, *Proceedings of the ION 2017 Pacific PNT Meeting*, Honolulu, Hawaii, May 2017, pp. 429-438.

7. Koppanyi, Z., Toth, C. K., Grejner-Brzezinska, D. (2017): UXO Mapping with UWB/IMU integration, *Proceedings of ION GNSS++*, Portland, Oregon, Sept 25-29, 2017

8. Toth, C. K., Koppanyi, Z., Navratil, V., Grejner-Brzezinska, D. (2017): Georeferencing in GNSS-Challenged Environment: Integrating UWB and IMU Technologies, *Int. Arch. Photogramm. Remote Sens. Spatial Inf. Sci.*, XLII-1/W1, 175-180, 2017

9. Zoltan Koppanyi, Charles K. Toth and Dorota A. Grejner-Brzezinska, (2015): Positioning in Challenging Environments Using Ultra-Wideband Sensor Networks, *GPS World*, Vol. 26, No. 3, pp. 44-49, March 2, 2015, Innovation Column, URL: http://gpsworld.com/innovation-where-are-we/

10. Dierenbach, K., Ostrowski, S., Jozkow, G., Toth, K. C., Grejner-Brzezinska, A. D., Koppanyi, Z. (2015): UWB for Navigation in GNSS compromised Environments, In: *Proceedings of ION GNSS 2016+*, 2015

11. Koppanyi, Z., Toth, C. K. (2014): Indoor Ultra-Wide Band Network Adjustment using Maximum Likelihood Estimation, In: *ISPRS Annals of the Photogrammetry, Remote Sensing and Spatial Information Sciences*, Vol. II-1, 2014, pp. 31-35., ISSN 2194-9042

12. Koppanyi, Z., Toth, C. K., Grejner-Brzezinska, D. A., Jozkow, G (2014): Performance Analysis of UWB Technology for Indoor Positioning, In*: Institute of Navigation International Technical Meeting 2014,* 2014, pp. 154-165., ISBN: 9781632660800

## APPENDIX B POINTS OF CONTACT

The main points of contact (POC) involved in the demonstration are listed below.

| POINT OF CONTACT Name | ORGANIZATION Name Address | Phone Fax E-mail | Role in Project |
|---|---|---|---|
| Herb Nelson | ESTCP<br>4800 Mark Center Drive, Suite 17D03,<br>Alexandria, VA 22350-3605 | 571-372-6400 (W)<br>202-215-4844 (C)<br>herbert.h.nelson10.civ@mail.mil | Director and<br>MR Program Manager |
| Michael Book | Noblis<br>2002 Edmund Halley Drive<br>Reston VA 20191 | 703-610-2118 (W)<br>michael.book@noblis.org | MR Program Assistant |
| Jack Kaiser | ARL – BP<br>15000 Blossom Point Road<br>Welcome, MD 20693 | 301-394-1534 (W)<br>john.e.kaiser8.civ@mail.mil | Garrison Manager |
| Charles Toth | OSU<br>470 Hitchcock Hall,<br>2070 Neil Ave.,<br>Columbus, OH 43210 | 614-292-7681 (W)<br>614-975-8018 (C)<br>toth.2@osu.edu | PI<br>AGT system |
| Zoltan Koppanyi | OSU<br>470 Hitchcock Hall,<br>2070 Neil Ave.,<br>Columbus, OH 43210 | 614-804-9057 (C)<br>zoltan.koppanyi@gmail.com | AGT data logging and processing |
| Dan Steinhurst | Nova Research, Inc.<br>1900 Elkin Street, Suite 230<br>Alexandria, VA 22308 | 202-767-3556 (W)<br>703-850-5217 (C)<br>daniel.steinhurst.ctr@nrl.navy.mil | co-PI<br>EMI data processing |
| Tom Bell | Leidos Corp., Maritime Solutions Division<br>4001 N Fairfax Dr.,<br>Arlington, VA 22203 | 301-712-7021 (C)<br>thomas.h.bell@leidos.com | Co-PI<br>EMI Data QC / Ground Truth |
| Glenn Harbaugh | Nova Research, Inc.<br>1900 Elkin Street, Suite 230<br>Alexandria, VA 22308 | 804-761-5904 (C)<br>glenn.harbaugh.ctr@nrl.navy.mil | Site Safety Officer |
| Andrey Soloviev | QuNav, Inc. | 740-541-1529 (C)<br>soloviev@qunav.com | SDR data processing |

*Page Intentionally Left Blank*

# APPENDIX C TARGETS AND LOCALIZATION ERRORS

| Seed ID | X UTM 18N [m] | Y UTM 18N [m] | Grid Value [mv/A, grid] | Localization Error [m] | Comments |
|---|---|---|---|---|---|
| **SESSION A1** | | | | | |
| 11 | 316718.40 | 4254546.10 | 34.40435028 | 0.14 | |
| 6 | 316712.40 | 4254551.60 | 36.05703354 | 0.11 | |
| 5 | 316710.90 | 4254554.90 | 48.31309128 | 0.16 | |
| 3 | 316712.50 | 4254557.50 | 88.08999634 | 0.10 | |
| 2 | 316713.60 | 4254559.80 | 66.59302521 | 0.08 | |
| 1 | 316710.00 | 4254560.20 | 47.87307358 | 0.14 | |
| 4 | 316716.00 | 4254558.60 | 26.31162453 | 0.09 | Centroid of Cluster |
| 8 | 316716.90 | 4254551.30 | 39.75291061 | 0.15 | Centroid of Cluster |
| 9 | 316715.70 | 4254549.80 | 45.2385025 | 0.07 | Centroid of Cluster |
| 10 | 316720.70 | 4254548.25 | 204.9919739 | 0.11 | Centroid of Cluster |
| 7 | 316717.20 | 4254554.20 | 51.75437164 | 0.18 | Centroid of Cluster |
| **SESSION A2** | | | | | |
| 5 | 316710.70 | 4254554.70 | 36.55809784 | 0.13 | |
| 3 | 316712.40 | 4254557.50 | 67.13149261 | 0.14 | |
| 2 | 316713.90 | 4254559.70 | 61.2253418 | 0.30 | |
| 1 | 316710.10 | 4254560.30 | 40.43009186 | 0.27 | |
| 4 | 316716.05 | 4254558.60 | 39.01179504 | 0.12 | Centroid of Cluster |
| 7 | 316717.17 | 4254554.17 | 61.18341827 | 0.14 | Centroid of Cluster |
| 6 | 316712.35 | 4254551.55 | 33.80296707 | 0.13 | Centroid of Cluster |
| 8 | 316716.80 | 4254551.20 | 33.31505203 | 0.04 | Centroid of Cluster |
| 9 | 316715.73 | 4254549.87 | 55.16459274 | 0.11 | Centroid of Cluster |
| 11 | 316718.20 | 4254546.15 | 31.78515244 | 0.09 | Centroid of Cluster |
| 10 | 316720.70 | 4254548.15 | 205.9895325 | 0.21 | Centroid of Cluster |
| **SESSION A5** | | | | | |
| 10 | 316720.60 | 4254547.90 | 259.19 | 0.48 | |
| 7 | 316717.30 | 4254554.10 | 57.19 | 0.20 | |
| 5 | 316710.80 | 4254554.90 | 44.7 | 0.09 | |
| 1 | 316710.10 | 4254559.87 | 48.29 | 0.24 | Centroid of Cluster 1 |
| 2 | 316713.75 | 4254559.55 | 64.27 | 0.22 | Centroid of Cluster 2 |
| 3 | 316712.55 | 4254557.45 | 80.86 | 0.08 | Centroid of Cluster 3 |
| 6 | 316712.35 | 4254551.5 | 31.05 | 0.13 | Centroid of Cluster 4 |
| 8 | 316716.95 | 4254551.25 | 31.93 | 0.16 | Centroid of Cluster 5 |
| 9 | 316715.70 | 4254549.70 | 50.64 | 0.14 | Centroid of Cluster 6 |
| 4 | 316716.05 | 4254558.85 | 25.95 | 0.35 | Centroid of Cluster 7 |
| 11 | 316718.27 | 4254546.37 | 31.09 | 0.19 | Centroid of Cluster 8 |
| **SESSION B3** | | | | | |
| 13 | 316732.00 | 4254523.20 | 19.21060371 | 0.45 | |
| 6 | 316731.40 | 4254535.90 | 62.35877991 | 0.33 | |
| 10 | 316728.50 | 4254525.10 | 35.6537323 | 0.25 | Centroid of Cluster |
| 12 | 316733.15 | 4254526.65 | 72.63007355 | 0.06 | Centroid of Cluster |
| 11 | 316735.30 | 4254528.95 | 32.11502838 | 0.14 | Centroid of Cluster |
| 9 | 316732.95 | 4254530.70 | 55.79240417 | 0.13 | Centroid of Cluster |
| 8 | 316727.70 | 4254529.40 | 41.27000046 | 0.08 | Centroid of Cluster |
| 7 | 316730.00 | 4254532.45 | 47.73563385 | 0.01 | Centroid of Cluster |

| Seed ID | X UTM 18N [m] | Y UTM 18N [m] | Grid Value [mv/A, grid] | Localization Error [m] | Comments |
|---|---|---|---|---|---|
| 5 | 316723.43 | 4254533.43 | 34.1165657 | 0.13 | Centroid of Cluster |
| 4 | 316726.25 | 4254535.65 | 41.92740631 | 0.20 | Centroid of Cluster |
| 1 | 316723.75 | 4254537.00 | 62.45170593 | 0.12 | Centroid of Cluster |
| 3 | 316727.55 | 4254537.90 | 31.25642776 | 0.13 | Centroid of Cluster |
| 2 | 316729.03 | 4254540.30 | 24.11397934 | 0.28 | Centroid of Cluster |
| **SESSION B4** | | | | | |
| 12 | 316733.20 | 4254526.50 | 79.15653229 | 0.21 | |
| 2 | 316728.75 | 4254540.20 | 33.72660065 | 0.04 | Centroid of Cluster |
| 3 | 316727.55 | 4254537.85 | 38.56863022 | 0.12 | Centroid of Cluster |
| 1 | 316723.80 | 4254537.20 | 57.12543869 | 0.11 | Centroid of Cluster |
| 4 | 316726.05 | 4254535.48 | 40.36207581 | 0.06 | Centroid of Cluster |
| 5 | 316723.30 | 4254533.47 | 24.7919445 | 0.22 | Centroid of Cluster |
| 7 | 316730.25 | 4254532.75 | 50.92269135 | 0.39 | Centroid of Cluster |
| 8 | 316727.66 | 4254529.27 | 37.71480179 | 0.11 | Centroid of Cluster |
| 9 | 316733.15 | 4254530.75 | 55.44271088 | 0.18 | Centroid of Cluster |
| 10 | 316728.76 | 4254525.13 | 43.44649124 | 0.02 | Centroid of Cluster |
| 13 | 316732.70 | 4254523.20 | 22.34028816 | 0.25 | Centroid of Cluster |
| 11 | 316735.40 | 4254528.85 | 25.0182724 | 0.03 | Centroid of Cluster |
| 6 | 316731.10 | 4254535.90 | 49.11999893 | 0.05 | Centroid of Cluster |
| **SESSION B5** | | | | | |
| 13 | 316732.30 | 4254523.20 | 27.74632645 | 0.15 | |
| 10 | 316728.80 | 4254525.10 | 38.03986359 | 0.05 | |
| 9 | 316733.00 | 4254530.70 | 30.55208015 | 0.10 | |
| 7 | 316730.20 | 4254532.50 | 59.54671478 | 0.20 | |
| 5 | 316723.50 | 4254533.40 | 27.16765404 | 0.12 | |
| 4 | 316726.00 | 4254535.40 | 29.50962067 | 0.15 | |
| 6 | 316731.30 | 4254536.00 | 63.6923027 | 0.27 | |
| 1 | 316723.80 | 42545370.00 | 66.83625793 | 0.10 | |
| 3 | 316727.60 | 4254537.90 | 37.97335434 | 0.18 | |
| 2 | 316728.80 | 4254540.30 | 28.99530983 | 0.13 | |
| 12 | 316733.10 | 4254526.65 | 59.31694794 | 0.08 | Centroid of Cluster |
| 11 | 316735.40 | 4254528.80 | 18.4076786 | 0.04 | Centroid of Cluster |
| 8 | 316727.70 | 4254529.40 | 29.54029846 | 0.08 | Centroid of Cluster |
| **SESSION B6** | | | | | |
| 13 | 316732.60 | 4254523.1 | 34.92255402 | 0.16 | |
| 10 | 316728.50 | 4254525.1 | 34.34999847 | 0.25 | |
| 12 | 316733.10 | 4254526.6 | 83.27456665 | 0.12 | |
| 8 | 316727.90 | 4254529.4 | 30.35094833 | 0.16 | |
| 9 | 316732.80 | 4254530.7 | 15.46608067 | 0.26 | |
| 7 | 316730.20 | 4254532.6 | 68.37150574 | 0.25 | |
| 5 | 316723.40 | 4254533.2 | 37.3470192 | 0.11 | |
| 3 | 316727.40 | 4254538.0 | 39.00791931 | 0.14 | |
| 2 | 316728.80 | 4254540.4 | 32.89575195 | 0.22 | |
| 11 | 316735.55 | 4254528.9 | 23.32940102 | 0.19 | Centroid of Cluster |
| 4 | 316726.15 | 4254535.50 | 37.55976868 | 0.05 | Centroid of Cluster |
| 6 | 316731.25 | 4254536.05 | 18.98483276 | 0.26 | Centroid of Cluster |
| 1 | 316723.80 | 4254537.10 | 42.96276474 | 0.03 | Centroid of Cluster |

# APPENDIX D VISUALIZATION OF EMI RESULTS

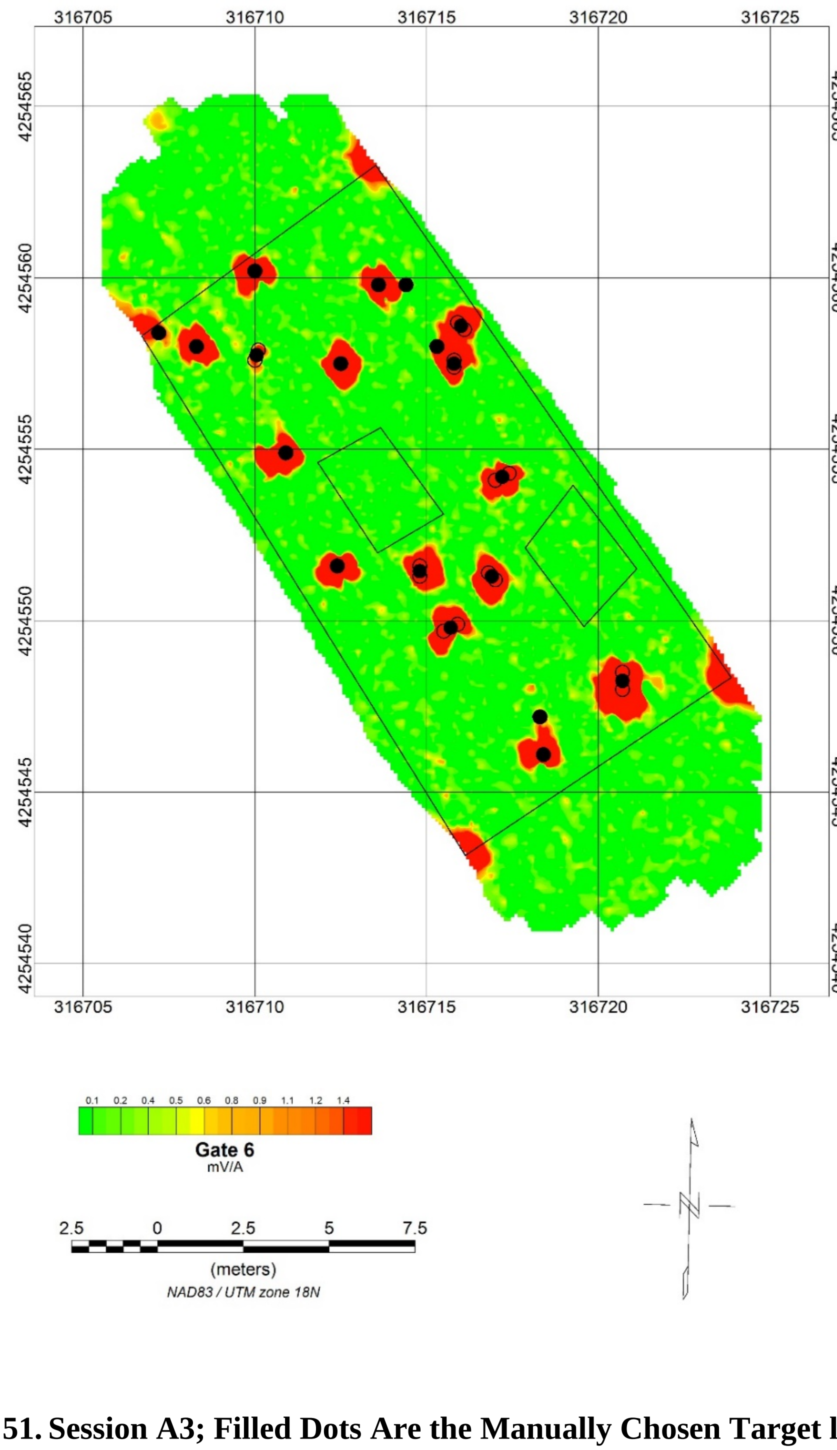


**Figure 51. Session A3; Filled Dots Are the Manually Chosen Target locations.**

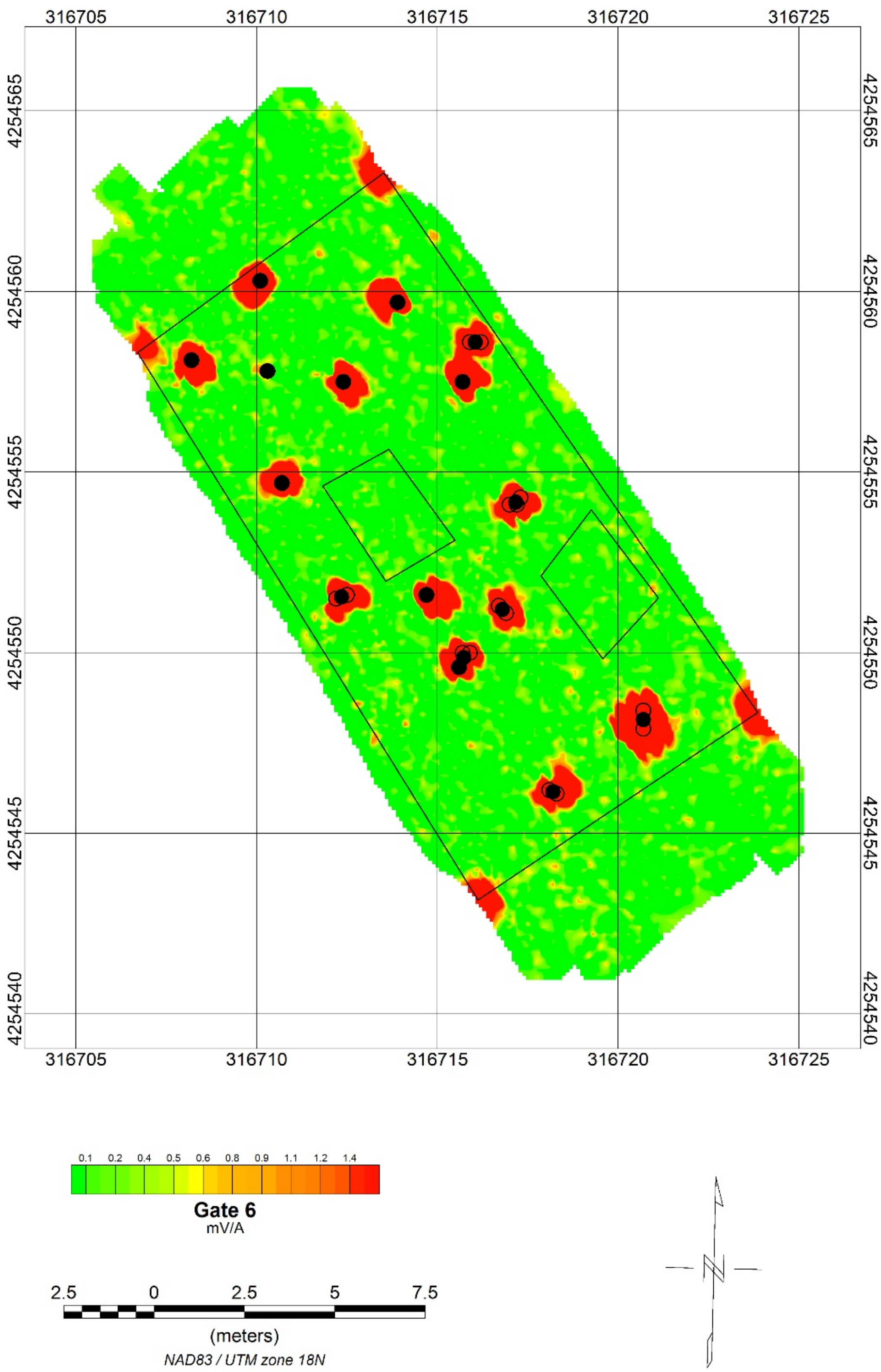


**Figure 52. Session A4; Filled Dots Are the Manually Chosen Target Locations.**

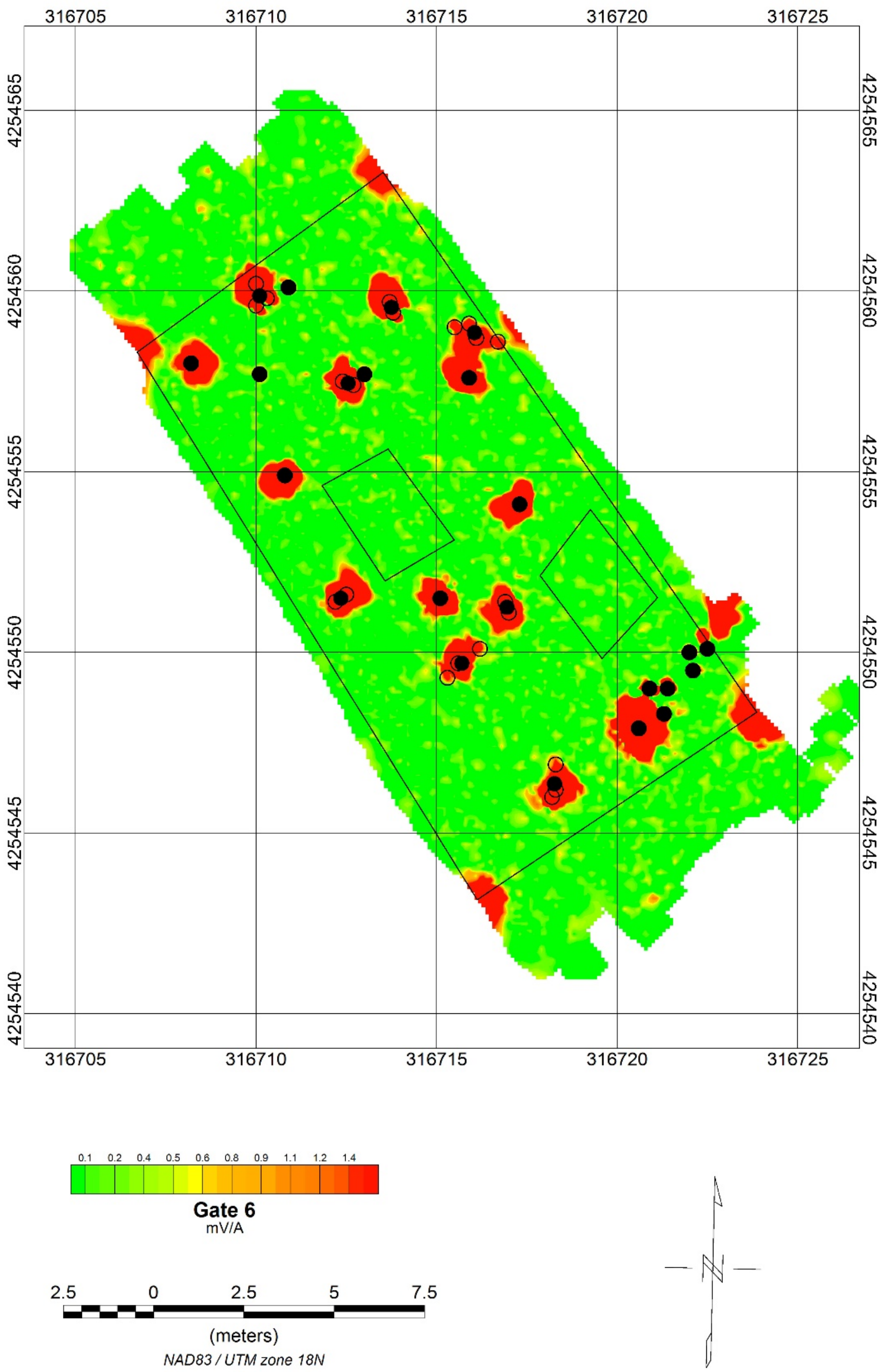


**Figure 53. Session A5; Filled Dots Are the Manually Chosen Target Locations.**

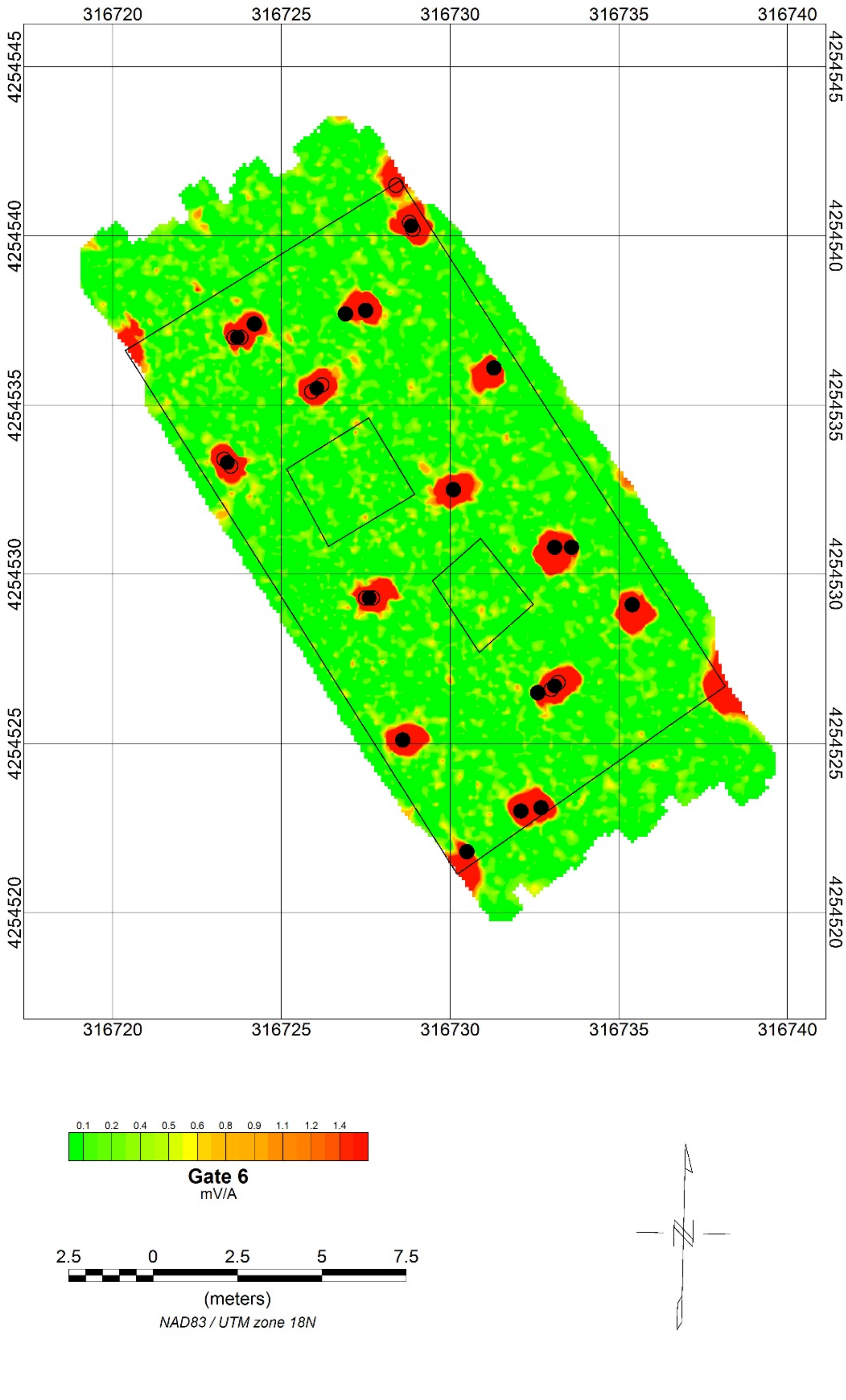


**Figure 54. Session B3; Filled Dots Are the Manually Chosen Target Locations.**

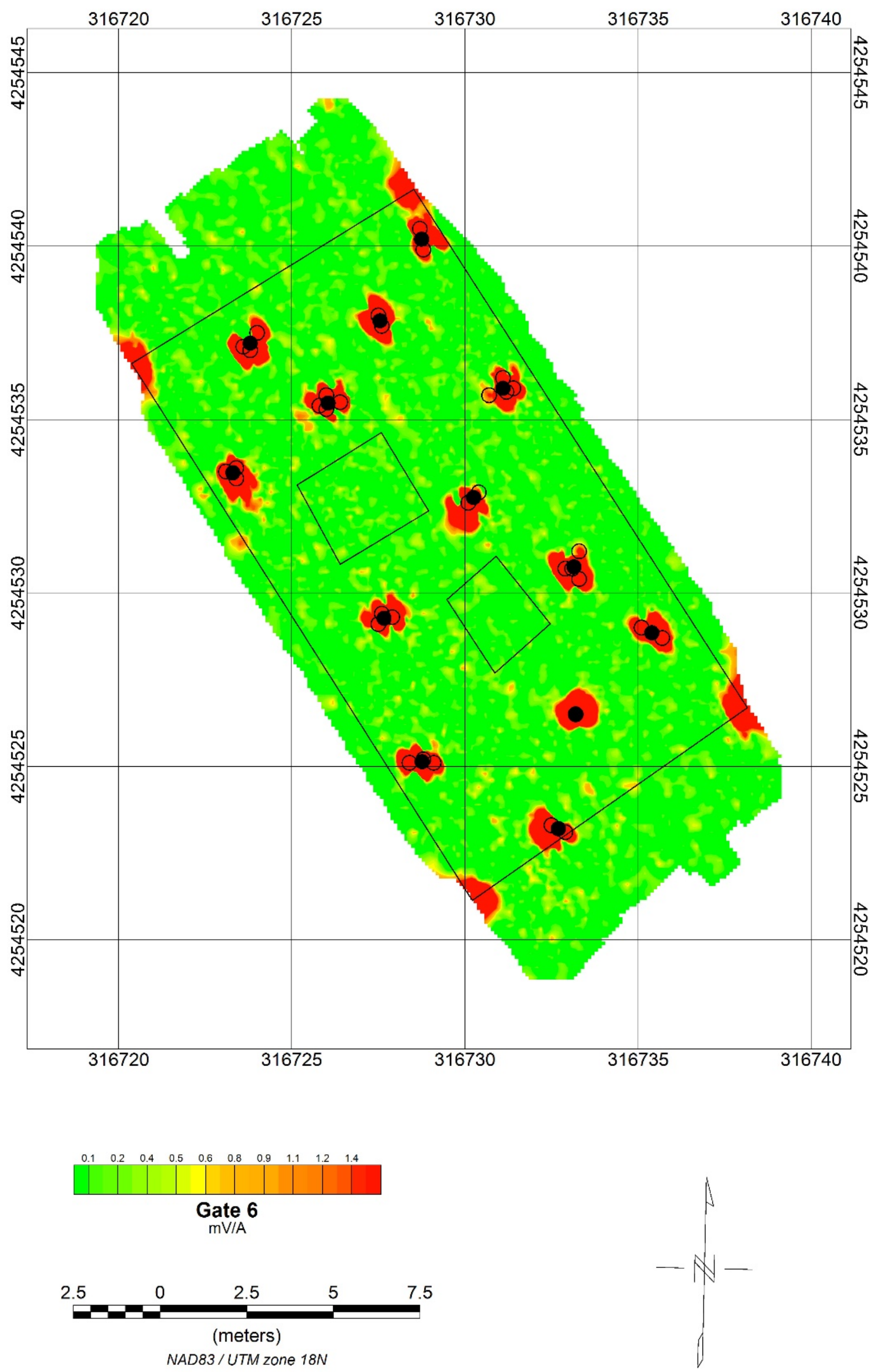


**Figure 55. Session B4; Filled Dots Are the Manually Chosen Target Locations.**

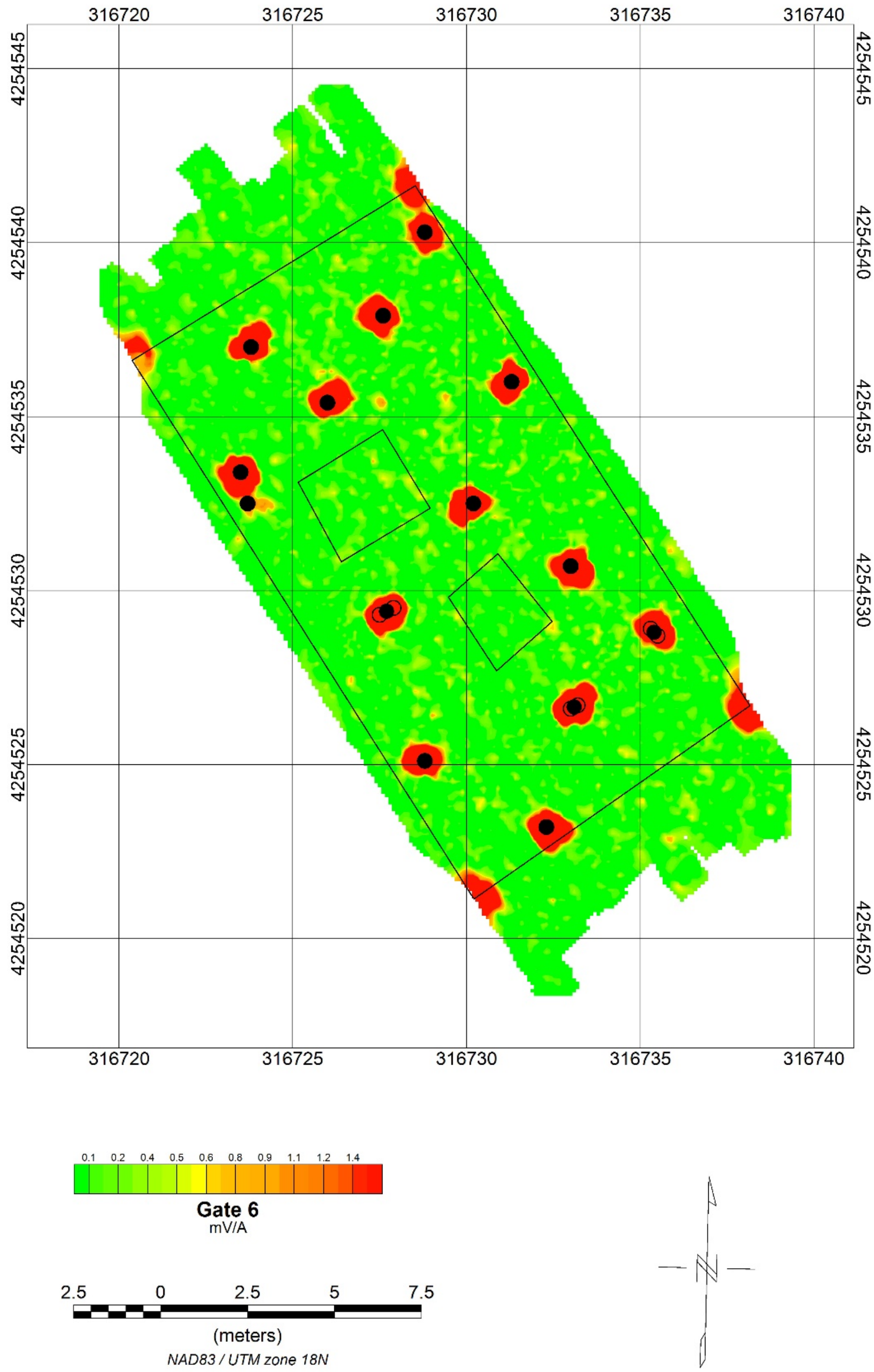


**Figure 56. Session B5; Filled Dots Are the Manually Chosen Target Locations.**

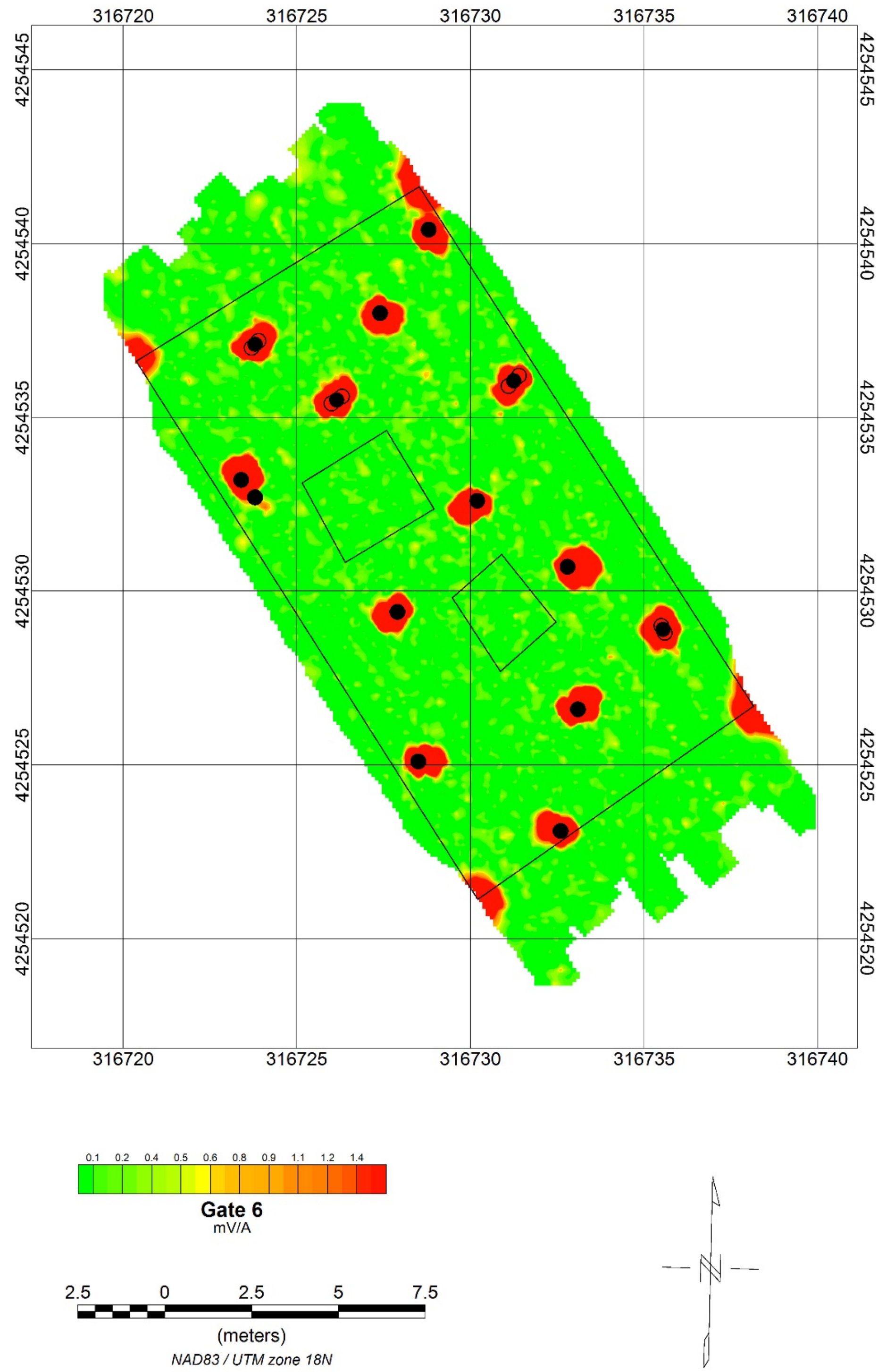


**Figure 57. Session B6; Filled Dots Are the Manually Chosen Target Locations.**